“The important thing is not to stop questioning.

Curiosity has its own reason for existing.”

Albert Einstein

University of Alberta

Development of Empirical Models to Predict Deposition of Aerosols in the Extrathoracic Airways of Children

by

Laleh Golshahi

A thesis submitted to the Faculty of Graduate Studies and Research
in partial fulfillment of the requirements for the degree of

Doctor of Philosophy

Department of Mechanical Engineering

Spring 2012
Edmonton, Alberta

DEDICATION

It is my great pleasure to dedicate this thesis to my better half, Reza, for his friendship, humor, endless support and encouragement.

ABSTRACT

The experimental studies described in this thesis were performed with the goal of measuring deposition of aerosols, inhaled either nasally or orally, in the extrathoracic airways of children in different age groups. We pursued *in vitro* methods and characterized the deposition of aerosols in the extrathoracic airway models of children to address the current concerns in the area of pediatric dosimetry. Using rapid prototyping, nasal airways of ten adults and fourteen children 4-14 years old as well as oral airways of nine children 6-14 years old were replicated from CT scans and MRI images during the course of this research. In addition to these 33 plastic replicas, ten previously-built nasal airway replicas of infants were also used to develop three empirical models to predict the deposition of ultrafine aerosols in nasal airways of infants and the deposition of micrometer-sized particles in the nasal and oropharyngeal airways of children. One of the goals of this study was also to develop a simplified idealized child throat model that could simulate the average oropharyngeal deposition among the children 6-14 years old. The resulting idealized child model presented here will hopefully simplify and accelerate the development of new inhalable drugs for the pediatric population suffering from respiratory diseases.

ACKNOWLEDGEMENTS

I have been waiting for a chance to express my sincere gratitude to my Ph.D. advisor, Professor Warren Finlay, who has been a great mentor to me and has literally held my hands when I have been taking my baby steps during the course of this study. I fell a lot, but picked myself up because I have had the chance to rely on his unconditional support. It may sound unreal, but I would have done my Ph.D. with him again if I were given a second chance to do so. He has had a strong influence on my academic life and writing this thesis to graduate has been a very hard decision to make since I have never felt that I have learned enough from his very broad and deep knowledge of aerosol science. Thank you for having me as your graduate student, Dr. Finlay. I am always grateful and honored for having the chance to do a Ph.D. with a brilliant researcher like you.

In addition to Dr. Finlay, the rest of my committee members Professors Sunalene Devadason, Carlos Lange, Michelle Noga, Jason Olfert and Reinhard Vehring have provided me with their invaluable feedback on this research. Their time and expertise are very much appreciated.

I would like to thank Professor Michelle Noga once more for providing the CT images of the nasal airways, coordinating the imaging of oral airways and providing guidance on ethics approval procedure. I cannot envision having this thesis completed without her help and support. The incredible staff of the PET/CT center at the Stollery Children's hospital, especially Mr. Scott Warren and Greg Wandzilak have been immensely helpful and have gone beyond their job descriptions to make a major part of the CT recordings possible. Professor Richard Thompson is also acknowledged for providing the MRI images of the nasal airways of adults, recruited by John Storey-Bishoff. Thanks also to Professor Carlos Flores-Mir and the staff at the Dentistry Department of the University of Alberta, especially Ms. Susan Helwig, for providing CBCT images at the preliminary stages of the oral airway studies.

The expertise of the staff of the Institute for Reconstructive sciences in Medicine (iRSM) in image processing and rapid prototyping has been vital to make this research possible. Special thanks to Mr. Andrew Grosvenor and Ben King for printing the airway replicas and answering my questions regarding image processing and rapid prototyping. Dr. Diana Shaw at iRSM has been more than a collaborator and her support has made the fabrication of models an enjoyable experience.

The talents of the professionals in the Department of Mechanical Engineering's machine shop and electronic engineering facility are highly acknowledged. They have generously helped me with my endless questions and requests. My special thanks go to Mr. Bernie Faulkner, Rick Conrad, Andrew Campbell, Dave Waege, Rick Bubenko, and Roger Marchand.

The staff at the main office of the Mechanical Engineering Department have been wonderful to me and I would like to especially thank Ms. Doris Riedner for patiently helping me with the imaging reimbursement fees for more than two years and Ms. Teresa Gray for being helpful with my frequent complicated expense claims. Also, I would like to thank Ms. Gail Dowler, the Department's Secretary of Graduate Studies, for her extensive help and support since the very beginning of my Ph.D.

Thanks to all the current and former members of ARLA lab during the long years of my Ph.D. studies. Especially, John Storey-Bishoff for answering my questions even long after his graduation, Roberto Martinez for answering my coding questions during my early attempts and Andriy Roshchenko for the interesting discussions that we have had during my experiments. Thank you to Stacey Yuen and Gillian Redman for their friendship and boundless energy. Thank you also to all the recently-joined ARLA members for their friendship, interesting questions, comments and their patience with the delays in their studies caused by my never-ending experiments. I also would love to very sincerely thank Ms. Helena

Orszanska. Helena, you made this study feasible in your own way. You made my days in the lab colorful with your spirit and vast knowledge of books and music. You made me believe there are lots left to be learned and I will never forget your subtle way of kindness. I have only got the chance to meet Dr. Kevin Stapleton at the final stages of my research, but his honest and friendly pieces of advice during our very short encounter have helped me to dust myself off at a pivotal point close to the end of this study. I am truly grateful for such honesty and guidance, Kevin.

Thanks to my family for always allowing me to grow and follow my passion with a peaceful mind. They have a special place in my heart for forming the core of my life's philosophy and teaching me to strive to be an honest person and a fair player no matter what life brings on my way. My mother is a heroin and the way she sets her life standards always inspires me. My father has been the reason that I have been driven into health-related research and I hope once more in a near future, I can be held effortlessly in his arms and be told that I have been a good daughter.

My genuine, bottom-hearted appreciation is reserved for my best friend and kind husband, Dr. Reza Mohammadi. He has patiently waited for me to get to the end of this journey. I believe it was not an easy road for him either, but he kept having faith in me and reminded me that this will end too. We did this together and I cannot see myself being able to do this alone or with anyone else. He stepped into my chaotic graduate student life in Calgary and since then he has been there for me despite my long hours either in the labs or lost in thoughts, my continuous doubts in myself and my sulfur-smelled clothes and hair on our very first date! His love and support have always been beyond my understanding and I feel incredibly lucky for getting to know his pure and beautiful soul. His family have also been incredibly supportive and their cheerful voices on the phone have made me smile and forget my day-to-day research problems.

Many friends inside and outside of the University of Alberta have made my life happier during my time at the U of A. Thanks to Oxana Malysheva, Haide Razavy

and her family for their friendship, my lovely friends at PIE readers book club, my incredible Corinne Lillo at Lillo's music school and Marjan Akhbari who has recently been discovered!

Finally, financial support from the Alberta Innovates (AIF), the Natural Sciences and Engineering Research Council of Canada (NSERC) and the University of Alberta are gratefully acknowledged. This thesis is materialized as a result of such generous financial support.

Laleh Golshahi
January 22nd, 2012
Edmonton, AB, Canada

Table of Contents

CHAPTER 1 : INTRODUCTION 1
1.1 Background 1
1.2 Objectives 3
1.3 Overall Structure of the Thesis 4
1.4 Bibliography 5
CHAPTER 2 : DEPOSITION OF INHALED ULTRAFINE AEROSOLS IN REPLICAS OF NASAL AIRWAYS OF INFANTS 10
2.1 Introduction 10
2.2 Experimental Procedure 14
2.3. Results and Discussion 22
2.3.1. Method Validation 22
2.3.2. Comparison of Infant Data with Existing Adult Correlations 25
2.3.3. Predictive Correlations for Infants 31
2.3.4. Use of Infant Correlation for Adults 39
2.4. Conclusions 41
2.5 Bibliography 42
CHAPTER 3 : *IN VITRO* DEPOSITION MEASUREMENT OF INHALED MICROMETER-SIZED PARTICLES IN EXTRATHORACIC AIRWAYS OF CHILDREN AND ADOLESCENTS DURING NOSE BREATHING 50
3.1 Introduction 50
3.2 Experimental Methods 53
3.3. Results and Discussion 62
3.3.1. Method Validation 63
3.3.2. Nasal Deposition in Child Replicas 65
3.3.3. Comparison of Deposition in Normal vs. Congested Nose 76
3.3.4. Comparison of Deposition across Different Age Groups 79
3.4 Conclusions 81
3.5 Bibliography 82
CHAPTER 4 : DEPOSITION OF INHALED MICROMETER-SIZED PARTICLES IN OROPHARYNGEAL AIRWAY REPLICAS OF CHILDREN AT CONSTANT FLOW RATES 89
4.1 Introduction 89
4.2 Experimental Methods 92
4.2.1 Imaging of the Airways 92
4.2.2. Fabrication of Replicas 94
4.2.3. Deposition Measurement Experiments 97
4.3. Results and Discussion 99
4.4 Conclusions 106
4.5 Bibliography 107

CHAPTER 5 : AN IDEALIZED CHILD THROAT THAT MIMICS AVERAGE PEDIATRIC OROPHARYNGEAL DEPOSITION 113
5.1 Introduction 113
5.2 Methods 115
5.3 Results and Discussion 117
5.4 Conclusions 120
5.5 Bibliography 121
CHAPTER 6 : COMPARISON OF THE LUNG DOSE IN ADULTS AND CHILDREN USING THE DEVELOPED CORRELATIONS FOR EXTRATHORACIC DEPOSITION 125
6.1 Introduction 125
6.2 Methods 126
6.3 Results and Discussion 127
6.4 Conclusions 132
6.5 Bibliography 133
CHAPTER 7 : CONCLUSIONS 134
7. 1 Summary and Conclusions 134
7.2 Future Work 135
7.3 Bibliography 136
Appendix A: Experimental Deposition Data i
A.1 List of Deposition Data Presented in Chapter 2 i
A.2 List of Deposition Data Presented in Chapter 3 vi
A.3 List of Deposition Data Presented in Chapter 4 xiii
A.4 List of Deposition Data Presented in Chapter 5 xviii

List of Tables

Table 2.1 Adult subject parameters 16
Table 2.2 Summary of equations in the literature for predicting deposition of ultrafine particles in nasal airways of adults and their related R^2 values when fitted to our infant data 26
Table 2.3 Characteristic diameters that are suggested in literature and tested in this study for calculation of dimensionless parameters to reduce intersubject variability 32
Table 2.4 *R*-squared values of equation (2.12) fitted to infant data using different characteristic diameters 34
Table 2.5 Values of constants in equations (2.12) and (2.13) for four diameters with the highest R^2 values for infant data 35
Table 2.6 Nasal resistance dependent characteristic diameter of infants 38
Table 2.7 Nasal resistance dependent characteristic diameter of adults 40
Table 3.1 Geometrical parameters including volume (V), surface area (A_s) and path length (L) of the five nasal replicas of adults used for comparison with *in vivo* data given in the literature 54
Table 3.2 Child subject parameters. V is the volume of airway, A_s is the surface area of the airway lumen, L_{nose} is the length of nasal cavity to the end of septum, L_t is the length of the remaining part of the nasal airway (oropharynx) to the level of upper trachea, A_{min} is the minimum cross section of the airway measured for each cross section at 3 mm intervals perpendicular to the possible streamline of air going through the nasal airway, $P_{nostril}$ is the perimeter of nostrils, N_l is the length of nostril (larger dimension of an ellipse) and N_w is the width (smaller dimension) of nostrils. 56
Table 3.3 Characteristic diameters and their corresponding references in the literature in case they have previously been used. $A_{nostril}$ is the cross sectional area of the nostrils, which is defined as the length of the nostril times its width, herein. E_{mean} is the average ellipticity of the two nostrils for each subject, whereby

ellipticity is defined as the ratio of each nostril's height to its width. R_{nose} is the resistance of the nose, which is defined in Eq. 3.12. 70
Table 3.4 *R*-squared values for different combinations of characteristic diameters used in defining combination of the nondimensional numbers in the deposition parameter, *X* (given in Eq. 3.9). The exponent values *a*, *b* (from Eq. 3.9), *c*, *d*, *e* (given below) are different in each case and chosen to minimize R^2 via least squares..... 71
Table 4.1 Relevant information of the subjects including their sex, age (in years), height (in cm) and weight (in kg) 94
Table 4.2 Geometrical parameters of the replicas post-build: volume (mm^3), surface area (mm^2) and length (mm) 96
Table 6.1 List of the developed extrathoracic deposition equations and their related parameters and references. Parameters *V*, *L* and A_s are the volume, centerline length and surface area of the airways, respectively. 127

List of Figures

Figure 2.1 Nasal airways of one infant subject and two adult subjects (one male and one female) are shown. 17
Figure 2.2 Schematic diagram of the experimental setup. 18
Figure 2.3 Pressure drop data points across six adult human nasal replicas as a function of inspiratory air flow rate compared with available *in vivo* and *in vitro* measurements in the literature. 23
Figure 2.4 Deposition data for adults at a flow rate of 20 L/min compared to available *in vivo* and *in vitro* data. 24
Figure 2.5 Pressure drop data for inspiratory flows in infant subjects. 25
Figure 2.6 The correlation of Swift et al. (1992) developed for adults is shown with our infant deposition data. Error bars on our experimental data points are approximately the same size as the symbols and so are not shown. 27
Figure 2.7 The correlation of Cheng et al. (1995) developed for older children (1.5-, 2.5- and 4-year-olds) is shown with infant deposition data in this study. ... 28
Figure 2.8 Comparison of deposition in infant replicas vs. particle diameter (d_p) using tidal breathing (solid markers) and constant flow rate (empty markers). ... 30
Figure 2.9 Comparison of deposition in adult replicas vs. particle diameter (d_p) using tidal breathing (solid markers) and constant flow rate (empty markers). ... 31
Figure 2.10 Deposition in infant replicas vs. non-dimensional deposition parameter using characteristic diameter defined as $d_c = (0.0181\ L_{nose}/R_{nose})^{4/19}$ .. 36
Figure 2.11 Deposition in infant replicas vs. non-dimensional deposition parameter using characteristic diameter $d_c = \overline{A_c}/L$ 39
Figure 3.1 Fourteen nasal airways of children 4-14 years old. The subjects are arranged based on their numerical label from left to right on each row (subject 1 is the top left airway). 55
Figure 3.2 Schematic diagram of the experimental setup for measuring deposition of particles in nasal airways of adults and children. 58
Figure 3.3 Deposition in our five adult replicas (subjects 2, 5, 6, 8, and 9) compared to *in vivo* data in the literature. 64

Figure 3.4 Comparison of deposition data from *in vivo* studies (Becquemin *et al*. (1991), 20 subjects 5.5-15 years old, and Bennett *et al.* (2008), 12 subjects 6-10 years old) with our deposition values in 13 replicas of children 4-14 years old vs. the impaction parameter (d_a^2Q)..... 66
Figure 3.5 Deposition in children's replicas vs. the deposition parameter including intranasal pressure drop ($d_a^2\Delta p$)..... 67
Figure 3.6 Deposition of micrometer-sized particles in children replicas vs. non-dimensional deposition parameter X from Eq. 3.9 including a characteristic diameter defined as (a) $d_c=A_s/L$ (b) $d_c=\sqrt{V/L}$ 75
Figure 3.7 Comparison of deposition in one six year old subject with a congested nose with our thirteen healthy subjects. 78
Figure 3.8 Deposition versus impaction parameter d_a^2Q across different ages (infants, children, adults). 80
Figure 4.1 The dimensions of the mouthpiece (LC star nebulizer's mouthpiece), through which the children inhaled at the time of CT imaging. 93
Figure 4.2 Nine oral airway replicas of children 6-14 years old. The replicas are arranged in an ascending order based on their numerical label from left to right on each row. 95
Figure 4.3 Schematic diagram of the experimental setup we used for measuring deposition of particles in oropharyngeal airway replicas of children and the 'Alberta Idealized Throat'..... 98
Figure 4.4 Deposition in children's replicas vs. the impaction parameter (d_a^2Q) for flow rates of 30-150 L/min and particles in the aerodynamic size range of 0.5- 5.3 μm. 100
Figure 4.5 Comparison of the deposition in our children replicas with the estimated values using a correlation developed for adults by Grgic et al. (2004) (Eq. 4.1) when the x-axis contains the children's geometrical dimensions. 102
Figure 4.6 Deposition of micrometer-sized particles in oropharyngeal replicas of children vs. non-dimensional deposition parameter (X) as a combination of

Stokes and Reynolds numbers that include a characteristic diameter defined as $d_c = \sqrt{V/L}$ 103

Figure 4.7 The deposition of micrometer-sized particles in oropharyngeal replicas of children vs. non-dimensional deposition parameter, X, as a combination of Stokes and Reynolds numbers. These numbers include a characteristic diameter defined as $d_c = V/A_s$ 105

Figure 5.1 Schematic of the Idealized Child Throat. The lengths of the sections a, b and c (62.7, 40.6 and 38.7 mm, respectively) are the summations of polylines shown in each section. 116

Figure 5.2 The deposition of orally inhaled micrometer-sized particles in the Idealized Child Throat versus the impaction parameter compared to that of nine children replicas in our previous study (Golshahi et al. 2011b). 118

Figure 5.3 Deposition in the Idealized Child Throat and children's anatomically accurate replicas (Golshahi et al. 2011b) versus the deposition parameter $X = \mathrm{Stk}^{1.5}\mathrm{Re}^{0.69}$ where Stk and Re are Stokes and Reynolds numbers that use a subject specific length scale V/A_s. 120

Figure 6.1 Lung doses for different age groups, normalized to the body mass and the adult inhaled dose, versus particle's aerodynamic diameter. 129

Figure 6.2 Lung doses for different age subjects, normalized to the adult inhaled dose and the subjects' body surface area, versus aerodynamic diameter of particles. 130

Figure 6.3 Lung doses for different age group subjects, normalized to the adult inhaled dose and the body surface area of different age groups, versus the inertial impaction parameter $d_a^2 Q$. 132

CHAPTER 1 : INTRODUCTION

1.1 Background

Deposition in the extrathoracic region of the respiratory system plays an important role in determining the dose delivered to the lungs since this region filters the inhaled aerosols on their way to the lungs. Extrathoracic airways are generally defined as oral/buccal cavity, nasal passages, pharynx, larynx and the proximal region of the trachea (Stahlhofen *et al*. 1980, 1983). Thus, there have been extensive studies with the focus on characterizing deposition in both nasal and oral airways of adults in order to understand the deposition mechanisms in the extrathoracic airways and, thus, determining the dose delivered to the lungs.

Deposition in oral airways is lower than nasal airways; therefore, oropharyngeal airways are considered as the preferred route of inhalation drug delivery, which is a favorite method of drug delivery due to its noninvasive nature. This path of inhalation has been extensively studied for drug delivery by our group (DeHaan and Finlay, 2001, 2004; Grgic *et al*. 2004 a, b, 2006) and others (Cheng *et al*. 1999, 2001; Swift, 1992; Zhou *et al*. 2011). Moreover, attempts have been made to simplify such complicated geometries in the form of idealized models to facilitate development of new drug formulations. The United States Pharmacopia (USP) throat is an example of such developments. This throat has been used with the hope of simulating the average oropharyngeal deposition among adults. The failure of this model (USP throat) in the deposition estimations, however, has been hypothesized to be due to its significant difference from the actual anatomical geometries because of its excessive simplifications

(Srichana *et al*. 2000; Zhang *et al*. 2007; Zhou *et al*. 2011). Thus, the 'Alberta Idealized Throat' has been developed in our group based on the actual airway geometry of adults and has successfully been commercialized to simulate the average oropharyngeal deposition among adults (Grgic *et al*. 2004 a, b; Stapleton *et al*., 2000; Zhang *et al*. 2007; Zhou *et al*. 2011).

Despite the progress that has been made in the prediction of extrathoracic deposition among adults, little data exists on oral airway deposition in children. *In vivo* studies are not easily feasible due to the ethical concerns regarding exposure of human subjects, especially children, to radiation. Thus, there are only limited numbers of *in vivo* studies with a focus on measuring total deposition of aerosols in the children's respiratory tract (Becquemin *et al*. 1991; Bennett and Zeman, 1998, 2004; Schiller-Scotland *et al*. 1992) and a few more on oropharyngeal and lung deposition of aerosols emitted from specific inhalers (Agertoft *et al*. 2003; Devadason *et al*. 1997, 2003; Geller *et al*. 1998; Roller *et al*. 2007; Schueepp *et al*. 2009).

In vitro studies, on the other hand, have proven to be successful in improving our understanding of respiratory deposition among adults over the years. However, long imaging time, a major issue considering the short attention span common among children, and tedious resin cast production have hindered the necessary progress in the area of pediatric respiratory deposition. Recent advances in high resolution imaging and 3D printing have facilitated studies in the field of *in vitro* pulmonary deposition. Thus, only recently attempts have been made to address the shortcomings of *in vivo* measurements by taking an *in vitro*

approach (Janssens *et al*. 2001; Minocchieri *et al*. 2008; Corcoran *et al*. 2003; Laube *et al*. 2010). Most of these studies however, have been focused on a limited number of nose-breathing subjects (mostly just one subject) or just with specific inhalers (Wachtel *et al*. 2010). A comprehensive study has been done in our group with the focus on minimizing the intersubject variability apparent in deposition of micrometer-sized particles in the nasal airways of infants 3-18 months (Storey-Bishoff *et al*. 2008). This thesis was planned to complete such measurements by expanding the age range of the pediatric subjects, inhalation route (i.e. nasal and oral) and the particle sizes.

1.2 Objectives

The main goal of this study is to characterize the deposition of aerosols of various sizes in the extrathoracic airways of children of different ages during various breathing patterns through the nose or mouth. In order to achieve this goal, the development of nasal and oral airway replicas of children was one of the prerequisites. Further measurements of aerosol deposition in the developed replicas and correlating the deposition data to the related non-dimensional numbers, which include the geometrical dimensions of the extrathoracic airways of each subject, were targeted to reduce intersubject variability and to enhance individualized prediction of extrathoracic deposition. Eventually, the development of a simple geometry that could simulate the average deposition of aerosols in the children's oral airways (as the preferred route of drug delivery), was deemed to be

within the scope of this research. Such a simple geometry may have a major impact on simplifying bench-top testing of new inhalation drug formulations.

1.3 Overall Structure of the Thesis

This thesis is presented in mixed-format, which includes published and as-yet under review research. The current chapter, Chapter 1, is a brief introductory chapter to the entire thesis and is written to describe the motivation behind this research and to explain the connections among the next chapters. Development of a method to measure the deposition of ultrafine aerosols (13-100 nm) in nasal airway replicas of ten infants is described in Chapter 2. This study is useful in exposure studies since ultrafine particles are ubiquitous in the environment and infants, as explicitly nose-breathers, are a high risk population. To extend our understanding of nasal deposition, the fabrication of fourteen nasal airway replicas of children 4-14 years old and the measurements of deposition of micrometer-sized particles in these replicas were undertaken, the procedure and results of which is presented in Chapter 3. This chapter will be useful for exposure studies and for potential inhalation drug delivery methods involving face masks. Since the preferred route of drug delivery to the lungs is the oral airways, the development of nine oral airway replicas and deposition measurements of micrometer-sized particles in these replicas are explained in Chapter 4. The results of Chapter 4 were used to develop an Idealized Child Throat model based on the previously made 'Alberta Idealized Throat' for the simulation of average extrathoracic deposition in adults. Chapter 5 introduces such an idealized child

throat model. Chapter 6 examines the usage of the developed correlations in Chapters 3 and 4. In this Chapter, the delivered dose to the lungs of children is also compared with those of adults and infants based on the previously-developed correlations (Grgic *et al*. 2004a; Storey-Bishoff *et al*. 2008) for the two latter age groups. Finally, summary of the whole thesis is given in Chapter 7 as the conclusions and suggested future works.

1.4 Bibliography

Agertoft, L., Laulund, L. W., Harrison, L. I., Pedersen, S. (2003). Influence of particle size on lung deposition and pharmacokinetics of beclomethasone dipropionate in children. *Pediatric Pulmonology*, 35, 192-199.

Becquemin, M. H., Yu, C. P., Roy, M., and Bouchikhi, A. (1991). Total deposition of inhaled particles related to age: comparison with age dependent model calculations. *Radiation Protection Dosimetry*, 38, 23-28.

Bennett, W. D., and Zeman, K. L. (1998). Deposition of fine particles in children spontaneously breathing at rest. *Inhalation Toxicology*, 10, 831-842.

Bennett, W. D., and Zeman, K. L. (2004). Effect of body size on breathing pattern and fine-particle deposition in children. *Journal of Applied Physiology*, 97, 821-826.

Cheng, Y. S., Zhou, Y., and Chen, T. B. (1999). Particle deposition in a cast of human oral airways. *Aerosol Science and Technology*, 31, 286-300.

Cheng, Y. S., Yazzie, D., and Zhou, Y. (2001). Respiratory deposition patterns of salbutamol pMDI with CFC and HFA-134a formulations in a human airway replica. *Journal of Aerosol Medicine*, 14(2), 255-266.

Corcoran, T.E., Shortall, B.P., Kim, I.K., Meza, M.P., Chigier, N. (2003). Aerosol drug delivery using heliox and nebulizer reservoirs: Results from an MRI-based pediatric model. *Journal of Aerosol Medicine*, 16, 365-271.

DeHaan, W. H., and Finlay, W. H. (2001). *In vitro* monodisperse aerosol deposition in a mouth and throat with six different inhalation devices. *Journal of Aerosol Medicine*, 14(3), 361-367.

DeHaan, W. H., and Finlay, W. H. (2004). Predicting extrathoracic deposition from dry powder inhalers. *Journal of Aerosol Science*, 35(3), 309-331.

Devadason, S. G., Everard, M. L., MacEarlan, C., Roller, C., Summers, Q. A., Swift, P., Borgstrom, L., and Le Souef, P. N. (1997). Lung deposition from the Turbuhaler in children with cystic fibrosis. *The European Respiratory Journal*, 10, 2023-2028.

Devadason, S. G., Huang, T., Walker, S., Troedson, R., and Le Souef, P. N. (2003). Distribution of technetium-99m-labelled QVAR™ delivered using an Autohaler™ device in children. *The European Respiratory Journal*, 21, 1007-1011.

Geller, D. E., Eigen, H., Fiel, S. B., Clark, A., Lamarre, A. P., Johnson, C. A., Konstan, M. W. (1998). Effect of smaller droplet size of dornase alfa on lung function in mild cystic fibrosis. *Pediatric Pulmonology*, 25, 83-87.

Grgic, B., Finlay W. H., Burnell, P. K. P., Heenan, A. F. (2004a). *In vitro* intersubject and intrasubject deposition measurements in realistic mouth-throat geometries. *Journal of Aerosol Science*, 35, 1025-1040.

Grgic, B., Finlay W. H., Heenan, A. F. (2004b). Regional aerosol deposition and flow measurements in an idealized mouth and throat. *Journal of Aerosol Science*, 35, 21-32.

Grgic, B., Martin, A. R., and Finlay W. H. (2006). The effect of unsteady flow rate increase on *in vitro* mouth-throat deposition of inhaled boluses. *Journal of Aerosol Science*, 37, 1222-1233.

Janssens, H.M., De Jongste, J.C., Fokkens, W.J., Robben, S.G.F., Wouters, K., Tiddens, H.A.W.M. (2001). The Sophia anatomical infant nose-throat (saint) model: A valuable tool to study aerosol deposition in infants. *Journal of Aerosol Medicine*, 14, 433-441.

Laube, B.L., Sharpless, G., Shermer, C., Nasir, O., Sullivan, V., Powell, K. (2010). Deposition of albuterol aerosol generated by pneumatic nebulizer in the Sophia Anatomical Infant Nose-Throat (SAINT) model. *Pharmaceutical Research*, 27, 1722-1729.

Minocchieri, S., Burren, J.M., Bachmann, M.A., Stern, G., Wildhaber, J., Buob, S., Schindel, R., Kraemer, R., Frey, U.P., Nelle, M. (2008). Development of the premature infant nose throat-model (PrINT-Model)-an upper airway replica of a premature neonate for the study of aerosol delivery. *Pediatric Research*, 64,141-146.

Roller, C. M., Zhang, G., Troedson, R. G., Leach, C. L., Le Souef, P. N., and Devadason, S. G. (2007). Spacer inhalation technique and deposition of extrafine aerosol in asthmatic children. *The European Respiratory Journal*, 29, 299-306.

Schiller-Scotland, C. H. F., Hlawa, R., Gebhart, J., Wonne, R., and Heyder, J. (1992) Total deposition of aerosol particles in the respiratory tract of children during spontaneous and controlled mouth breathing. *Journal of Aerosol Science*, 23(Suppl. 1), S457-S460.

Schueepp, K. G., Devadason, S. G., Roller, C., Minocchieri, S., Moeller, A., Hamacher, J., and Wildhaber, J. H. (2009) Aerosol delivery of nebulised budesonide in young children with asthma. *Respiratory Medicine*, 103, 1738-1745.

Srichana, T., Martin, G., and Marriott, C. (2000). A human oral-throat cast integrated with a twin-stage impinger for evaluation of dry powder inhalers. *Journal of Pharmacy and Pharmacology*, 52, 771-778.

Stahlhofen, W., Gebhart, J., and Heyder, J. (1980). Experimental determination of the regional deposition of aerosol particles in the human respiratory tract. *American Industrial Hygiene Association Journal*, 41(6), 385-398a.

Stahlhofen, W., Gebhart, J., Heyder, J., Scheuch, G. (1983). New regional deposition data of the human respiratory tract. *Journal of Aerosol Science*, 14(3), 186-188.

Stapleton, K. W., Guentsch, E., Hoskinson, M. K., and Finlay, W. H. (2000). On the suitability of k-ε turbulence modeling for aerosol deposition in the mouth and throat: a comparison with experiment. *Journal of Aerosol Science*, 31,739-749.

Storey-Bishoff, J., Noga, M. and Finlay, W. H. (2008). Deposition of micrometer-sized aerosol particles in infant nasal airway replicas. *Journal of Aerosol Science*, 39, 1055-1065.

Swift, D. L. (1992). Apparatus and method for measuring regional distribution of therapeutic aerosols and comparing delivery systems. *Journal of Aerosol Science*, 23(Suppl. 1), S495-S498.

Wachtel, H., Bickmann, D., Breitkreutz, J., Langguth, P. (2010). Can Pediatric Throat Models and Air Flow Profiles Improve Our Dose Finding Strategy. In *Respiratory Drug Delivery 2010*, pp. 195-204, ed. Dalby, R.N., Byron, P. R., Peart, J., Suman, J. D., Farr, S. J., Young, P.M., Davis Healthcare, Rivergrove, Illinois.

Zhang, Y., Gilbertson, K., and Finlay, W. H. (2007). *In vivo-in vitro* comparison of deposition in three mouth-throat models with Qvar and Turbuhaler inhalers. *Journal of Aerosol Medicine*, 20: 227-35.

Zhou, Y., Sun, J., and Cheng Y. S. (2011). Comparison of deposition in the USP and physical mouth-throat models with solid and liquid particles. *Journal of Aerosol Medicine and Pulmonary Drug Delivery*, 24, 1-8.

CHAPTER 2 : DEPOSITION OF INHALED ULTRAFINE AEROSOLS IN REPLICAS OF NASAL AIRWAYS OF INFANTS[1]

A very similar version of this chapter has been published as:

Golshahi, L., Finlay, W. H., Olfert, J. S., Thompson, R. B., and Noga, M. L. (2010). Deposition of Inhaled Ultrafine Aerosols in Replicas of Nasal Airways of Infants. *Aerosol Science and Technology*, 44,741-752.

2.1 Introduction

Ultrafine particles (UFP, with a diameter of less than 100 nm) are ubiquitous in ambient and indoor air from several natural and anthropogenic sources. Epidemiological studies have raised concerns over adverse health effects associated with exposure to ultrafine particles (Kreyling *et al*. 2006). The cardiovascular and pulmonary systems have been diagnosed as the main targets of this unwanted exposure. However, recent studies have shown stronger affiliations between inhaled particles and respiratory failure compared to cardiovascular outcomes (Halonen *et al*. 2009). Exposure to radon and its progeny, which attaches to dusts and airborne particles, is associated with an increased risk of lung cancer (NRC 1988). Viral lower respiratory tract infections in infants and young children are also a major public health issue (Van Woensel *et al*. 2003). On the other hand, effects of UFPs on organs other than the lungs, especially, the brain and central nervous system (CNS) have received special attention recently.

[1] Reproduced with permission from Taylor & Francis, Copyright 2010.

Researchers have found that the CNS can be a target of ultrafine aerosols and the most probable mechanism behind this process is from deposits on the olfactory mucosa in the nasopharyngeal region of the respiratory tract and subsequent translocation via the olfactory nerve (Oberdorster *et al*. 2004).

Nanomedicine, including the use of nanoparticles, has potential for the therapeutic treatment of diseases via manipulation of particle characteristics such as size, surface chemistry, surface charge, and surface area (Gill *et al*. 2007). Conceptually, drug delivery directly to the site of infection reduces the systemic side effects of therapeutic agents, which in turn makes pulmonary targeted drug delivery of ultrafines a plausible research area. Moreover, deposition of inhaled pharmaceutical aerosols in the olfactory region may be an efficient method for treatment of central nervous system disorders. However, the dosimetry, which involves regional deposition patterns in the respiratory tract and the biokinetic fate of inhaled ultrafine particles, is not yet fully understood (Kreyling *et al*. 2006).

Human extrathoracic airways filter inhaled pharmaceutical particles and hinder their penetration to targeted regions in the lung. Therefore, knowledge of the filtration efficiency of the upper airways (naso/oropharyngeal regions) and the influence of intersubject differences on this mechanism is essential for evaluating delivered dose to the lungs, as well as assessing the risks of exposure to toxic ultrafine particles in different environments. In an attempt to understand how physical properties of particles and respiratory parameters influence the deposition of aerosols in extrathoracic airways of adults, many experimental

measurements (*in vivo* and *in vitro*), numerical analyses and computational fluid dynamics (CFD) studies have been performed. For example, *in vivo* adult studies have been performed by Cheng, Y. S. *et al*., Cheng, K. H. *et al*., and Swift and Strong (1996). These *in vivo* studies have demonstrated that considerable intersubject variability is present in the diffusion deposition regime (Cheng 2003). Although *in vivo* studies on human subjects are desirable, the invasive and hazardous nature of the employed aerosols limits the extent of such studies. Experimental measurements of deposition of ultrafine particles in physical casts of extrathoracic airways (*in vitro*) have been used as a substitute for *in vivo* studies (Cheng *et al*. 1988, 1990, 1993; Swift *et al*. 1992; Yamada *et al*. 1988; Gradon and Yu 1989; Guilmette *et al*. 1994; Kelly *et al*. 2004). Computational fluid dynamic (CFD) simulations have been useful for improving our understanding of deposition mechanisms correlated to flow patterns in nasal airways (Yu *et al*. 1998; Zamankhan *et al*. 2006; Shi *et al*. 2006; Wang *et al*. 2009; Xi and Longest 2008).

In spite of all the above noted progress on aerosol deposition in adults, our knowledge of aerosol behavior in children and specifically in infants is limited. Practical difficulties with using *in vivo* imaging in infants and children could be one of the reasons for this limitation. The youngest subject for which *in vitro* deposition of ultrafine particles in extrathoracic airways has been measured is reported in the study of Cheng *et al*. (1995). They measured the deposition of ultrafine particles and radon progeny within three nasal airways replicas of 1.5-, 2.5- and 4-year-old children using monodispersed NaCl and Ag aerosols ranging

from 0.0046 μm to 0.2 μm in diameter at inspiratory and expiratory flow rates of 3 L/min, 7 L/min and 16 L/min. In that study, the deposition efficiency was found to decrease with increasing age for a given particle size between 0.001 to 0.2 μm. To our knowledge, however, no studies have measured the deposition of ultrafine particles in the extrathoracic airways of children younger than 1.5 years (i.e., infants).

For micron-sized particles, comparison of the deposition data of Swift (1991), Minocchieri *et al*. (2008) and the SAINT replica (Schuepp *et al*. 2005) raised the following question: assuming there are large intersubject variations in extrathoracic airways of infants, as there are in adults, how much of the variability in deposition is due to differences in airway morphology or breathing pattern at a given age and how much is due to age alone? (Finlay 2008) While Storey-Bishoff *et al*. (2008) address this question for micron-sized particles, ultrafine aerosol deposition in infants has not been explored in this regard.

It has been suggested that infants breathe exclusively through their nose from birth to between 6 weeks and 6 months of age (Polgar and Kong 1965). Moreover, face masks are normally used for pharmaceutical aerosol administration to infants because infants are unable to use the mouthpieces associated with standard inhalers and nebulizers; therefore, predicting deposition of aerosols in nasal airways of infants is important in exposure assessments and determining lung drug dose.

Comparisons of ultrafine particle deposition in models and live subjects confirm *in vitro* measurement as an acceptable method for the simulation of

particle behavior in human nasal airways (Martonen and Zhang 1992). Experiments using nasal replicas are popular because they can be used for systematic studies in laboratories without the ethical limitations of human studies. Given that nasal airway cross sections do not change noticeably during the breathing cycle (Arens *et al*. 2005), collecting images of infant extrathoracic airways is an alternative option to avoid the complexities of subject recruitment and *in vivo* studies. Moreover, although deposition of ultrafine aerosols in replicas with nasal hair is higher than without nasal hair for adults (Cheng *et al*. 1993), this is not an issue for infants because they do not yet have any nasal hair. Also, surface roughness characteristics of replicas have not been found to be important in deposition of ultrafine particles less than 150 nm in diameter (Kelly *et al*. 2004). For the above reasons, *in vitro* measurements of deposition in infants nasal airways are expected to be an acceptable alternative to *in vivo* studies.

In the present study we characterize ultrafine particles deposition in nasal airways of infants, supplementing a recent communication whose focus was on the deposition of micrometer-sized particles in replicas of nasal airways of infants (Storey-Bishoff *et al*. 2008).

2.2 Experimental Procedure

For the infant part of our study, computed tomography (CT) scans of upper airways of ten infants (3-18 months) were obtained from the medical imaging archive at Stollery Children's Hospital, Edmonton, Canada with the approval of the Alberta Health Research Ethics Board. The replicas included the

face, nostrils and nasal airways to the level of the upper trachea. Details of model construction and subject parameters can be found in a recent communication (Storey-Bishoff *et al*. 2008).

For validation purposes, magnetic resonance imaging (MRI) scans of six adults during nasal breathing were obtained in coronal slices using a Turbo Spin Echo sequence using a Siemens MRI scanner (Sonata, Siemens Healthcare, Erlangen, Germany) with a standard head coil for signal reception under the approval of the University of Alberta Health Research Ethics Board. In-plane spatial resolution in the coronal plane was 0.33 mm with a slice thickness of 1.5 mm. Coronal slice orientations ensured the lower resolution slice-dimension was oriented predominantly along the length of the nasal passages, while the high resolution in-plane dimensions were oriented perpendicular to the nasal wall. Manual dynamic region growing using Mimics (Materialise, Leuven, Belgium) was used for segmenting airways in the MRI data. Replicas included all facial features and smoothed nasal airways proximal to trachea were subtracted from the face. Figure 2.1 shows smoothed nasal airways of one male (subject 3), one female (subject 5), and one of the infants (subject 2). The replicas were built in an Invision SR 3-D printer (3D Systems, Rock Hill, SC, USA) in three parts using an acrylic-build material and wax support, which was melted and removed later from the replicas by heating them to 60 °C. Some geometrical parameters of the adult subjects are given in Table 2.1.

Table 2.1 Adult subject parameters

Subject	Sex	V (mm^3)	A_s (mm^2)	L (mm)
1	M	52338	28444	234
2	F	44567	28718	241
3	M	56218	31507	274
4	F	40410	26422	231
5	F	35857	23532	210
6	M	50125	31345	269

V, volume; A_s, surface area; L, length of the airways.

To facilitate the tube connections, noses of all replicas (adults and infants) were fitted with size 1 PARI BABY^{TM} nebulizer silicone face masks (PARI, Inc. Midlothian, VA, USA). This method was chosen instead of using an exposure chamber because our preliminary experiments using an exposure chamber resulted in excessive fluctuations of concentration at the sampling point and close to the nostrils due to diffusion of particles as well as flow circulation within the chamber.

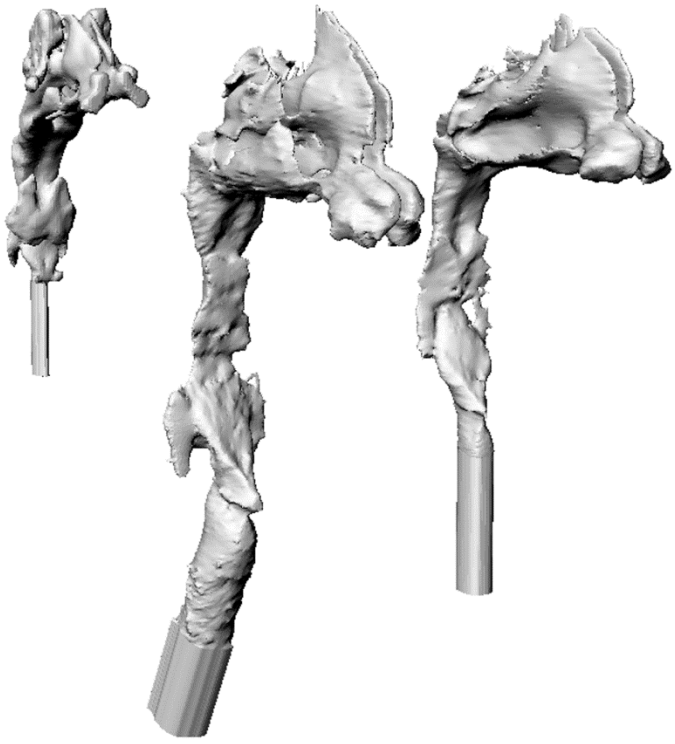

Figure 2.1 Nasal airways of one infant subject and two adult subjects (one male and one female) are shown.

Polydisperse salt particles were generated from saline solution at a solution concentration of 0.24±0.028 mg/ml using a 6-jet Collison atomizer (BGI, Inc., Waltham, MA, USA). Aerosol was passed through a silica gel diffusion dryer and subsequently passed through a Kr-85 neutralizer (Model 3054, TSI, Inc., St-Paul, MN, USA). To reduce coagulation, aerosol was then diluted upstream of the nasal replica with clean dry dilution air at a flow rate of 17 L/min (infant setup) or 31 L/min (adult setup). A mass flow meter (Model 4043, TSI, Inc., St-Paul, MN, USA) was used to measure flow rates of dilution air. Since a tidal breathing pattern was simulated, an outlet was provided to release the excess

dilution air out of the system. A Traceable Digital Hygrometer Thermometer Dew point (Fisher Scientific, USA) was used to measure the relative humidity just upstream of the nasal replica; the maximum relative humidity was 31%. Dry salt particles are achieved (complete crystallization) below a relative humidity of 40% (Orr *et al*. 1958; Tang and Murkelwitz 1984). The deposition efficiency for ultrafine particles in the size range of 13-100 nm in diameter in nasal replicas was measured using the setup illustrated in Figure 2.2. Different components of the experimental setup were all connected using Teflon tubes (TSI, Inc., St-Paul, MN, USA) and metal fittings.

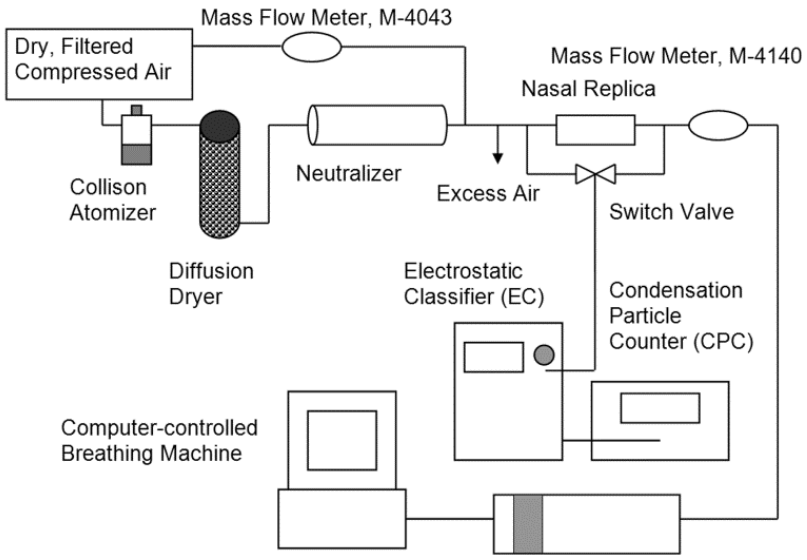

Figure 2.2 Schematic diagram of the experimental setup.

Two flow rates that were physiologically compatible with natural tidal breathing in infants were programmed and generated with an in-house breathing machine to produce a sinusoidal breathing pattern. For the present subjects,

resting tidal volumes of 30-88 mL and breathing rate of 44-34 bpm, respectively, have been considered physiologically realistic (Storey-Bishoff *et al*. 2008). A mass flow meter (Model 4140, TSI, Inc., St-Paul, MN, USA) was used for recording tidal breathing patterns. Periodic patterns were used since previous researchers have shown differences in total deposition of particles during tidal and steady flow through airway replicas at an equal average velocity (Haussermann *et al*. 2002; Shi *et al*. 2006). Only the inhalation half of the breathing pattern was used. Actual values of breaths/min and tidal volume for each test were measured by analyzing recorded flow patterns vs. time, given that the tidal volume is the area under the curve. The following measured breathing patterns were used: 42.09±0.16 breaths/min (bpm) with average flow rate 3.07±0.03 L/min, and 33.98±0.09 bpm with average flow rate 7.06±0.06 L/min, corresponding to minimum and maximum flow rates. Dividing average flow rate by twice the breaths per minute gives the tidal volume for a sinusoidal wave. To determine the effect of flow rate on deposition for three subjects (2, 6 and 10), a third flow pattern with a middling flow rate (5.34±0.25 L/min, 39.78±0.12 bpm) was also tested. Similarly, a small number of tests were done with two infant subjects (subjects 3 and 8) at two constant flow rates similar to two tested tidal flow patterns (3 and 7 L/min).

For six adult replicas, three constant flow rates of 4, 10 and 20 L/min were used to allow comparison with literature data. An additional set of experiments was performed with three adult subject replicas (subjects 1, 3 and 6) using two physiological tidal flow patterns with the average of approximately 9.7±0.03

L/min (9.6±0.05 bpm and tidal volume V_t=0.506±0.002 L) and 19.6±0.4 L/min (16.86±0.34 bpm and V_t=0.58±0.02 L) to obtain preliminary data on the difference in deposition between constant vs. tidal flow.

A scanning mobility particle sizer (Model 3936, TSI, Inc., Shoreview, MN, USA), consisting of an electrostatic classifier (EC, Model 3080, TSI, Inc., Shoreview, MN, USA) with a nano differential mobility analyzer (DMA, 3085, TSI, Inc., Shoreview, MN, USA) and a condensation particle counter (CPC, Model 3776, TSI, Inc., Shoreview, MN, USA), was used to count the particles. Deposition efficiency (η) was determined based on the number concentration before (C_{in}) and after (C_{out}) each nasal airway replica, as follows:

$$\eta = \left(\frac{C_{in} - C_{out}}{C_{in}} \right) \times 100 \tag{2.1}$$

A typical experiment consisted of two 125-second samples from each side of the replica at ten sizes of particles (13 and 20-100) at 10 nm size interval increments (20, 30 nm, etc.). Preliminary experiments showed that one minute after switching valves, the concentration was steady; therefore, a one-minute time interval occurred between the two aforementioned samples to eliminate errors due to valve switching. Each deposition data point is an average of three experiments. Error bars are not displayed because they were approximately the same size of symbols. The first set of measurements for each replica was excluded after realizing that it was higher than the other measurements due to electrostatic surface charge on the airway surfaces of replicas, which was eliminated after having enough mass deposited on those surfaces. A single CPC was used after realizing that concentration was steady during the time of each test (310 seconds)

for the selected particle sizes. Using a single CPC also eliminated any systematic error in determining the deposition efficiency. Count concentration of smaller particles (<13 nm) was too variable over the time of experiment (coefficient of variation- COV>5%) due to the low concentration of those particles coming out of the Collison atomizer; therefore, only deposition of particles larger than 13 nm was determined.

Correction was needed for multicharged particles passing through the DMA with the mobility of the singly-charged target size. For example, when the electrostatic classifier was set at 30 nm (n=1), in actuality a fraction of 43 nm (n=2) and 54 nm (n=3) particles would also be counted by the CPC. Therefore, C_{in} and C_{out} in Equation (2.1) for 30 nm particles are in fact given by:

$$C_{\text{in}} = f_{+1}N_{30} + f_{+2}N_{43} + f_{+3}N_{54} \tag{2.2}$$

$$C_{\text{out}} = P_{30}f_{+1}N_{30} + P_{43}f_{+2}N_{43} + P_{54}f_{+3}N_{54} \tag{2.3}$$

where the fraction of particles with one, two and three positive charges are f_{+1}, f_{+2} and f_{+3}, respectively. The fraction of particles that carry multiple charges (f) was estimated using the equations given by Wiedensohler (1988). Continuing with the example of 30 nm particles, penetrations of 30, 43 and 54 nm particles (P_{30}, P_{43} and P_{54}) are the parameters needing correction. Penetration curves that were obtained without corrections were used as an initial guess for penetration values. Numbers of particles (N_{30}, N_{43} and N_{54}) were calculated by considering the size distribution of the Collison atomizer and multiplying the transfer function of the DMA (Ω) by the size distribution with the mobility as its x-axis. The transfer function gives the fraction of particles with mobilities that will be included in the

sample to the CPC and is calculated according to the equation given by Wang and Flagan (1990). Corrected penetration values were obtained by matching both sides of Equation (2.3) for each subject at each flow rate; however, those corrections did not change the deposition values significantly (maximum change 0.5%). Losses of the lines were also subtracted from the deposition data.

Since pressure drop measurements are a means of indirectly validating the build procedure of the models, the pressure drop across each infant and adult replica was measured with a low range digital manometer (OMEGA HHP-103). Steady inspiratory flow rates in the ranges of 4-75 L/min and 0-16 L/min were used to obtain pressure measurements for the adult and infant replicas, respectively. The pressure drops of the connections were subtracted from the total pressure drop and the presented net values are averages of triplicate measurements.

2.3. Results and Discussion

2.3.1. Method Validation

The transnasal pressure drop measurements in our six adult replicas for inspiratory flow rates ranging from 4-75 L/min are compared to literature values in Figure 2.3. Comparison of the *in vitro* data of Cheng *et al*. (1988, 1990) and Garcia *et al.* (2009) as well as the *in vivo* measurements of pressure drop across the nasal passages and nasopharynx on human volunteers performed by Pattle (1961), Hounam *et al*. (1971) and Heyder and Rudolf (1977) shows that despite all the obvious intersubject variability, airway resistance across our adult replicas

is within the range of existing data in the literature. This gives us confidence that the methodology we have chosen for fabricating replicas is adequate.

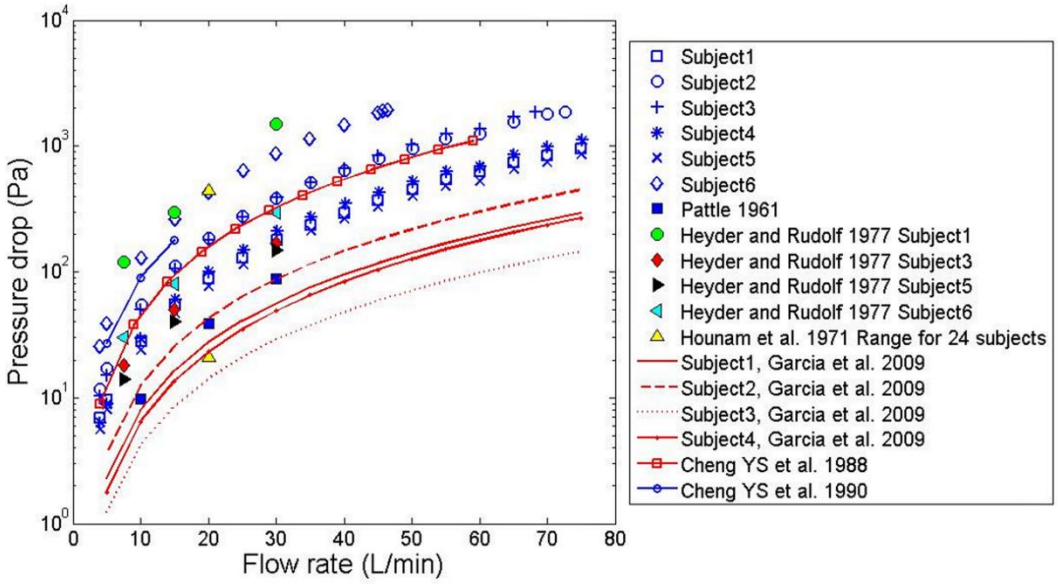

Figure 2.3 Pressure drop data points across six adult human nasal replicas as a function of inspiratory air flow rate compared with available *in vivo* and *in vitro* measurements in the literature.

Deposition in our six adult replicas is compared for a flow rate of 20 L/min with existing *in vivo* and *in vitro* data in Figure 2.4. Good agreement is seen. A paired t-test between mean deposition in six replicas vs. the mean of all previous studies at a given flow rate (4 and 10 L/min) and particle size (20, 50, and 100 nm) yielded no significant difference between our *in vitro* data and that given by these previous studies (p>0.05).

The above pressure and deposition data provides validation of our experimental method, given that no similar *in vivo* data on infants exists for validation purposes.

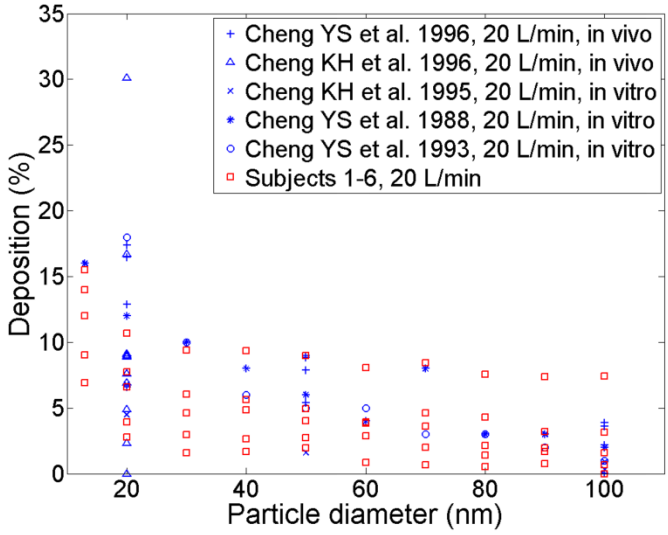

Figure 2.4 Deposition data for adults at a flow rate of 20 L/min compared to available *in vivo* and *in vitro* data.

The pressure drop data for inspiratory flow in ten infant replicas are shown in Figure 2.5. The range of *in vivo* physiologic data for upper airway resistance (ratio of pressure drop to airflow at a particular time) reported in the literature is 3.7-23.9 cm H_2O L^{-1} sec (362.85-2343.8 Pa L^{-1} sec) for Caucasian infants weighing 1.5-10.2 kg (Stocks and Godfrey 1978). The Janssens *et al*. (2001) Sophia Anatomical Infant Nose-Throat (SAINT) replica, an anatomically correct model of the upper airways of a 9-month old child, has previously been found to lie in this range. Figure 2.5 shows that our replicas have similar values.

Additional post-built validation of geometrical features of our replicas (volume, airway surface, minimum cross sectional area, and length) is given elsewhere (Storey-Bishoff *et al*. 2008).

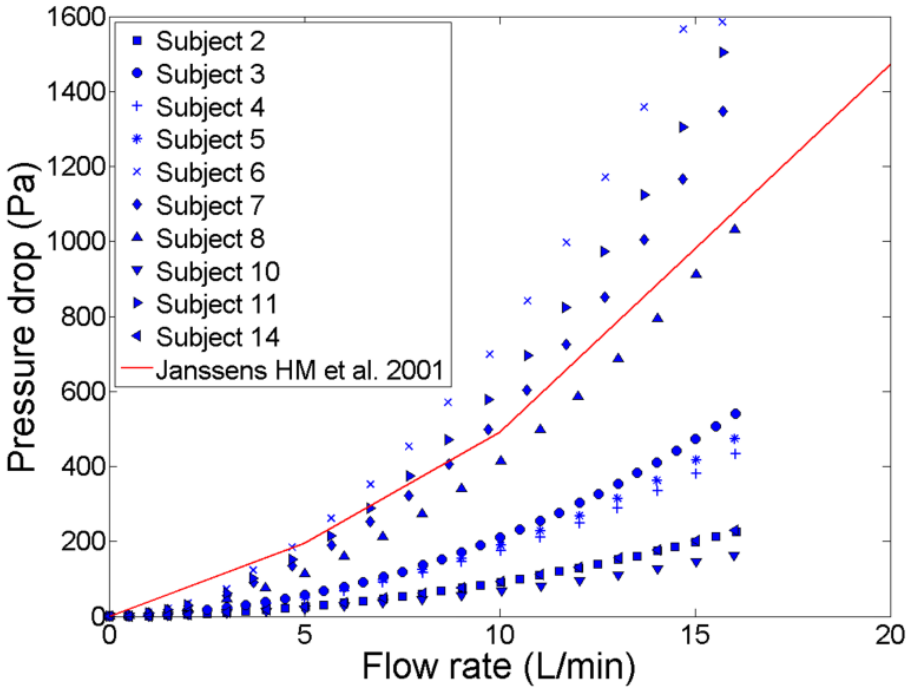

Figure 2.5 Pressure drop data for inspiratory flows in infant subjects.

2.3.2. Comparison of Infant Data with Existing Adult Correlations

Having obtained deposition measurements in our ten infant replicas, let us first examine whether this data can be predicted using existing correlations developed for adults. Table 2.2 summarizes all the available correlations that we have found in the literature for prediction of deposition of ultrafine particles in nasal airways of adults. They have been fitted to our infant data and their attributed R-squared values are given.

Table 2.2 Summary of equations in the literature for predicting deposition of ultrafine particles in nasal airways of adults and their related R^2 values when fitted to our infant data

Deposition Equation		Comments	R^2	Reference
$\eta = 1 - \exp((-16.6)D^{0.5}Q^{-0.28})$	(2.4)	Q (L/min)	0.58	Cheng (2003)
$\eta = 1 - \exp[-15.9D^{0.39}Q^{-0.28}]$	(2.5)	Q (cm^3/s)	0.32	Cheng, K. H. et al. (1996)
$\eta = 1 - \exp[-1.4\left(\frac{A_s}{A_{min}}\right)^{0.27}\left(\overline{S_f}\right)^{1.24}D^{0.39}Q^{-0.28}]$	(2.6)	Q (cm^3/s)	0.55	Cheng, K. H. et al. (1996)
$\eta = 1 - \exp\left(-11.8D^{0.5}Q^{-0.125}\right)$	(2.7)	Q (L/min)	0.55	Swift and Strong (1996)
$\eta = 1 - \exp[-12.65D^{0.5}Q^{-0.125}]$	(2.8)	Q (L/min)	0.64	Swift et al. (1992)
$\eta = 1 - \exp\left(-0.853\left(\frac{A_s}{\overline{A_c}}\right)^{0.75}\mathrm{Sc}^{-0.4}\mathrm{Re}^{-0.45}\right)$	(2.9)	$d_h = 4\overline{A_c}/\overline{Pr}$ $\mathrm{Re} = 4Q/\nu\overline{Pr}$ $\mathrm{Sc} = \upsilon/D$	0.27	Cheng, Y. S. et al. (1996)

D, diffusion coefficient (cm^2/s); *Q*, flow rate (unit is specified in each study); A_s, total surface area of the nasal airway; A_{min}, minimum cross-sectional area of nasal airway in a plane perpendicular to air flow; $\overline{S_f}$, average airway shape factor of the nasal turbinate region defined as the ratio of the airway perimeter to a reference perimeter that is the periphery of the rectangle bounding maximum horizontal and vertical boundaries of each 3 mm bilateral airway slice; $\overline{A_c}$, average cross-sectional area of nasal airway, which is calculated by dividing the volume of airways by the length of the centerline passing through the airways; d_h, hydraulic diameter for calculating Reynolds; Re, Reynolds number; Sc, Schmidt number; $\overline{Pr}$, average perimeter of the nasal airways; ν, kinematic viscosity.

Figure 2.6 compares deposition values calculated using an equation developed for adults by Swift *et al*. (1992), which gives the highest *R*-squared value when compared with our infant experimental data. Similar to Figure 2.6, we find that most of the literature equations (given in Table 2) pass through the cloud of our infant data. However, there is large intersubject variability that scatters the data and reduces the ability of any of the above equations to accurately predict deposition in a given individual.

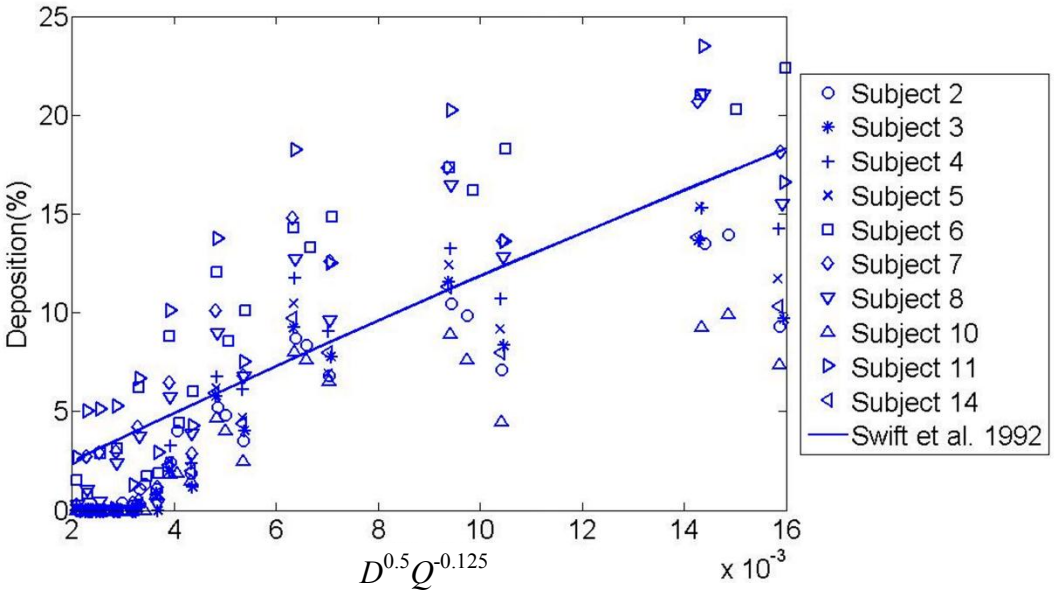

Figure 2.6 The correlation of Swift *et al*. (1992) developed for adults is shown with our infant deposition data. Error bars on our experimental data points are approximately the same size as the symbols and so are not shown.

The respiratory tract is still under development in children and the airway dimensions are a function of age (Phalen *et al*. 1985), which causes age-associated changes in nasal deposition. The effect of age on nasal deposition has

been included in the equation developed by Cheng *et al*. (1995) as given in Equation (2.10), in which parameter *a(t)* is a function of age in years as given in Equation (2.11):

$$\eta = 1 - \exp\left(-a(t)D^{0.5}Q^{-0.125}\right) \tag{2.10}$$

$$a(t) = 12.4 + \frac{12.9}{t} - \frac{2.21}{t^2} \tag{2.11}$$

Here, the diffusion coefficient (D) is in cm^2/s and Q is in L/min. Comparison of expected deposition in 5 of our infant replicas (subjects 2, 3, 4, 5, and 6) using Equations (2.10) and (2.11) is given with our measured experimental data in Figure 2.7.

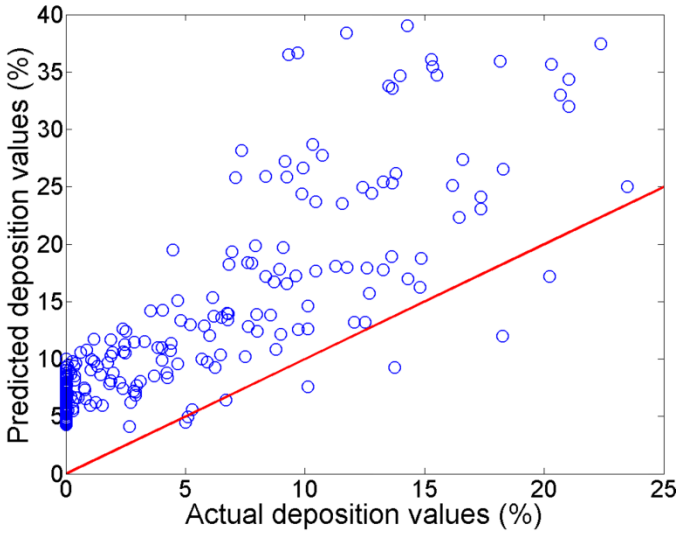

Figure 2.7 The correlation of Cheng *et al*. (1995) developed for older children (1.5-, 2.5- and 4-year-olds) is shown with infant deposition data in this study.

Previous authors provide predictions with much reduced intersubject variability by using dimensionless analysis with subject specific length scales (Storey-Bishoff *et al*. 2008; Garcia *et al*. 2009; Grgic *et al*. 2004). Developed for adults, Eqn. 2.9 includes the subject specific dimensionless parameters Sc and Re. However, it does not include a dimensionless parameter governing unsteady effects, which is reasonable for adults (Kelly *et al*. 2004; Swift and Strong 1996; Wang *et al*. 2009), but may not be reasonable in infants for particles governed by diffusion as is seen in Figure 2.8, where deposition with constant flow rate is compared to that occurring with sinusoidal tidal breathing. It is seen that deposition is higher for unsteady vs. steady flow rates. The breathing frequency in infants is much higher than adults and is apparently responsible for the increased importance of unsteadiness in infants. Haussermann *et al*. (2002) found unsteadiness to be important at high breathing frequency in adults for micron-sized particles.

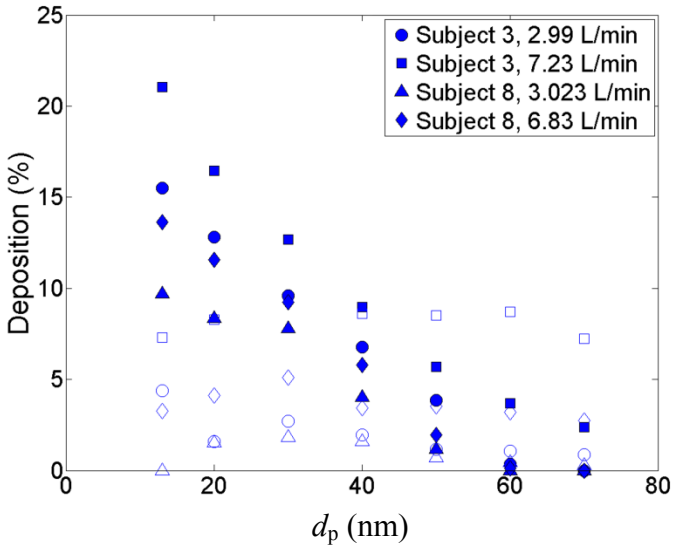

Figure 2.8 Comparison of deposition in infant replicas vs. particle diameter (d_p) using tidal breathing (solid markers) and constant flow rate (empty markers).

While the difference between steady and tidal flow deposition is noticeable in infants, this is in contrast to what we observe for adults as shown in Figure 2.9. Although our data for detailed comparison of inhalation patterns in adults is limited (since adults are not the focus of this study), careful examination of Figure 2.9 shows that in most cases tidal deposition is slightly higher than constant flow deposition. Heyder *et al*. (1982) noted enhanced deposition in adults with tidal flow patterns for micron sized particles compared to deposition using a controlled breathing pattern. However, Heyder *et al*. proposed that most of the intersubject variability was due to morphological parameters and the effect of physiological parameters was not significant in their study.

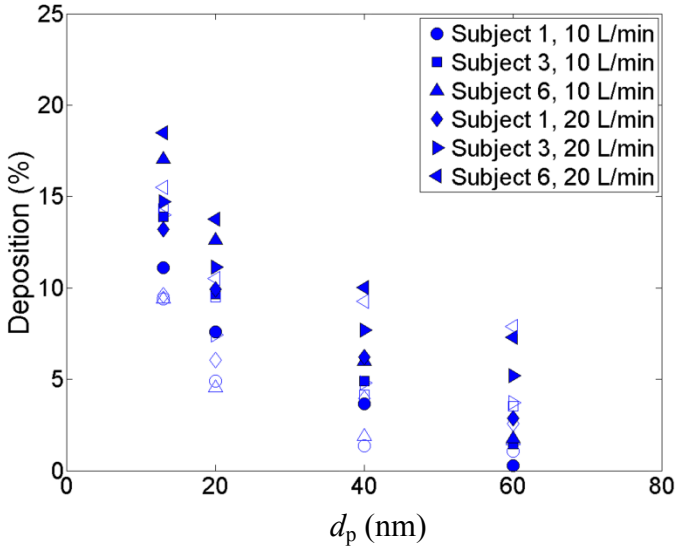

Figure 2.9 Comparison of deposition in adult replicas vs. particle diameter (d_p) using tidal breathing (solid markers) and constant flow rate (empty markers).

As will be noted later, prolonged residence in recirculation regions may play a stronger role in causing deposition in infants and may explain these differences between infant and adult deposition of ultrafine particles. In mass transport applications with large Peclet number, similar to this study, it is known that flow-assisted diffusion is present as a result of enhanced cross-stream advection due to recirculation regions and the recirculation zone resembles a well mixed region at steady-state with a resulting reduced distance for diffusive transport (Trevelyan *et al*. 2002).

2.3.3. Predictive Correlations for Infants

Given the above considerations, unsteadiness appears to be important in the deposition of ultrafine particles in infants and we therefore add the dimensionless

Womersley number, Wo (defined in Eqn. (2.15)), to the list of governing dimensionless dynamical parameters. Following Finlay and Martin (Finlay and Martin 2008), we then define the parameter X as a rational combination of the governing dimensionless parameters and determine the best fit form of X. However, it cannot be known *a priori* which characteristic diameter used in the calculation of dimensionless parameters will result in the best predictive fit. Some of the characteristic diameters that have been proposed in literature for reducing intersubject variability either in micron-sized or ultrafine range and tested in this study have been summarized in Table 2.3.

Table 2.3 Characteristic diameters that are suggested in literature and tested in this study for calculation of dimensionless parameters to reduce intersubject variability

Characteristic diameter (d_c)	Reference
V/A_s	Storey-Bishoff et al. (2008)
V/A_{min}	Storey-Bishoff et al. (2008)
L	Storey-Bishoff et al. (2008)
A_s/L	Storey-Bishoff et al. (2008)
$\sqrt{V/L}$	Grgic et al. (2004)
$\overline{A_c}/L$	This study
$\sqrt{A_{min}/\pi}$	Cheng Y. S. 2003
$(0.0181\ L_{nose}/R_{nose})^{4/19}$	Garcia et al. (2009)
$4A_n/P_n$	This study
$4\overline{A_c}/\overline{Pr}$	Cheng, Y. S. et al. (1996)

V, volume of the nasal cavity; L, length of the representative line passing through airway; L_{nose},

V, volume of the nasal cavity; L, length of the representative line passing through airway; L_{nose}, length of the nasal airways from nostrils to the end of the septum; R_{nose}, nasal resistance; A_n, surface area of nostrils; P_n, perimeter of nostrils. All the other parameters have been introduced in the caption of Table 2.2.

Further study showed that the following equation gave the best fit to our deposition data:

$$\eta = aX^2 + eX + f \tag{2.12}$$

where f is a constant and:

$$X = \mathrm{Re}^b\ \mathrm{Sc}^c\ \mathrm{Wo}^d \tag{2.13}$$

Reynolds (Re), Womersley (Wo) , and Schmidt (Sc) numbers were calculated as:

$$\mathrm{Re} = \frac{\rho Q}{d_c \mu} \tag{2.14}$$

$$\mathrm{Wo} = d_c \sqrt{2\pi f_i / \upsilon} \tag{2.15}$$

$$\mathrm{Sc} = \upsilon / D \tag{2.16}$$

d_c is the characteristic diameter for each subject. Breathing frequency (f_i) is the number of inhaled breaths per minute. Note that in mass transfer, the product of Reynolds and Schmidt numbers is considered a Sherwood number (Sh).

Using different combinations of non-dimensional numbers to define X with various choices of characteristic diameters, R-squared values were obtained for each combination and are given in Table 2.4. Table 2.4 shows that the characteristic diameter denoted in the third row from the bottom of Table 2.3, which uses the length of the nasal airway and its resistance, gives the best fit compared to other characteristic diameters.

Table 2.4 *R*-squared values of equation (2.12) fitted to infant data using different characteristic diameters

TABLE 4

R-squared values of equation (12) fitted to infant data using different characteristic diameters

Deposition Parameter (X)	$d_c=V/A_s$	$d_c=V/A_{min}$	$d_c=L$	$d_c=A_s/L$	$d_c=\sqrt{V/L}$
Sc[c]	0.70	0.70	0.70	0.70	0.70
Re[b] Sc[c]	0.77	0.78	0.72	0.73	0.75
Re[b] Sc[c] Wo[d]	0.84	0.80	0.72	0.73	0.81
Re[b] Sc[c] (d_c/d_{c_ave})[g]	0.84	0.80	0.72	0.73	0.81

Deposition Parameter (X)	$d_c=\overline{A_c}/L$	$d_c=\sqrt{A_{min}/\pi}$	$d_c=(0.0181\ L_{nose}/R_{nose})^{4/19}$	$d_c=4A_n/P_n$
Sc[c]	0.70	0.70	0.70	0.70
Re[b] Sc[c]	0.79	0.71	0.79	0.70
Re[b] Sc[c] Wo[d]	0.82	0.71	0.89	0.71
Re[b] Sc[c] (d_c/d_{c_ave})[g]	0.82	0.73	0.89	0.72

Deposition Parameter (X)	$d_c=4\overline{A_c}/\overline{Pr}$
Sc[c]	0.70
Re[b] Sc[c]	0.71
Re[b] Sc[c] Wo[d]	0.83
Re[b] Sc[c] (d_c/d_{c_ave})[g]	0.83

It can be seen that including the Womersley number also gives a better fit with a higher R-squared value. Although including the ratio of d_c/d_{c_ave}, where d_{c_ave} is the average characteristic diameter for all subjects, improves R-squared values as much as including Womersley number does, Womersley number is included in the following further exploration of the parameter X due to our observed effect of unsteady flow. Inclusion of the Womersley number may be

expected to improve the fit compared to inclusion of the ratio of characteristic diameters if the number of breaths per minute varies by a few orders of magnitude, however, such range in breathing frequency is not physiologically realisitic; therefore it has not been explored.

The values of the six constants (*a-f*) of equations 2.12 and 2.13 were obtained using least squares fitting and their values are given in Table 2.5. The exponent *b* involving Re is much smaller than the exponent *d* including Wo, indicating that breathing frequency is more important than flow rate in affecting deposition. This supports our earlier supposition that breathing frequency underlies the explanation for the importance of unsteadiness in infants.

TABLE 5

Table 2.5 Values of constants in equations (2.12) and (2.13) for four diameters with the highest R^2 values for infant data

Values of constants in equations (12) and (13) for four diameters with the highest R^2 values for infant data

Constant values	$d_c = (0.0181\ L_{nose}/R_{nose})^{4/19}$	$d_c = V/A_s$	$d_c = 4\overline{A_c}/\overline{Pr}$	$d_c = \overline{A_c}/L$
a	-4.58	-3.49	2.83	-2.14
b	0.04	0.05	0.01	0.14
c	-0.19	-0.22	-0.04	-0.32
d	-0.51	-0.59	-0.07	-0.45
e	3.51	2.59	-2.05	1.63
f	-0.20	-0.17	0.17	-0.10

Figure 2.10 shows the best fit using characteristic diameter defined as $d_c = (0.0181\ L_{nose}/R_{nose})^{4/19}$ from Equations (2.12) and (2.13).

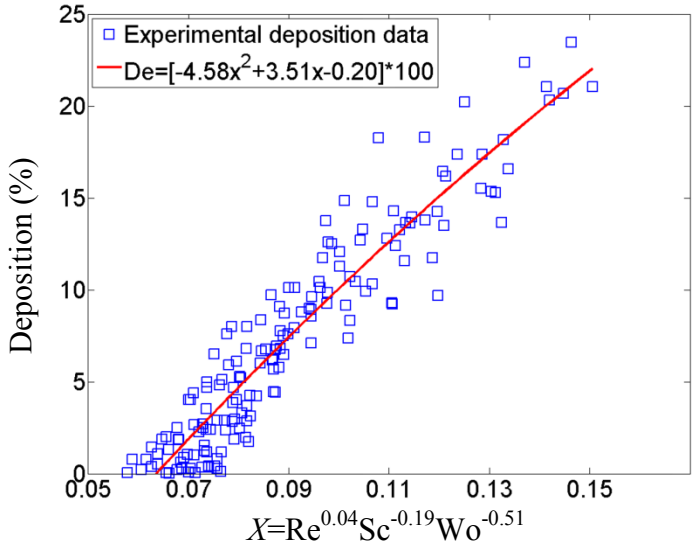

Figure 2.10 Deposition in infant replicas vs. non-dimensional deposition parameter using characteristic diameter defined as $d_c = (0.0181\ L_{nose}/R_{nose})^{4/19}$.

The characteristic diameter $d_c = (0.0181\ L_{nose}/R_{nose})^{4/19}$ was introduced by Garcia *et al*. (2009) as the best parameter for the estimation of deposition of micron-sized particles in adult nasal airways. To examine the validity of using the correlation for turbulent flow pressure drops in a pipe of diameter d and length L for nasal airways, given by (Blasius H. 1911)

$$\Delta P = 0.241 L \rho^{3/4} \mu^{1/4} d^{-19/4} Q^{1.75} \tag{2.17}$$

the value of the power of flow rate in the pressure drop- flow rate correlation was calculated by fitting the following correlation to measured pressure drop data in our infant replicas:

$$\Delta P = aQ^b \tag{2.18}$$

Values of the parameter b for infants were 1.8-2 (mean 1.91±0.06), which is close to the value of 1.75 seen in the turbulent flow pressure drop correlation for pipes (Equation (2.17)). Therefore, nasal resistance R_{nose} was calculated by fitting the following equation to our measured infant replica pressure drop data:

$$\Delta P = R_{\text{nose}} Q^{1.75} \tag{2.19}$$

A characteristic diameter attributed to R_{nose} is then calculated as follows (Garcia *et al*. 2009):

$$d_{\text{c}} = \left(0.0181 L_{\text{nose}} / R_{\text{nose}}\right)^{4/19} \tag{2.20}$$

Nasal resistance values and characteristic diameters for our infant replicas are given in Table 2.6. The values of L_{nose} (the length of the nasal airways from nostrils to the end of the septum) were determined using the electronic CAD files of the infant replicas.

Table 2.6 Nasal resistance dependent characteristic diameter of infants

Subjects	L_{nose} (mm)	$R_{nose} \times 10^{-8}$ (Pa/(m^3/sec)$^{1.75}$)	d_c (mm)
2	40.32	3.92	3.4
3	43.99	9.19	2.9
4	38.72	7.51	2.9
5	44.41	8.17	3.0
6	49.02	31.0	2.3
7	51.75	23.6	2.5
8	49.29	17.9	2.6
10	60.56	2.87	3.9
11	52.88	26.6	2.4
14	55.15	4.00	3.6

Although the diameter that includes nasal resistance (d_c = (0.0181 L_{nose}/R_{nose}) $^{4/19}$) yields the highest *R*-squared value for our infant data, other diameters ($d_c=V/A_s$, $d_c = 4\overline{A_c}/\overline{Pr}$, and $d_c = \overline{A_c}/L$) may be more convenient for use in *a priori* prediction of a deposition in a given subject. The constants used in defining the fits with those diameters are given in Table 2.5. Among $d_c=V/A_s$, $d_c = 4\overline{A_c}/\overline{Pr}$, and $d_c = \overline{A_c}/L$, if subject specific predictions are desired, both $d_c=V/A_s$ and $d_c = 4\overline{A_c}/\overline{Pr}$ require knowledge of the given subjects' airway dimensions and thus require imaging of the nasal airway. However, to quantify $d_c = \overline{A_c}/L$, acoustic rhinometry can be used to measure the volume and length of the nasal airways in a given subject. Average cross section can be calculated as volume

divided by length. Thus, while the R-squared value is not as high, $d_c = \overline{A_c}/L$ may be more convenient to use than these other diameters. The fit function using $d_c = \overline{A_c}/L$ is shown in Figure 2.11.

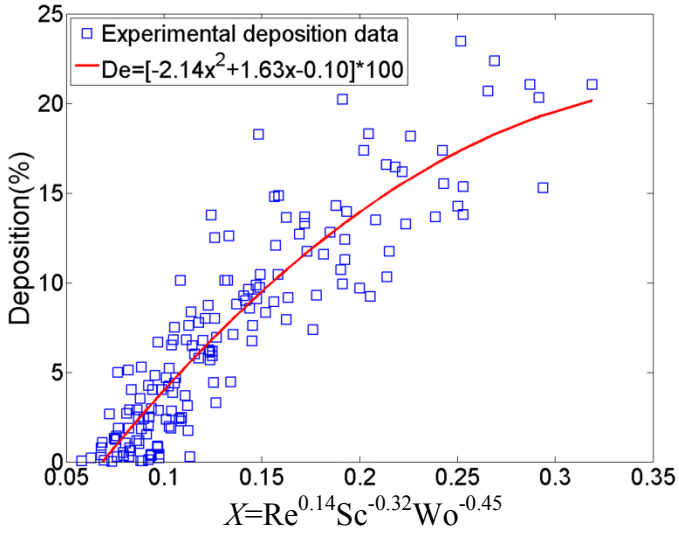

Figure 2.11 Deposition in infant replicas vs. non-dimensional deposition parameter using characteristic diameter $d_c = \overline{A_c}/L$.

2.3.4. Use of Infant Correlation for Adults

While the correlation shown in Figure 2.10 provides good prediction of our infant deposition data, it is interesting to explore whether this correlation is suitable for predicting deposition in adults. For this reason, the values of L_{nose} and R_{nose} for three adult subjects that had been tested by us with tidal breathing patterns were quantified similarly and the values of those parameters are given in Table 2.7.

Table 2.7 Nasal resistance dependent characteristic diameter of adults

Nasal resistance dependent characteristic diameter of adults

Subjects	L_{nose} (mm)	$R_{nose} \times 10^{-8}$ (Pa/(m^3/sec)$^{1.75}$)	$d_c = (0.0181\ L_{nose}/R_{nose})^{4/19}$ (mm)
1	88.4	1.1256	5.2
3	87.8	2.5474	4.4
6	81.8	5.3457	4.3

We compared our measured adult deposition data with the values obtained from Equations (2.12) and (2.13) with related Reynolds and Womersley numbers. The fit is much worse than that for infants and gives a low R-squared value (R^2= 0.37). The number of adult subjects that were tested for tidal flow rate is not appropriate for an extensive comparison of adult deposition with our curve-fit obtained for infants; however, based on our relatively small dataset, the equation predicts somewhat higher deposition values in infants compared with adults at a fixed X value. This suggests that nasal deposition increases with decreasing age within the range of experiments in this study. Cheng *et al*. (1995) also found higher nasal deposition in younger children (1.5-year-old) compared with 2.5 and 4-year-old children.

The utility of our infant correlation to predict our adult data may also be reduced by the fact that deposition in adults is largely unaffected by unsteadiness, so that the inclusion of the Womersley number is not appropriate in adults. As mentioned earlier, the higher breathing frequency in infants appears to make unsteadiness important and cause this difference between infant and adult

deposition for ultrafine particles. Unsteadiness is known to reduce entrainment of jets and affect deposition of micrometer sized particles in the larynx in adults (Grgic *et al*. 2006). From a fluid mechanics perspective, reduced entrainment in separated shear regions may enhance the size of recirculation regions in our infant replicas with unsteady flow. Increased residence time in such enhanced recirculation regions may result in enhanced diffusional deposition and could explain the importance of unsteady effects in infants that we observe. This explanation is supported by other studies where it is found that the presence of recirculation regions significantly enhances cross-stream diffusional mass transport (Trevelyan *et al*. 2002).

2.4. Conclusions

Deposition within a subject (intrasubject variability) is found to be a function of Reynolds number, Schmidt number, and Womersley number. Strong dependence of deposition on the steady vs. unsteady nature of the flow was noticed within the range of this study, with deposition using tidal breathing found to be higher than deposition using a constant flow pattern. These observations may be due to the fact that in unsteady flow patterns, a higher proportion of the flow area is part of recirculating flows having lower than average velocity. Enhanced recirculation regions would increase particle residence time and diffusional deposition. For adults, however, deposition for tidal flow was almost identical to deposition using steady flow rates. This may be due to the much lower

breathing frequency in adults, and concomitant reduction in differences in recirculating regions between steady and unsteady flow rates.

For our ten infant replicas, the best fit correlation to our data is $\eta = -4.58(\mathrm{Re}^{0.04}\,\mathrm{Sc}^{-0.2}\mathrm{Wo}^{-0.51})^2 + 3.51(\mathrm{Re}^{0.04}\,\mathrm{Sc}^{-0.2}\mathrm{Wo}^{-0.51}) - 0.20$, where $d_c = (0.0181 L_{nose}/R_{nose})^{4/19}$, introduced by Garcia *et al*. (2009) and obtained by fitting pressure-flow data with equations (2.19) and (2.20), is used as the length scale for calculating Reynolds and Womersley numbers. The average value of $d_c = (0.0181 L_{nose}/R_{nose})^{4/19}$ for our infants is 2.95 mm. This equation requires knowledge of nasal resistance to predict deposition in a given subject. A correlation that fits nearly as well, but which requires only geometric information is $\eta = -2.14(\mathrm{Re}^{0.14}\,\mathrm{Sc}^{-0.32}\mathrm{Wo}^{-0.45})^2 + 1.63(\mathrm{Re}^{0.14}\,\mathrm{Sc}^{-0.32}\mathrm{Wo}^{-0.45}) - 0.10$ where $d_c = \overline{A_c}/L$, defined as the ratio of the average cross-sectional area to a representative length of the nose from the nostrils to the trachea, is used as the length scale for calculating Reynolds and Womersley numbers. The average value of $d_c = \overline{A_c}/L$ for our infants is 1.1 mm. Use of either of these correlations allows fairly accurate subject specific predictions of ultrafine particle deposition in the nasal airways of infants. Such predictive capabilities may be useful in the development of improved health effect models for infants.

2.5 Bibliography

Arens, R., Sin, S., McDonough, J. M., Palmer, J. M., Dominguez, T., Meyer, H., Wootton, D. M., and Pack, A. I. (2005) Changes in upper airway size during tidal

breathing in children with obstructive sleep apnea syndrome. *American Journal of Respiratory and Critical Care Medicine*, 171, 1298-1304.

Blasius, H. (1911) The similarity law in friction processes. *Physikalische Zeitschrift*, 12, 1175-1177.

Cheng, Y. S., Yamada, Y., Yeh, H. C., and Swift, D. L. (1988) Diffusional deposition of ultrafine aerosols in a human nasal cast. *Journal of Aerosol Science*, 19(6), 741-751.

Cheng, Y. S., Yamada, Y., Yeh, H. C., and Swift, D. L. (1990) Deposition of ultrafine aerosols in a human oral cast. *Aerosol Science and Technology*, 12(4), 1075-1081.

Cheng, Y. S., Su, Y. F., Yeh, H. C., and Swift, D. L. (1993) Deposition of thoron progeny in human head airways. *Aerosol Science and Technology*, 18(4), 359-375.

Cheng, Y. S., Smith, S. M., Yeh, H. C., Kim, D. B., Cheng, K. H., and Swift, D. L. (1995) Deposition of ultrafine aerosols and thoron progeny in replicas of nasal airways of young children. *Aerosol Science and Technology*, 23, 541-552.

Cheng, Y. S., Yeh, H. C., Guilmette, R. A., Simpson, S. Q., Cheng, K. H., and Swift, D. L. (1996) Nasal deposition of ultrafine particles in human volunteers and its relationship to airway geometry. *Aerosol Science and Technology*, 25, 274-291.

Cheng, K. H., Cheng, Y. S., Yeh, H. C., Guilmette, R. A., Simpson, S.Q., Yang, S. Q., and Swift, D. L. (1996) *In vivo* measurements of nasal airway dimensions

and ultrafine aerosols depositing in human nasal and oral airways. *Journal of Aerosol Science*, 27(5), 785-801.

Cheng, Y. S. (2003) Aerosol deposition in the extrathoracic region. *Aerosol Science and Technology*, 37, 659-671.

Finlay, W. H. (2008) At the frontiers of understanding: inhaled aerosols in neonates. *Pediatric Research*, 64(2), 121-122.

Finlay W. H., and Martin, A. R. (2008) Recent advances in predictive understanding of respiratory tract deposition. *Journal of Aerosol Medicine Pulmonary Drug Delivery*, 21(2), 1-17.

Garcia, G. J. M., Tewksbury, E. W., Wong, B. A., and Kimbell, J. S. (2009) Interindividual variability in nasal filtration as a function of nasal cavity geometry. *Journal of Aerosol Medicine Pulmonary Drug Delivery*, 22(2), 139-155.

Gill, S., Lobenberg, R., Ku, T., Azarmi, S., Roa, W. and Prenner, E. J. (2007) Nanoparticles: characteristics, mechanisms of action and toxicity in pulmonary drug delivery- a review. *Journal of Biomedical Nanotechnology*, 3, 107-119.

Grgic, B., Finlay, W. H., Burnell, P. K. P., and Heenan, A. F. (2004) *In vitro* intersubject and intrasubject deposition measurements in realistic mouth-throat geometries. *Journal of Aerosol Science*, 35, 1025-1040.

Grgic, B., Martin, A. R., and Finlay W. H. (2006) The effect of unsteady flow rate increase on *in vitro* mouth-throat deposition of inhaled boluses. *Journal of Aerosol Science*, 37, 1222-1233.

Guilmette, R. A., Cheng, Y. S., Yeh, H. C., Swift, D. L. (1994) Deposition of 0.005-12 μm monodisperse particles in a computer-milled, MRI based nasal airway replica. *Inhalation Toxicology*, 6(s1), 395-399.

Halonen, J. I., Lanki, T., Yli-Tuomi, T., Tiittanen, P., Kulmala, M., and Pekkanen, J. (2009) Particulate air pollution and acute cardiorespiratory hospital admissions and mortality among the elderly. E*pidemiology*, 20(1), 143-153.

Haussermann, S., Bailey, A. G., Bailey, M. R., Etherington, G., and Youngman, M. (2002) The influence of breathing patterns on particle deposition in a nasal replicate cast. *Journal of Aerosol Science*, 33, 923-933.

Heyder, J., and Rudolf, G. (1977) Deposition of aerosol particles in the human nose. In: Walton, W. H., editor. *Inhaled Particles* IV, Pergamon Press; Oxford, UK, 107-126.

Heyder, J., Gebhart, J., Stahlhofen, W., and Stuck, B. (1982) Biological variability of particle deposition in the human respiratory tract during controlled and spontaneous mouth-breathing. *Annals of Occupational Hygiene*, 26 (1-4), 137-147.

Hounam, R. F., Black, A., and Walsh, M. (1971) The deposition of aerosol particles in the nasopharyngeal region of the human respiratory tract. *Journal of Aerosol Science*, 2, 47-61.

Janssens, H. M., De Jongste, J. C., Fokkens, W. J., Robben, S. G. F., Wouters, K., and Tiddens, H. A. W. M. (2001) The Sophia anatomical infant nose-throat (Saint) model: a valuable tool to study aerosol deposition in infants. *Journal of Aerosol Medicine*, 14(4), 433-441.

Kelly, J. T., Asgharian, B., Kimbell, J. S., Wong, B. (2004) Particle deposition in human nasal airway replicas manufactured by different methods. Part II: Ultrafine particles, *Aerosol Science and Technology*, 38, 1072-1079.

Kreyling, W. G., Semmler-Behnke, M., and Moller, W. (2006). Ultrafine particle-lung interactions: does size matter? *Journal of Aerosol Medicine*, 19, 74-83.

Martonen, T. B., and Zhang, Z. (1992) Comments on recent data for particle deposition in human nasal passages. *Journal of Aerosol Science*, 23(6), 667-674.

Minocchieri, S., Burren, J. M., Bachmann, M. A., Stern, G., Wildhaber, J., Buob, S., Schindel, R., Kraemer, R., Frey, U. P., Nelle, M. (2008) Development of the premature neonate for the study of aerosol delivery. *Pediatric Research*, 64(2), 141-146.

National research council (NRC) (1988). Health risks of radon and other internally deposited alpha emitters. Committee on the biological effects of ionizing radiations, National Academy Press, Washington, DC.

Oberdorster, G., Sharp, Z., Atudorei, V., Elder, A., Gelein, R., Kreyling, W., Cox. C. (2004) Translocation of inhaled ultrafine particles to the brain. *Inhalation Toxicology*, 16, 437-445.

Orr, C., Hurd, F. K., and Corbett, W. J. (1958) Aerosol size and relative humidity. *Journal of Colloid Science*, 13, 472-482.

Park, S. H., Kim, H. O., Han, Y. T., Kwon, S. B., and Lee, K. W. (2001) Wall loss rate of polydispersed aerosols. *Aerosol Science and Technology*, 35, 710-717.

Pattle, R. E. (1961) The retention of gases and particles in the human nose. In: Davies C. N., editor. *Inhaled Particles and Vapors*, Pergamon Press; New York, US, 302-309.

Phalen, R. F., Oldham, M. J., Beaucage, C. B., Crocker, T. T., Mortensen, J. D. (1985) Postnatal enlargement of human tracheobronchial airways and implications for particle deposition. *Anatomical Record*, 212, 368-380.

Polgar, G., Kong, G. P. (1965) The nasal resistance of newborn infants. *Journal of Pediatrics*, 67, 557-567.

Schlichting, H. (1968) Boundary layer theory (Translated by Kestin, J.) McGraw-Hill, Stanford.

Schuepp, K. G., Jauernig, J., Janssens, H. M., Tiddens, H. A., Straub, D. A., Stangl, R., Keller, M., and Wildhaber, J. H. (2005) *In vitro* determination of the optimal particle size for nebulized aerosol delivery to infants. *Journal of Aerosol Medicine*, 18, 225-235.

Shi, H., Kleinstreuer, C., Zhang, Z. (2006) Laminar airflow and nanoparticle or vapor deposition in a human nasal cavity model. *Journal of Biomechanical Engineering*, 128, 697-706.

Stocks, J., Godfrey, S. (1978) Nasal resistance during infancy. *Respiratory Physiology*, 34, 233-246.

Storey-Bishoff, J., Noga, M., and Finlay, W. H. (2008). Deposition of micrometer-sized aerosol particles in infant nasal airway replicas. *Journal of Aerosol Science*, 39, 1055-1065.

Swift, D. L., Cheng, Y. S., Su, Y. F., and Yeh, H. C. (1990) In Indoor radon and lung cancer: reality and myth? (F. Cross, eds.). 29th Hanford symposium on health and the environment, Richland, Washington, p.213.

Swift, D. L. (1991) Inspiratory inertial deposition of aerosols in human nasal airway replicate casts: implications for the proposed NCRP lung model. *Radiation Protection Dosimetry*, 38, 29-34.

Swift, D. L., Montassier, N., Hopke, P. K., Kim, K. H., Cheng, Y. S., Su, Y. F., Yeh, H. C., and Strong, J. C. (1992) Inspiratory deposition of ultrafine particles in human nasal replicate cast. *Journal of Aerosol Science*, 23(1), 65-72.

Swift, D. L., and Strong, J. C. (1996) Nasal deposition of ultrafine 218Po aerosols in human subjects. *Journal of Aerosol Science*, 27(7), 1125-1132.

Tang, I. N., and Murkelwitz, H. R. (1984) An Investigation of Solute Nucleation in Levitated Solution Droplets. *Journal of Colloid and Interface Science*, 98(2), 430-438.

Trevelyan P.M.J., Kalliadasis, S., Merkin, J. H., and Scott, S. K. (2002) Mass-transport enhancement in regions bounded by rigid walls. *Journal of Engineering Mathematics*, 42, 45-64.

Van Woensel, J. B. M., Van Aalderen, W. M. C., Kimpen, J. L. L. (2003). Viral lower respiratory tract infection in infants and young children. *British Medical Journal*, 327, 36-40.

Vincent, J. H. (2005) Health-related aerosol measurement: a review of existing sampling criteria and proposals for new ones. *Journal of Environmental Monitoring*, 7, 1037-1053.

Wang, S. C., and Flagan, R. C. (1990) Scanning electrical mobility spectrometer. *Aerosol Science and Technology*, 13(2), 230-240.

Wang, S. M., Inthavong, K., Wen, J., Tu, J. Y., and Xue, C. L. (2009) Comparison of micron- and nanoparticle deposition patterns in a realistic human nasal cavity. *Respiratory Physiology and Neurobiology*, 166, 142-151.

Wiedensohler, A. (1988) An approximation of the bipolar charge distribution for particles in the submicron size range. *Journal of Aerosol Science*, 19(3), 387-389.

Xi, J., Longest, P. W. (2008). Effects of oral airway geometry characteristics on the diffusional deposition of inhaled nanoparticles. *Journal of Biomechanical Engineering*, 130, 011008:1-16.

Xi, J., and Longest, P. W. (2008) Numerical predictions of submicrometer aerosol deposition in the nasal cavity using a novel drift flux approach. *International Journal of Heat and Mass Transfer*, 51, 5562-5577.

Yamada, Y., Cheng, Y. S., Yeh, H. C., and Swift, D. L. (1988) Inspiratory and expiratory deposition of ultrafine particles in a human nasal cast. *Inhalation Toxicology*, Premier Issue 1:1-11.

Yu, G., Zhang, Z., Lessman, R. (1998) Fluid flow and particle deposition in the human upper respiratory system. *Aerosol Science and Technology*, 28, 146-158.

Zamankhan, P., Ahmadi, G., Wang, Z., Hopke, P.H., Cheng, Y.S., Su, W. C., Leonard, D. (2006) Airflow and deposition of nano-particles in a human nasal cavity. *Aerosol Science and Technology*, 40, 463-476.

CHAPTER 3 : *IN VITRO* DEPOSITION MEASUREMENT OF INHALED MICROMETER-SIZED PARTICLES IN EXTRATHORACIC AIRWAYS OF CHILDREN AND ADOLESCENTS DURING NOSE BREATHING[2]

A very similar version of this chapter has been published as:

Golshahi, L., Noga, M. L., Thompson, R. B., and Finlay, W. H. (2011). *In vitro* deposition measurement of inhaled micrometer-sized particles in extrathoracic airways of children and adolescents during nose breathing. *Journal of Aerosol Science*, 42(7), 474-488.

3.1 Introduction

Exposure to toxic aerosols in working and living environments causes certain health related problems depending on several parameters such as the size of inhaled particles, the region of respiratory tract deposition, breathing rate, type of breathing (oral vs. nasal), and anatomical features of airways (U.S. EPA 1994; Ginsberg *et al*. 2008). Environmental standards were developed to regulate health related risks once the size dependency of deposition in the respiratory tract became apparent (Vincent 2005). However, risk assessment methods have focused on adults, with children addressed typically by extrapolation, despite behavioral and physiological differences between adults and children, such as spending more time playing outdoors and greater ventilation rate per body weight and lung surface area (Ginsberg *et al*. 2008). As a result of such extrapolations, age-specific uncertainties exist in particulate deposition prediction using current

[2] Reproduced with permission from Elsevier, Copyright 2011.

exposure models such as the ICRP human respiratory tract model (ICRP 1994; Harvey and Hamby 2002). The uncertainty in regional deposition in airways (extrathoracic, tracheobronchial, and alveolar), which is dependent upon age, sex, and breathing pattern, contribute to total uncertainty in inhalation dose estimates (Harvey and Hamby 2002); thus, focusing on decreasing uncertainties in each region solidifies our understandings of exposure to unwanted aerosol and can also be used to optimize pharmaceutical aerosol delivery via face masks.

Nasal breathing is the preferred mode of breathing at rest among all ages and the contribution of nasal breathing is also significant at higher activity levels compared to oral breathing (Bennett *et al.* 2008). Nasal airways filter inhaled aerosols on their way to the lungs; however, local deposition in nasal airways may cause allergic responses and cancers due to accumulation with time (Cheng 2003). Moreover, extrathoracic deposition of micrometer-sized pharmaceutical aerosols from inhalers and nasal sprays determines the efficiency of drug delivery. Hence, improved protection of children and enhanced drug delivery via nasal inhalers and face masks requires knowledge of the deposition of inhaled micrometer-sized aerosols. Such aerosols are ubiquitous in the environment as allergens and toxicants, and on the other hand therapeutic particles.

Despite numerous *in vivo* (Landahl and Black 1947; Landahl and Tracewell 1949; Pattle 1961; Hounam *et al.* 1969, 1971; Lippmann 1970; Giacomelli-Maltoni *et al.* 1972; Heyder and Rudolf 1977; Heyder *et al.* 1986; Kesavanathan *et al.* 1998; Kesavanathan and Swift 1998; Keck *et al.* 2000; Rasmussen *et al.* 1990, 2000;Wiesmiller *et al*. 2003; Bennett and Zeman 2005),

in vitro (Itoh *et al.* 1985; Swift 1991; Guilmette *et al.* 1994; Swift and Kesavanathan 1996; Yeh *et al.* 1997; Zwartz and Guilmette 2001; Kelly *et al.* 2004, 2005; Dai *et al.* 2007; Garcia *et al.* 2009), computational fluid dynamics (CFD) (Kimbell 2006; Liu *et al.* 2007, 2009, 2010; Shi *et al.* 2007; Wang *et al.* 2009), and theoretical modeling (Scott *et al.* 1978; Yu *et al.* 1981; Cheng *et al.* 1991) studies on deposition of micrometer-sized particles that give correlations including airway dimensions and flow patterns to predict deposition of micrometer-sized particles in nasal airways of adults, only a few studies have focused on children. Two studies involving children (Becquemin *et al.* 1991; Bennett *et al.* 2008) (one for 5.5-15 year olds and the other for 6-10 year olds) included only a few monodisperse particle sizes and we are not aware of any empirical nasal correlation including geometry and breathing pattern of children based on the measured deposition data. Furthermore, existing results are inconsistent since some report higher deposition in nasal airways of children (Phalen *et al.* 1989) while others report lower deposition compared to adults (Becquemin *et al.* 1991; Bennett *et al.* 2008). In order to address such uncertainties and fill the available knowledge gaps, we have performed an *in vitro* study characterizing deposition of micrometer-sized particles in multiple nasal airway replicas of school-aged children and adolescents (4-14 years old). Considering compliance related and relevant ethical issues in pediatric *in vivo* deposition measurements, and the existence of well validated *in vitro* deposition measurement methods for adults, such *in vitro* methodologies are attractive. Previously, a study focusing on deposition of micrometer-sized particles in nasal

airways of infants has been presented by our group (Storey-Bishoff *et al.* 2008). In addition, a study by Swift (1991) used a cast of a six-week old infant and studies using Sophia Anatomical Infant Nose-Throat (SAINT) replica used an anatomical model of the nasal airways of a 9-month-old girl (Janssens *et al.* 2001). This manuscript extends the aforementioned work with measurements of deposition of micrometer-sized particles (0.5-5.3 μm) in replicas of older children (4-14 years old) to develop correlations including geometric dimensions of airways and breathing patterns as a predictive tool for future potential improvements in environmental and pharmaceutical standards.

3.2 Experimental Methods

We started our experimental procedure by choosing five replicas of adults (three males and two females) including the face (from chin to forehead including both cheeks), nostrils and nasal airways to the level of upper trachea of those individuals that were used by us in recent work on deposition of nanoparticles in nasal airways of infants (Golshahi *et al.* 2010). In brief, MRI images of ten adults were obtained under the approval of the University of Alberta Health Research Ethics Board and the regions of interest were identified in those images based on grayscale level using the Mimics software package (Materialise, Ann Arbor, MI). A rapid prototyping machine (Invision SR 3-D printer, 3D Systems, Rock Hill, SC, USA) was used for building the processed 3D computer models with natural color acrylic plastic build material and wax as the support. We measured the pressure drops of replicas using a low range digital manometer (OMEGA HHP-

103) at constant flow in the range of 4-75 L/min. Afterwards, we chose five of the ten adult replicas, two at the minimum, two in the middle and one with the maximum pressure drop to cover the full range of deposition values for comparison with available *in vivo* data in adults. The reasoning for this type of selection relied upon our previous experiments indicating strong correlations between pressure drop and deposition among infants (Storey-Bishoff *et al.* 2008) and similarly for adults according to the literature (Garcia *et al.* 2009). It should be noted that *in vivo* data do not include the larynx and nasopharynx but the nasopharynx and the larynx of our adult replicas were built as a separate piece, which allowed us to exclude the pressure drop of those regions from the total pressure drop before comparison with the *in vivo* pressure drop data. Some geometrical parameters of those adult subjects are given in Table 3.1.

Table 3.1 Geometrical parameters including volume (V), surface area (A_s) and path length (L) of the five nasal replicas of adults used for comparison with *in vivo* data given in the literature

Subject	Sex	V (mm^3)	L (mm)	A_s (mm^2)
2	F	44567	241	28718
5	F	35857	210	23532
6	M	50125	269	31345
8	M	47264	223	28936
9	M	45267	239	25086

A similar build procedure was followed for building replicas of thirteen healthy children and one with congested airways in the age range of 4-14 years,

including both males and females. However, instead of MRI we used CT images of the children for creating the 3D models of their airways, illustrated in Figure 3.1.

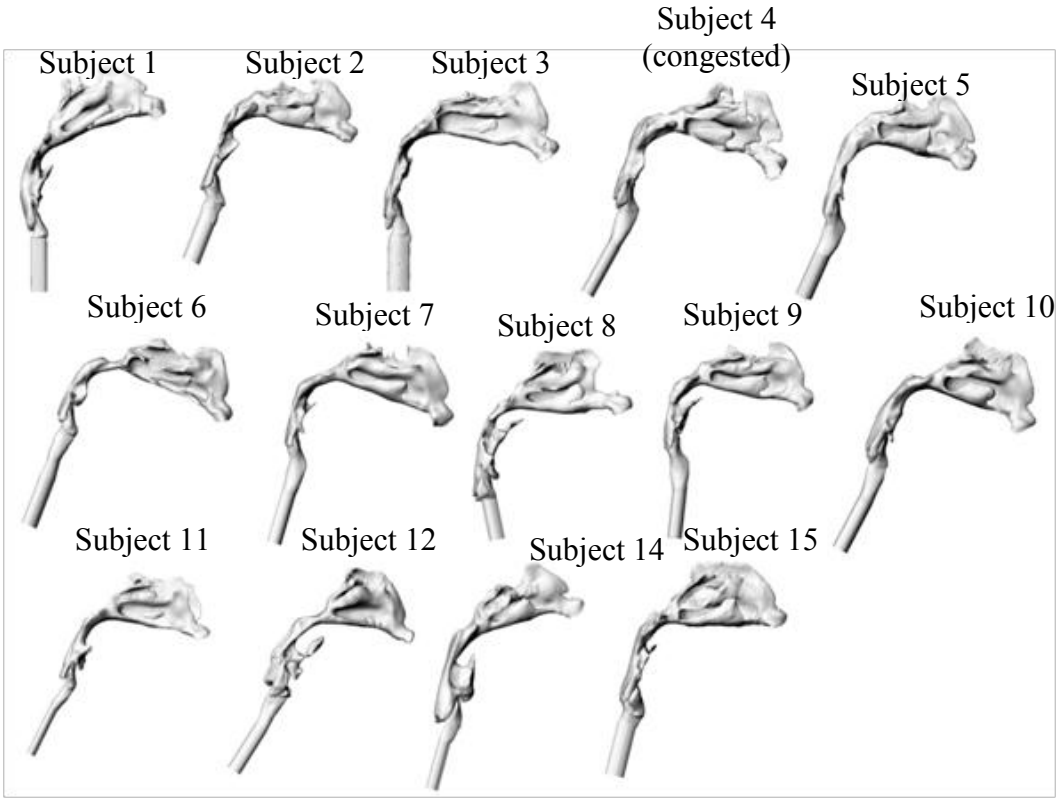

Figure 3.1 Fourteen nasal airways of children 4-14 years old. The subjects are arranged based on their numerical label from left to right on each row (subject 1 is the top left airway).

The imaging mode was helical with reconstructed slices at the axial thickness ranging from 0.6 to 1.25 mm and in plane resolution ranging from 266 to 430 μm. More details on building replicas using CT images and comparison of

the post-built scans with the original scans have previously been given by our group (Storey-Bishoff *et al.* 2008). In this study we visually inspected post-build CT scans of our replicas to ensure the critical geometries of the airways match the original scans and no blocked sections were apparent. An extension of 3 mm was added beyond the trachea to each nasal replica by extruding the most distal cross section for easier connection to downstream tubing.

We measured transnasal pressure drops using the same digital manometer that we used for the adult replicas (OMEGA HHP-103) at constant flow in the range of 5-45 L/min for all replicas of children to compare to available *in vivo* data as a tool for validating our build procedure and subject selection. Similar to adult replicas, we had the nasopharynx and the larynx of our children replicas built as a separate piece, which gave us the opportunity to subtract the pressure drop in those regions from the total pressure drop of the replica before comparison with the *in vivo* data. Subject parameters including volume, length, surface area, minimum cross section of the airways, height and width of their nostrils (used for calculating ellipticity (E), i.e. the nostril length to width ratio according to the literature (Kesavanathan *et al.* 1998)) are given in Table 3.2.

Table 3.2 Child subject parameters. V is the volume of airway, A_s is the surface area of the airway lumen, L_{nose} is the length of nasal cavity to the end of septum, L_t is the length of the remaining part of the nasal airway (oropharynx) to the level of upper trachea, A_{min} is the minimum cross section of the airway measured for each cross section at 3 mm intervals perpendicular to the possible streamline of

air going through the nasal airway, $P_{nostril}$ is the perimeter of nostrils, N_l is the length of nostril (larger dimension of an ellipse) and N_w is the width (smaller dimension) of nostrils.

Child Subject Number	Age (yr)	Sex	V (mm^3)	A_s (mm^2)	L_{nose} (mm)	L_t (mm)	Bilateral A_{min} (mm^2)	$P_{nostril}$ Left, right (mm)	N_l Left, right (mm)	N_w Left, right (mm)
1	4	F	17944.6	12776.5	78.1	86.1	63.9	21.6, 24.6	9.2,10.2	4.1,4.8
2	12	F	41638.1	22240.0	81.9	146.8	155.1	34.5, 38.7	13.1,13.5	6.5,7.4
3	12	M	27348.8	19459.1	79.9	118.5	114.8	36.7, 40.1	15.4,16.9	4.8,6.3
4	6	M	26296.3	17330.0	74.2	130.6	47.6	34.4, 35.2	13.1,15.2	8.1,4.9
5	14	M	39530.3	22585.4	77.0	140.7	114.3	43.6, 41.8	17.6,17.4	8.2,6.9
6	6	F	22755.1	16277.1	77.4	135.1	113.4	31.4, 33.1	11.4,11.5	5.7,6.4
7	8	M	22411.8	16999.0	80.7	133.2	91.1	28.6, 31.6	11.5,13.6	3.9,3.1
8	13	M	41937.8	24726.2	90.6	126.0	106.3	40.9, 42.6	17.2,17.6	6.4,7.1
9	10	F	32818.8	19864.0	82.0	126.4	167.0	37.2, 37.6	13.4,14.5	7.2,7.8
10	6	M	22844.9	17596.8	71.9	126.0	78.7	35.2, 34.7	14.6,13.9	6.4,6.0
11	4	M	13620.0	11934.4	66.9	110.8	66.6	24.9, 25.2	9.9,9.3	4.3,5.6
12	6	F	26664.1	16195.2	64.7	128.8	90.5	27.8, 26.5	9.2,9.3	6.3,5.4
14	6	M	23784.4	14871.5	68.8	119.0	60.4	31.4, 29.7	13.0,11.7	5.2,5.3
15	9	M	23391.0	20694.1	76.6	115.0	104.2	33.2, 33.8	12.5,13.3	5.4,4.9

Figure 3.2 shows a schematic diagram of the experimental setup that we used for measuring deposition. The replicas were placed in an exposure chamber made from transparent acrylic plastic that has been designed and built in-house. We selected its dimensions according to calculations given for dynamic (with airflow) inhalation exposure systems with the goal of reaching theoretical equilibrium concentrations across the box within a reasonable time (max. 42 min) considering the chamber volume and airflow (Dorato and Wolff 1991). The box is 0.6 m × 0.6 m × 0.6 m and its dimensions correspond approximately to a quarter scale residential room, which is a manageable size to work with. It is small enough to reach equilibrium quickly and large enough to simulate particle behavior in rooms (Thatcher *et al.* 1996). It has two parts, one for mixing (with a height of 10 cm) including one aerosol inlet, two dilution air inlets and a mixing fan while the other section is for exposure (45 cm high). The two sections are

separated by an aluminum hexagonal mesh honeycomb (Plascore, Zeeland, MI, USA) with a thickness of 5 cm with the hexagonal cells having a width of 6 mm and a length of 7 mm to act as a flow straightener after the mixing section. This divider keeps the distribution in the exposure part homogeneous and unaffected by the mixing. Polydisperse sunflower oil particles with a size distribution having a count median aerodynamic diameter (CMAD) of 0.4 μm and geometric standard deviation (GSD) of 3.1 were generated using a Collison atomizer (BGI, Inc., Waltham, MA, USA) and were directed into the box. Two dilution air inlets were left open to allow enough air for the tidal flow patterns that were generated by a computer controlled piston-type breathing machine (Pulmonary Waveform Generator, model: PWG S/N904, MH Custom Design & Mfg. LC, Midvale, Utah, USA) at inhalation mode only by using a one way valve to release the exhalation section of the respiratory cycle.

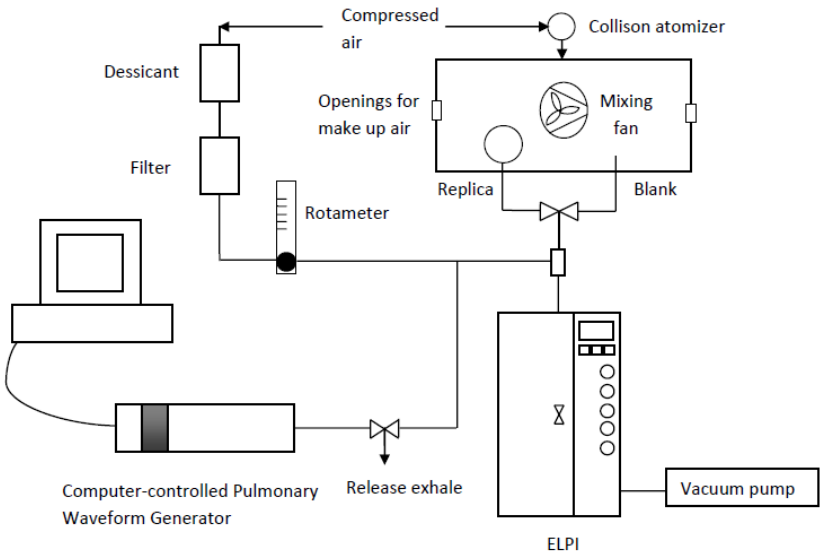

Figure 3.2 Schematic diagram of the experimental setup for measuring deposition of particles in nasal airways of adults and children.

Four types of sinusoidal physiological breathing patterns for the children at the two age groups of 5.5-12 and 12-15 years old at two different levels of activity (i.e. at rest and moderate exercise) were generated using the breathing machine according to the data given in the literature (Becquemin *et al.* 1991; Bennett *et al.* 2008). The tidal volume (V_t) and breathing frequency for each simulated subject were measured based on recorded flow using a digital mass flow meter (Model 4043, TSI, Inc., St.Paul, MN, USA) downstream of each replica individually when the atomizer was not on and there was no aerosol in the box. On average the following breathing patterns were used: 1) 22.6± 0.07 breaths/min (bpm) and tidal volume V_t =0.215±0.017 L, 2) 17.7± 0.07 bpm and tidal volume V_t =0.360±0.031 L, 3) 29.4± 0.16 bpm and tidal volume V_t =0.313±0.034 L, and 4) 24.6± 0.15 bpm and tidal volume V_t =0.498±0.058 L.

In the same setup, deposition of micrometer-sized particles in our five adult replicas was measured while a tidal flow pattern was passed through the replicas. For the adult replicas, the tidal volume and breathing frequency were determined using the recorded breathing patterns downstream of each replica. Average tidal volume for the adult replicas was 0.385±0.009 L and average breathing frequency was 14.8±0.045 bpm.

Samples were taken from the box using a tube with no replica and alternatively using a tube that was connected to the replica. A gate valve was used for switching the sampling line between the two lines at one minute intervals with a one minute stabilizing time after each switch used to exclude the effect of the valve on the sampled concentration after switching the valve. Each single test was

5 minutes: one minute from the blank line, one minute stabilizing time, one minute from the replica line, one minute stabilizing and a second one minute sample from the blank line. It should be noted that prior to each set of experiments with a new replica the uniformity of the concentration between the two points in the chamber were checked: one at the nostrils and one at the point where the sample was taken with the blank line. Also, the stability of the atomizer's output was examined for each experiment and no drift was noticed within the time of each experiment (i.e. 5 minutes). The samples were drawn into a manifold where an inlet of filtered dried dilution air on the side provided the additional flow needed for the Electrical Low Pressure Impactor (ELPI) (DEKATI, Tampere, Finland), followed by an outlet vertically down to the ELPI. The ELPI was used for size and concentration measurements. The amount of make up air for the ELPI (approx. 30 L/min, controlled by keeping a rotameter at a certain reading that was calibrated using Model 4043 TSI mass flow meter) was adjusted by checking that zero flow occurred through the box when the breathing machine was off. There was a three way connection on the way to breathing machine with one limb including the dilution line providing the sampling flow to ELPI, one limb to the breathing machine and one limb to the manifold upstream of the ELPI unit. Average number concentration of the blank line (C_1) and replica line (C_2) were obtained using the concentration profiles recorded at 40,000 fA with the application of ELPIVI 4.0 software including corrections for diffusion and particle bounce provided by Dekati Ltd. (Tampere, Finland). Deposition in the replicas for particles smaller than 0.5 μm in diameter, as far as diffusion was

not their dominant deposition mechanism, was close to zero and the number of particles larger than 5.3 μm was not large enough to allow meaningful data analysis; thus, we only used the concentration data for the ELPI stages with aerodynamic cut sizes within 0.5- 5.3 μm.

Due to additional flow resistance in the replica, corrections have been made to the particle counts measured via the blank line by multiplying the average concentration of samples taken via the blank line (C_1) by a correction factor to correct for the difference between the particle count through the blank line and the particle count of the sample that actually goes through the nostrils. The correction factor was calculated for each subject and flow rate separately by dividing the measured tidal volume of each subject at a given flow rate with the sample line by the measured tidal volume with the blank line at the same flow rate. Deposition efficiency (η) (equivalent to 1-penetration) was then determined using the corrected C_1 and C_2, as follows:

$$\eta = \frac{C_1 - C_2}{C_1} \times 100 \tag{3.1}$$

Five repetitions of each experiment have been used for each data point given in the results. All the curve fits were done based on least squares using functions available in the statistical toolbox of MATLAB. Student t-tests were used to determine significance with α=0.05.

3.3. Results and Discussion

Before we present our data, it is useful to first provide an outline of what follows. We begin by first comparing transnasal pressure drops of our replicas with *in vivo* pressure drop data available for both adults and children, in order to validate the build procedure we followed for making our replicas, since a direct relation between deposition and pressure drop is proposed in an *in vivo* study with adult subjects by Hounam *et al*. (1971). Next, due to the scarcity of *in vivo* data for children, we will compare deposition in our adult replicas with the *in vivo* data available for adults in order to assure ourselves of the close proximity of our *in vitro* data measurement with the *in vivo* measurements. Furthermore, we will compare the few *in vivo* deposition datapoints for children that are available for limited particle sizes with our systematically obtained *in vitro* data with children replicas. Next, we will initially examine the possibility of reducing intersubject variability with the application of dimensional deposition parameters that have previously been proposed by other researchers such as impaction parameter ($d_a^2 Q$) and a deposition parameter that includes transnasal pressure drop ($d_a^2 \Delta p$). Subsequently, we examine possible non-dimensionalized correlations that can be used for predicting deposition of aerosols with different particle sizes inhaled by children during different activity levels in a more general setting. This includes exploration of the applicability of multiple characteristic diameters, on the basis of anatomical dimensions of our replicas, in an equation that includes theoretically relevant non-dimensional numbers such as Reynolds and Stokes numbers. To emphasize that our proposed dimensionless correlation can only be

used to predict average amount of particle deposition in an anatomically normal population, we will look at a single anatomically abnormal replica. Finally, we will compare deposition within different age groups (i.e. infants, children, and adults).

3.3.1. Method Validation

3.3. 1.1. Transnasal Pressure Drop Values

The transnasal pressure drop data measured for our adult replicas (i.e. excluding the larynx and nasopharynx) were compared with *in vivo* and *in vitro* data given in the literature. The transnasal pressure drop for 24 subjects is given in an *in vivo* study by Hounam (1971) in the range 0.021-0.447 kPa at 20 L/min. At the same flow rate (i.e. 20 L/min) the range of pressure drop in an *in vitro* study by Garcia *et al.* (2009) is given in the range of 14-43 Pa for four healthy adults and for our adult replicas at 20 L/min the transnasal pressure drop (excluding the larynx and pharynx) is 0.028-0.042 kPa, which is in the range of the aforementioned studies. From the ten adult replicas, five subjects were selected for deposition measurements in order to span the range of pressure drop, as noted earlier.

Transnasal pressure drop across our children replicas (excluding the larynx and pharynx) were compared with *in vivo* data given by Becquemin *et al.* (1991), which is in the range of 0.012-0.449 (mean=0.105, stdev=0.115) kPa (at rest) to 0.076-1.097 (mean=0.256, stdev=0.306) (at moderate exercise) kPa for the range of flow rate that was in our interest. Our data approximately lie within the

range of the *in vivo* data and were 0.026-0.074 kPa (at rest) and 0.052-0.154 kPa (at moderate exercise).

3.3.1.2. Nasal Deposition in Adult Replicas

Deposition in our five adult replicas is compared with data in the literature in Figure 3.3. Standard deviations are given as error bars. Despite differences in the methodologies used to obtain the available *in vivo* data and significant scatter and intersubject variability in the *in vivo* data, deposition in our replicas lies within the range of *in vivo* data. This gives us confidence that our methodology should be acceptable for use in measuring deposition in children's replicas.

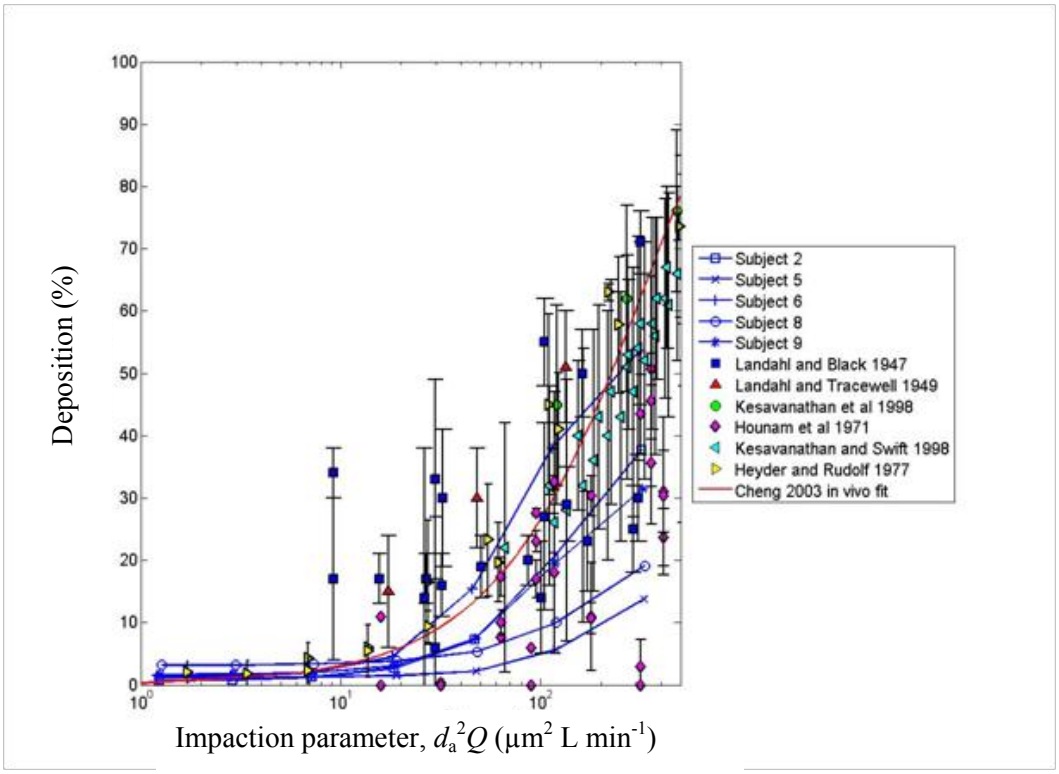

Figure 3.3 Deposition in our five adult replicas (subjects 2, 5, 6, 8, and 9) compared to *in vivo* data in the literature.

It is worth noting that our goal is to estimate the amount of aerosol delivered to the lungs; therefore, our deposition values have a larynx component included, which makes the comparison of our data with *in vivo* data more qualitative rather than quantitative. However, the larynx component in the deposition data can be estimated with predictive correlations given by ICRP (publication 66). Excluding the small deposition fraction in the larynx (<5%) will still result in deposition data within the range of *in vivo* deposition values.

3.3.2. Nasal Deposition in Child Replicas

Figure 3.4 shows a comparison of existing *in vivo* deposition data for children (5.5-15 (Becquemin *et al.* 1991) and 6-10 years old (Bennett *et al*. 2008)) with the data in our children's replicas. Our deposition data is similar to that seen *in vivo* in children, particularly considering intersubject variability. Large experimental variability for the lowest range of impaction parameters was reported by Becquemin *et al.* (1991), which may explain the constant deposition values for low impaction parameters in that *in vivo* study. Also, similar to adults, exclusion of the small deposition fraction in the larynx will still result in our deposition values being within the range of the *in vivo* data.

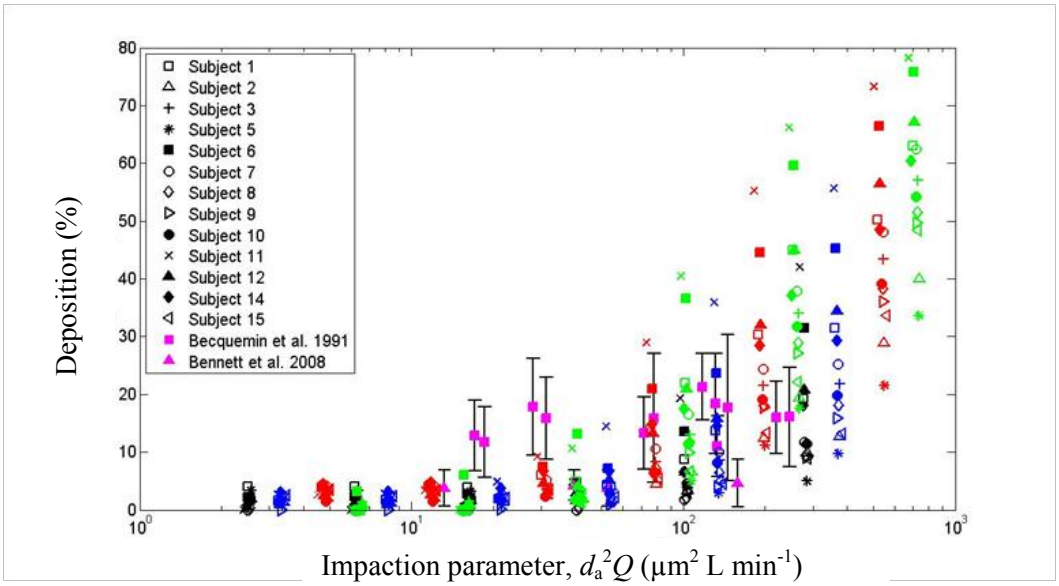

Figure 3.4 Comparison of deposition data from *in vivo* studies (Becquemin *et al*. (1991), 20 subjects 5.5-15 years old, and Bennett *et al.* (2008), 12 subjects 6-10 years old) with our deposition values in 13 replicas of children 4-14 years old vs. the impaction parameter (d_a^2Q). Deposition using four flow rates in an ascending order are illustrated in black (9.72 L/min), blue (12.7 L/min), red (18.4 L/min), and green (24.5 L/min).

Figure 3.4 shows the measured deposition data in our children's replicas versus the impaction parameter d_a^2Q. Deposition using four flow rates in an ascending order are illustrated in black (9.72 L/min), blue (12.7 L/min), red (18.4 L/min), and green (24.5 L/min). It can be seen that deposition increases with increasing flow rate and diameter, which is expected for impaction dominant deposition.

Hounam *et al*. (1971), among others, have suggested that plotting deposition vs. a parameter that includes the pressure drop Δp across the nasal

airways would reduce the scatter of deposition data in adults better than an impaction parameter. To assess the idea of scatter reduction using pressure drop, Figure 3.5 illustrates deposition in children versus $d_a^2\Delta p$. This pressure parameter does reduce the scatter of deposition data considerably.

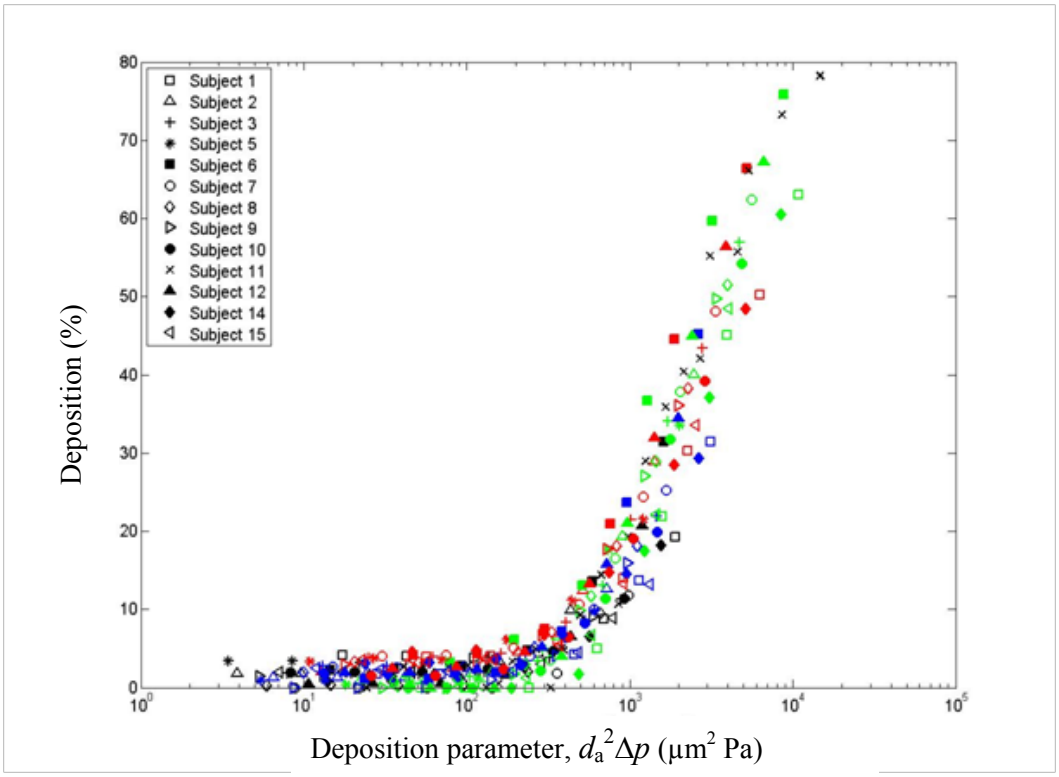

Figure 3.5 Deposition in children's replicas vs. the deposition parameter including intranasal pressure drop ($d_a^2\Delta p$).

Although the impaction parameter ($d_a^2 Q$) partly reduces the scatter of data and pressure drop parameter ($d_a^2\Delta p$) reduces it even more, these two parameters are both dimensional and therefore do not allow the application of the development of correlations that can be generalized e.g. to other gases and

individuals as has been done with dimensionless correlations (Finlay and Martin 2008). To provide a dimensionless correlation based on our child deposition data we first examined the Eq. 3.2 that Cheng (2003) has fitted to Swift's data (Swift 1991) based on a Stokes with minimum nasal cross-section area A_{min}, given as follows:

$$\eta=1-\exp(-100\mathrm{Stk});\ \mathrm{Stk}=\pi^{0.5}d_a^2Q/18\mu A_{min}^{1.5} \quad (3.2)$$

Eq. 3.2 reduced the scatter of deposition data in our children compared to the impaction parameter but the curve lay above the experimental data. Garcia *et al.* (2009) have also pointed out that the application of Stokes number defined in Eq. 3.2 only somewhat reduced the scatter of the deposition in their adult replicas.

To better reduce intersubject variability, it would be interesting to examine whether correlating deposition with a Stokes number calculated using a different optimum characteristic diameter (d_c, specific for each subject) can decrease the scatter of the data separately or in addition to other parameters such as non-dimensional intranasal pressure drop or Reynolds number. Stokes (Stk) and Reynolds (Re) numbers including d_c are defined as follows:

$$\mathrm{Re}=\frac{4\rho_{air}Q}{\pi\mu d_c} \quad (3.3)$$

$$\mathrm{Stk}=\frac{\rho_p d_p^{\ 2}C_c\,U}{18\mu d_c}=\frac{2\rho_{water}d_a^2C_cQ}{9\pi\mu d_c^3} \quad (3.4)$$

In the above equations ρ_{air} (1.2 kg/m^3) is the density of air, ρ_{water} is the density of water (1000 kg/ m^3), which is used with aerodynamic particle size d_a. The average inhaled flow rate (Q) is used in data analyses, which is calculated using tidal volume (V_t) and breathing frequency (f) as follows:

$$Q\,(l/\min) = 2 \times V_{\mathrm{t}}\,(l) \times f\,(\min^{-1}) \tag{3.5}$$

Dynamic viscosity (μ) for air is 1.8×10^{-5} (kg/(m s)). C_{c} is the Cunningham slip correction factor, which is defined as follows:

$$C_{\mathrm{c}} = 1 + 2.52\,\lambda/d_p \tag{3.6}$$

and λ is the mean free path of air.

A dimensionless pressure drop parameter can be defined using the Euler number:

$$\mathrm{Eu} = \Delta p / \rho_f U^2 = \pi^2 d_c^4 \Delta p / 16 \rho_f Q^2 \tag{3.7}$$

where Δp is the intranasal pressure drop. Various possible characteristic diameters (d_{c}) are given in Table 3.3 with their corresponding references if they have been used previously.

Comparison of the R^2 value obtained by fitting an equation that follows the trend of the deposition data was used to guide which non-dimensional numbers are characteristic determinants for prediction of deposition in addition to reducing intersubject variability. Cheng *et al*. (2003) have suggested an exponential type of equation given in Eq. 3.8, while Storey-Bishoff *et al.* (2008) have used the function given in Eq. 3.9.

$$\eta = 1 - \exp(-aX) \tag{3.8}$$

$$\eta = 1 - \left(\frac{a}{a+X}\right)^b \tag{3.9}$$

where a and b are constant values and X is a combination of different dimensionless parameters given in Table 3.4. R-squared values obtained by fitting the two aforementioned equations and visual inspection of one of the two best R^2 values obtained by the two types of equation demonstrated that a closer agreement

between the trend of data with the fitted equation could be obtained by using Eq. 3.9; therefore, we present the result of our analyses for children using Eq. 3.9.

Table 3.3 Characteristic diameters and their corresponding references in the literature in case they have previously been used. A_{nostril} is the cross sectional area of the nostrils, which is defined as the length of the nostril times its width, herein. E_{mean} is the average ellipticity of the two nostrils for each subject, whereby ellipticity is defined as the ratio of each nostril's height to its width. R_{nose} is the resistance of the nose, which is defined in Eq. 3.12.

Characteristic diameter (d_c)	Reference	Characteristic diameter (d_c)	Reference
V/A_s	Storey-Bishoff *et al*. (2008)	$\sqrt{V/L_{nose}}$	This study
V/A_{min}	Storey-Bishoff *et al*. (2008)	A_{min}/L and $A_{\text{min}}/ L_{\text{nose}}$	This study
L	Storey-Bishoff *et al*. (2008)	$\sqrt{A_{\text{min}}}$	Storey-Bishoff *et al*. (2008)
L_{nose}	This study	$\sqrt{A_{\text{min}}/E_{\text{mean}}}$	Kesavanathan *et al*. (1998)
A_s/L	Storey-Bishoff *et al*. (2008)	$\sqrt{A_s}$	This study
A_s/ L_{nose}	This study	$\sqrt{A_s/E_{\text{mean}}}$	This study
$\sqrt{V/L}$	Grgic *et al*. (2004)	$(0.0181L_{\text{nose}}/R_{\text{nose}})^{4/19}$	Garcia *et al*. (2009)
$4A_{\text{nostril}}/P_{\text{nostril}}$	Garcia *et al*. (2009)		

Table 3.4 *R*-squared values for different combinations of characteristic diameters used in defining combination of the nondimensional numbers in the deposition parameter, X (given in Eq. 3.9). The exponent values a, b (from Eq. 3.9), c, d, e (given below) are different in each case and chosen to minimize R^2 via least squares.

Deposition parameter (X)	$d_c = V/A_s$	$d_c = V/A_{min}$	$d_c = L$	$d_c = L_{nose}$	$d_c = A_s/L$
Stk[c]	0.74	0.68	0.73	0.78	0.88
Stk[c] Eu [d]	0.76	0.63	0.87	0.86	0.88
Stk[c] Re[d]	0.78	0.69	0.83	0.83	0.94
Stk[c] Re[d] $(D/D_{avg})^e$	0.80	0.80	0.83	0.83	0.94
Stk[c] Re[d] Eu [e]	0.79	0.69	0.94	0.94	0.94
Deposition parameter (X)	$d_c = A_s/L_{nose}$	$d_c = \sqrt{V/L}$	$d_c = \sqrt{V/L_{nose}}$	$d_c = A_{min}/L$	$d_c = A_{min}/L_{nose}$
Stk[c]	0.83	0.85	0.83	0.70	0.66
Stk[c] Eu [d]	0.79	0.86	0.84	0.70	0.67
Stk[c] Re[d]	0.87	0.91	0.88	0.70	0.67
Stk[c] Re[d] $(D/D_{avg})^e$	0.90	0.91	0.89	0.78	0.80
Stk[c] Re[d] Eu [e]	0.90	0.92	0.90	0.72	0.67
Deposition parameter (X)	$d_c = \sqrt{A_{min}}$	$d_c = \sqrt{A_{min}/E_{mean}}$	$d_c = \sqrt{A_s}$	$d_c = \sqrt{A_s/E_{mean}}$	$d_c = (0.0181 L_{nose}/R_{nose})^{4/19}$
Stk[c]	0.77	0.66	0.85	0.74	0.88
Stk[c] Eu [d]	0.79	0.67	0.88	0.77	0.88
Stk[c] Re[d]	0.81	0.68	0.92	0.77	0.95
Stk[c] Re[d] $(D/D_{avg})^e$	0.84	0.79	0.92	0.81	0.95
Stk[c] Re[d] Eu [e]	0.83	0.68	0.95	0.80	0.95
Deposition parameter (X)	$d_c = 4A_{nostril}/P_{nostril}$				
Stk[c]	0.73				
Stk[c] Eu [d]	0.79				
Stk[c] Re[d]	0.75				
Stk[c] Re[d] $(D/D_{avg})^e$	0.78				
Stk[c] Re[d] Eu [e]	0.81				

Following Storey-Bishoff *et al.* (2008), X values appearing in Eq. 3.9 could be combination of different non-dimensional numbers or just an individual non-dimensional number. Table 3.4 shows the R^2 values obtained using different combinations of three relevant non-dimensional numbers: Stokes number (Stk) to include aerodynamic diameter effects, Reynolds number (Re) to include flow

effects and Euler number (Eu) to include the dependence of deposition values on intranasal pressure drop that was seen in Figure 3.5.

Table 3.4 demonstrates that the addition of Euler number and the ratio of characteristic diameter D over the average diameter D_{avg} to the combination of Stokes and Reynolds numbers do not improve the fit significantly. Thus for simplicity of the proposed correlating equation we will not consider these parameters further.

We have also compared deposition in our children replicas at four constant flow rates vs. the four unsteady breathing patterns that have average flow rate similar to the constant values. Although deposition under unsteady breathing was consistently slightly higher than at constant flow rate (except at the highest flow rate in the subject with the maximum intranasal pressure drop), the difference between the two patterns was not statistically significant (P>0.05). Therefore, we did not examine the use of a dimensionless number, such as Womersley number, that has a component of breathing frequency in it. It is worth mentioning that Reynolds, Euler, and Womersley numbers that we considered herein come from the non-dimensionalized Navier-Stokes equation, whereas Stokes number comes from the non-dimensionalized particle equation of motion.

The characteristic diameter defined by Garcia *et al*. (2009), which results in the highest R^2 value, includes transnasal pressure drop. The considerable reduction in scatter of the data with the application of pressure drop has also previously been illustrated in Figure 3.5. Equation 3.10, gives the form of an

equation that can be used for predicting deposition using that characteristic diameter.

$$\eta = [1 - \left(\frac{1.414 \times 10^4}{1.414 \times 10^4 + X} \right)^{0.51}] \times 100 \; ; \quad X = \mathrm{Stk}^{1.30} . \mathrm{Re}^{1.36} \tag{3.10}$$

For our subjects, the average and standard deviations of the characteristic diameters proposed by Garcia *et al*. (2009) for calculation of the dimensionless numbers in Eq. 3.10 is 0.005±0.001 m.

In order to understand the strong correlation between deposition and pressure drop, it is useful to consider the Darcy-Weisbach equation, which relates pressure drop to duct diameter as follows (White 1999):

$$\Delta p = fL \frac{\rho Q^2}{2d^5} \tag{3.11}$$

where f is the friction factor, L is the length of the duct, Q is the flow rate, ρ is the density of the fluid and d is the diameter of the duct. It can be seen that the pressure drop is strongly dependent on the duct geometric dimension (i.e. d^{-5}); thus, even a small change in duct dimension will be magnified in the pressure drop. This magnified direct relation between geometry and pressure drop may be what collapses intersubject variability when using the pressure drop in the characteristic diameter.

Despite the high R^2 value obtained by the application of Garcia's characteristic diameter, calculations of this diameter involve the parameter R_{nose} that requires an extra step of mathematical curve fitting to pressure drop versus average flow rate data according to the following equation (Garcia *et al.* 2009):

$$\Delta p = R_{nose} Q^{1.75} \tag{3.12}$$

where pressure drop values are measured at a given constant flow pattern. To avoid this step and given that nearly as high an R^2 values is obtained with less work using other characteristic diameters, we will only consider two correlations (Eqs. 3.13 and 3.14) that include Stokes and Reynolds numbers calculated using the two characteristic diameters: A_s/L and $\sqrt{V/L}$. The first characteristic diameter, A_s/L, gives a high R^2 value (0.94) with Eq. 3.13 but requires post processing measurements of surface area, which is difficult to obtain *in vivo*. The second equation (Eq. 3.14) includes the dimensions of volume and the path length of the airways which can be readily measured *in vivo* by acoustic rhinometry but still gives a good fit (R^2=0.91).

$$\eta = [1 - \left(\frac{4.21 \times 10^{-3}}{4.21 \times 10^{-3} + X} \right)^{0.55}] \times 100 \; ; \quad X = \mathrm{Stk}^{1.25} . \mathrm{Re}^{1.32} \tag{3.13}$$

$$\eta = [1 - \left(\frac{119.4}{119.4 + X} \right)^{0.57}] \times 100 \; ; \quad X = \mathrm{Stk}^{1.23} . \mathrm{Re}^{1.28} \tag{3.14}$$

For our subjects, the average and standard deviations of the characteristic diameters A_s/L and $\sqrt{V/L}$ for calculation of the dimensionless numbers in Eqs. 3.13 and 3.14 are 0.090±0.014 and 0.011±0.001 m, respectively. Figure 3.6 (a) and (b) demonstrate Eqs. 3.13 and 3.14 passing through the deposition data.

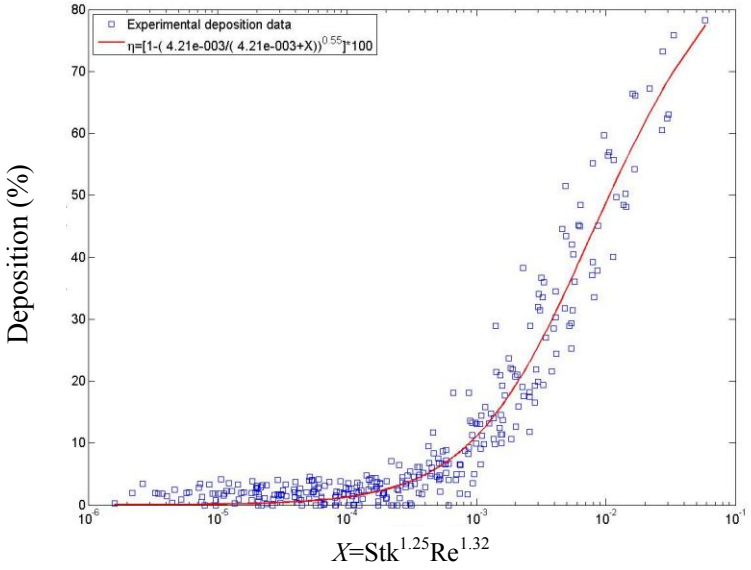

(a)

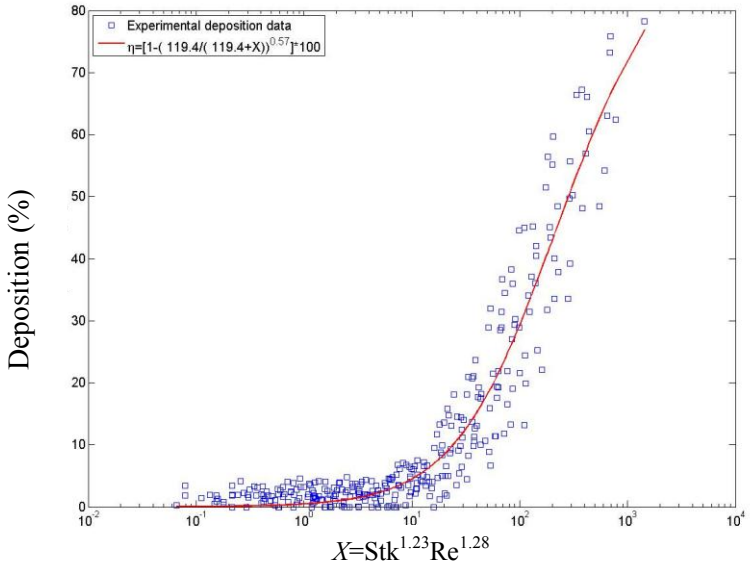

(b)

Figure 3.6 Deposition of micrometer-sized particles in children replicas vs. non-dimensional deposition parameter X from Eq. 3.9 including a characteristic diameter defined as (a) $d_c=A_s/L$ (b) $d_c=\sqrt{V/L}$.

Note that the characteristic diameter A_s/L and $\sqrt{V/L}$ that resulted in good fits are the average perimeter and the average cross section of the nasal airways, respectively. Both of these two diameters can be viewed as indicators of the distance between central flow streamlines and the wall of the nasal airways. This distance is directly correlated to the probability of deposition of particles by impaction (i.e. the shorter the distance the higher the probability of deposition by impaction), so that it is sensible that these characteristic diameters result in good collapse of the data.

3.3.3. Comparison of Deposition in Normal vs. Congested Nose

In addition to the thirteen healthy subjects that we have identified based on similarity between their intranasal pressure drop and the *in vivo* pressure drop values, we also had an additional replica of an individual (subject 4), which had an unusually high pressure drop. By examining a post build scan we knew that there was no residual wax build up in the replica and that abnormalities in the airways were apparent in the original *in vivo* scan as well. The abnormalities in this subject's airways are believed to have been due to congestion of the airways in that subject since isolated volumes of air were seen to be present surrounded by mucus in the proximal nasal regions, a feature not seen in any other subject. Deposition in this one congested replica of a six year old male is compared with other healthy subjects in Figure 3.7(a). Deposition for the congested subject is outside the range used to develop our proposed equations 3.13 and 3.14 and caution should thus be used in the application of equations developed for normal

populations to subjects with abnormalities such as congestion. It is worth noting that noticeable differences (approx. 60%) between normal and congested noses has previously been demonstrated for adults (see Figure 5 in Swift 1991). Following Swift's method for adults (Swift 1991) we defined a Stokes number which uses $\sqrt{A_{\min}/\pi}$ as the characteristic diameter (Cheng 2003) and fitted an equation to both congested and normal data in our children. The scatter was not reduced and the R^2 was 0.56. Similarly considering Reynolds number, calculated using $\sqrt{A_{\min}/\pi}$, with Stokes number did not collapse the data. Using $\sqrt{V/L}$ as the characteristic diameter in calculation of the deposition parameter also did not collapse the scatter in deposition in normal vs. the congested nose. It is speculated that this difference between healthy subjects and a congested subject may be due to the significant differences between the shape and features of a congested nose vs. normal ones. Apparently, the anatomical features are no longer geometrically similar enough to the normal population for the present dimensionless parameters to yield generalized correlations valid for such disparate geometries.

We have also plotted deposition in the congested replica (subject 4) together with the other subjects vs. $d_a^2\Delta p$ (Figure 3.7b). Although the scatter was noticeably less than the case with the impaction parameter as the *x*-axis, deposition for the congested nose remains distinguishably higher than the normal ones.

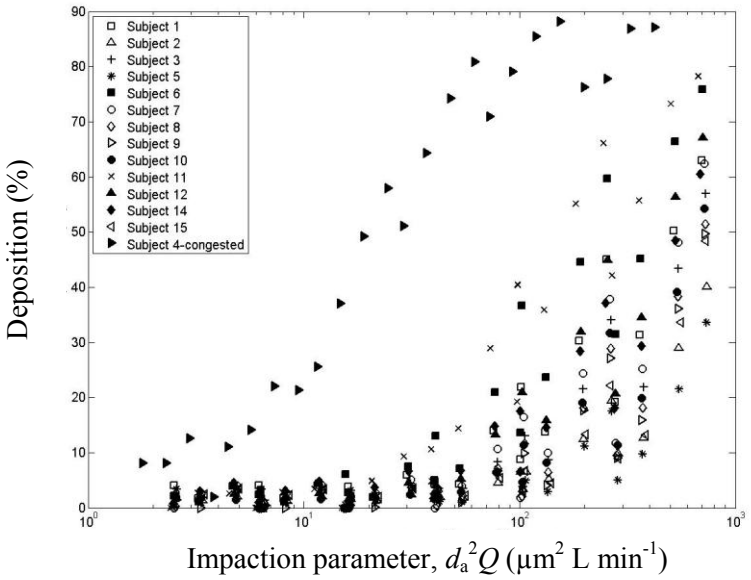

(a)

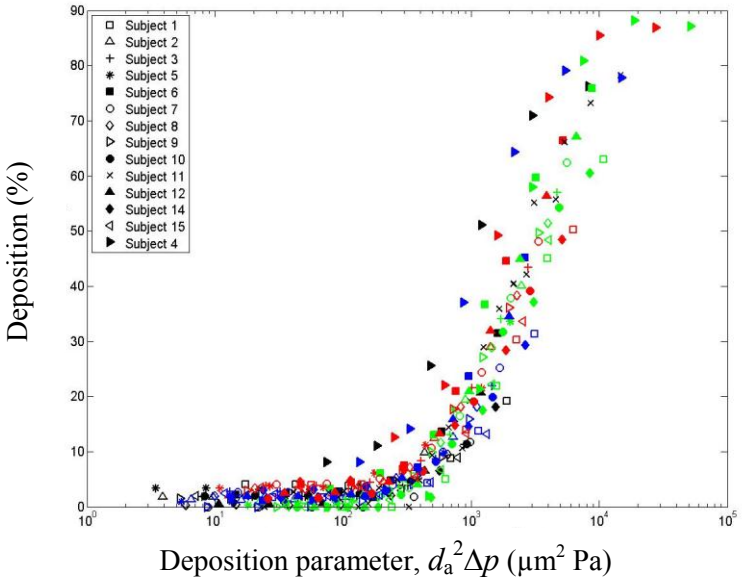

(b)

Figure 3.7 Comparison of deposition in one six year old subject with a congested nose with our thirteen healthy subjects.

3.3.4. Comparison of Deposition across Different Age Groups

One of our initial goals for carrying out this study was to determine the difference in deposition across different age groups. For that purpose we tried fitting our previously developed correlations (Storey-Bishoff *et al.* 2008) for eleven 3-18 month old infants using the characteristic diameters V/A_s and $\sqrt{V/L}$ to our deposition data from thirteen healthy subjects 4-14 years old. The infant correlations lay above our data, which indicates higher deposition in infants compared to our children at the same Stokes and Reynolds number. There was also significant scatter in the resulting plot of deposition data (approx. maximum 65% variation at a fixed X value with V/A_s and 40% with $\sqrt{V/L}$).

Since the equation for infants did not work well for children, in an attempt to have a single equation for prediction of deposition in infants and children, we tried fitting an equation to the deposition data for both age ranges vs. different deposition parameters as in Table 3.4. The best R^2 value that we obtained using Stokes number and Reynolds number ($d_c = V/A_s$) was 0.75 and the scatter of data was again significant (approx. maximum 60% variation). Data points corresponding to nonzero deposition values in infants were higher than the deposition in children at a given value of deposition parameter X; however, the data points of the two age groups had a partial overlap.

It is also instructive to compare our data in children to that seen in adults. Figure 3.8 shows our deposition data in our five chosen adult replicas, along with the data from Storey-Bishoff *et al.* (2008) for infants and our data in children.

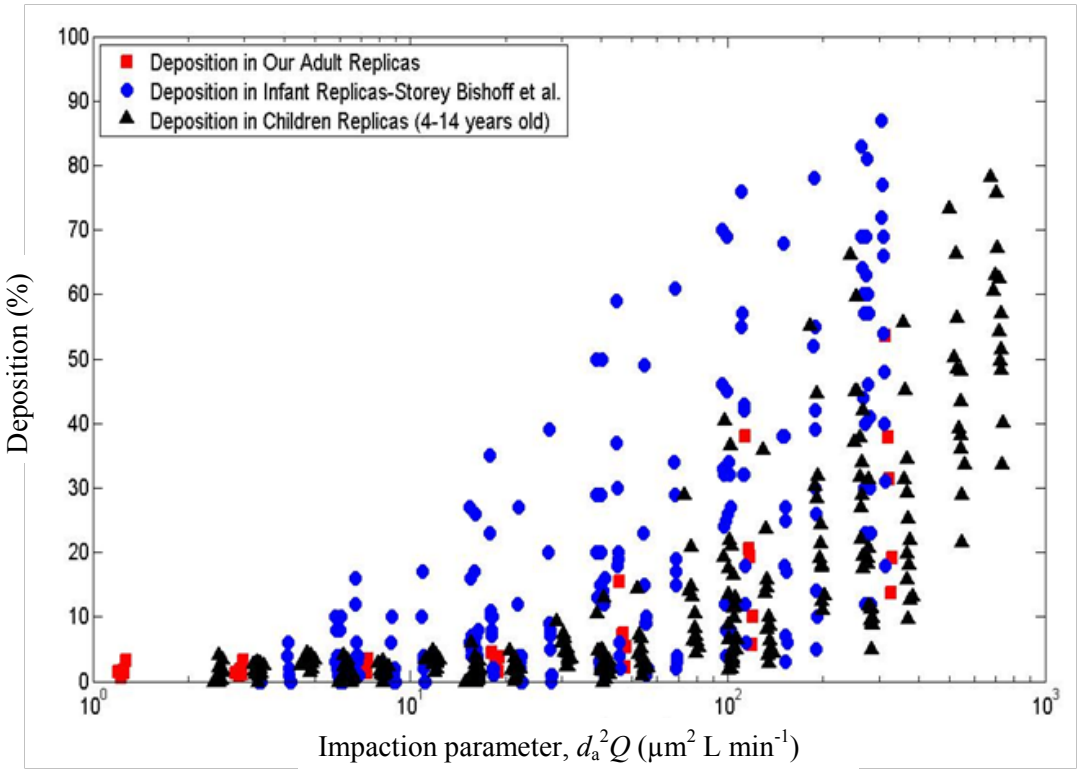

Figure 3.8 Deposition versus impaction parameter d_a^2Q across different ages (infants, children, adults).

For a given impaction parameter, Figure 3.8 shows that deposition in infants is generally higher than children and adults. Swift (1991) noted a similar higher deposition in a six week old female infant compared to a 57 year old man at a given impaction parameter. Overall, considering intersubject variability in both children and adults it also appears that the deposition values in adults and children are fairly close to each other. In order to explain the observed trends in Figure 3.8 we examined the relevant characteristic dimensions and basic dimensions of all age groups. The dimensions of our children are close to adult values, whereas infants have considerably smaller geometries as is seen by the average value of length of

nasal airways for our children (20.1±1.73 cm) being close to the average length for our adults (23.6±2.22 cm), whereas for infants it is 10.4±0.8 cm. It thus appears that the much smaller infant nasal dimensions, but not dissimilar dimensions between adults and children, explain the above noted age trends in Figure 3.8.

3.4 Conclusions

Considerable intersubject variability was observed in deposition of micrometer-sized particles in our fourteen children replicas if only impaction parameter is considered when plotting the data. When instead a characteristic diameter in the form of the ratio of surface area to the length of nasal airway is used for calculation of Reynolds and Stokes numbers, the scatter of the data largely collapses. However, since measuring the surface area of the airways *in vivo*, requires imaging, it is useful to note that a characteristic diameter including nasal airway volume and length (i.e $\sqrt{V/L}$), which can be measured by acoustic rhinometry, allows prediction of deposition with good accuracy (R^2= 0.91) via the following equation:

$\eta = [1 - \left(\frac{119.4}{119.4 + X} \right)^{0.57}] \times 100$ where ; $X = \mathrm{Stk}^{1.23}.\mathrm{Re}^{1.28}$.The average value of the characteristic diameter $\sqrt{V/L}$ used in Stokes and Reynolds for our thirteen healthy subjects is 1.1±0.14 cm. Comparing deposition across different age groups at a constant impaction parameter shows that deposition in infants is higher than in both adults and children, whereas deposition in our children is not significantly different from our five tested adults. The proposed equation can be used for

estimating the fraction of nasally inhaled aerosol that reaches the lungs of school aged children and adolescents.

3.5 Bibliography

Becquemin, M. H., Swift, D. L., Bouchikhi, A., Roy, M., and Teillac, A. (1991). Particle deposition and resistance in the noses of adults and children. *The European Respiratory Journal*, 4, 694-702.

Bennett, W. D., and Zeman, K. L. (2005). Effect of race on fine particle deposition for oral and nasal breathing. *Inhalation Toxicology*, 17, 641-648.

Bennett, W. D., Zeman, K. L., and Jarabek, A. M. (2008). Nasal contribution to breathing and fine particle deposition in children versus adults. *Journal of Toxicology and Environmental Health, Part A*, 71, 227-237.

Cheng, Y. S., Yeh, H. C., and Swift, D. L. (1991). Aerosol Deposition in Human Nasal Airway for Particles 1 nm to 20 μm: A Model Study. *Radiation Protection Dosimetry*, 38, 41-47.

Cheng, Y.S. (2003). Aerosol deposition in the extrathoracic region. *Aerosol Science and Technology*, 37, 659-671.

Dai, Y., Chang, C., Tu, L., and Hsu, D. (2007). Development of a Taiwanese head model for studying occupational particle exposure. *Inhalation Toxicology*, 19, 383-392.

Dorato, M. A., and Wolff, R. K. (1991). Inhalation exposure technology, dosimetry, and regulatory issues. *Toxicologic Pathology*, 19(4), 373-383.

Finlay, W. H., and Martin A. R. (2008). Recent advances in predictive understanding of respiratory tract deposition. *Journal of Aerosol Medicine and Pulmonary Drug Delivery*, 21(2), 189-205.

Garcia, G. J. M., Tewksbury, E. W., Wong, B. A., and Kimbell, J. S. (2009). Interindividual variability in nasal filtration as a function of nasal cavity geometry. *Journal of Aerosol Medicine and Pulmonary Drug Delivery*, 22(2), 139-155.

Giacomelli-Maltoni, G., Melandri, C., Prodis, V., and Tarroni, G. (1972). Deposition efficiency of monodisperse particles in human respiratory tract. *American Industrial Hygiene Association Journal*, 33(9), 603-610.

Ginsberg, G. L., Asgharian, B., Kimbell, J. S., Ultman, J. S., and Jarabek, A. M. (2008). Modeling approaches for estimating the dosimetry of inhaled toxicants in children. *Journal of Toxicology and Environmental Health*, *Part A*, 71, 166-195.

Golshahi, L., Finlay, W. H., Olfert, J. S., Thompson, R. B., and Noga, M. L. (2010). Deposition of Inhaled Ultrafine Aerosols in Replicas of Nasal Airways of Infants. *Aerosol Science and Technology*, 44 (9), 741-752.

Guilmette, R. A., Cheng, Y. S., Yeh, H. C., and Swift, D. L. (1994). Deposition of 0.005-12 μm monodisperse particles in a computer-milled, MRI-based nasal airway replica. *Inhalation Toxicology*, 6, 395-399.

Harvey, R. P., and Hamby D. M. (2002). Age-specific uncertainty in particulate deposition for 1 mm AMAD particles using the ICRP 66 lung model. *Health Physics*, 82(6), 807-816.

Heyder, J., and Rudolf, G. (1977). Deposition of aerosol in the human nose. In: W. H. Walton (Ed.), Inhaled Particle IV. Pergamon Press: Oxford, pp. 107-125.

Heyder, J., Gebhart, J., Rudolf, G., Schiller, C. F., and Stahlhofen, W. (1986). Deposition of particles in the human respiratory tract in the size range 0.005-15 μm. *Journal of Aerosol Science*, 17(5), 811-825.

Hounam, R. F., Black, A., and Walsh, M. (1969). Deposition of aerosol particles in the nasopharyngeal region of the human respiratory tract. *Nature*, 221, 1254-1255.

Hounam, R. F., Black, A., and Walsh, M. (1971). The deposition of aerosol particles in the nasopharyngeal region of the human respiratory tract. *Journal of Aerosol Science*, 2, 47-61.

International Commission on Radiological Protection (ICRP), Publication 66 (1994). Human respiratory tract model for radiological protection. Pergamon Press: Oxford.

Itoh, H., Smaldone, G. C., Swift, D. L., and Wagner, Jr., H. N. (1985). Mechanisms of aerosol deposition in a nasal model. *Journal of Aerosol Science*, 16, 529-534.

Janssens, H.M., De Jongste, J. C., Fokkens,W. J., Robben, S. G. F.,Wouters, K., and Tiddens,H.A.W.M. (2001). The Sophia Anatomical Infant Nose–Throat (Saint) Model: A Valuable Tool to Study Aerosol Deposition in Infants. *Journal of Aerosol Medicine and Pulmonary Drug Delivery*, 14(4), 433–441.

Keck, T., Leiacker, R., Klotz, M., Lindemann, J., Riechelmann, H., Rettinger, G. (2000). Detection of particles within the nasal airways during respiration. *European Archives of Oto-rhino-laryngology*, 257, 493-497.

Kelly, J. T., Asgharian, B., Kimbell, J. S., and Wong, B. A. (2004). Particle deposition in human nasal airway replicas manufactured by different methods. Part I: Inertial Regime Particles. *Aerosol Science and Technology*, 38, 1063-1071.

Kelly, J. T., Asgharian, B., and Wong, B. A. (2005). Inertial particle deposition in a monkey nasal mold compared with that in human nasal replicas. *Inhalation toxicology*, 17(14), 823-830.

Kesavanathan, J., Bascom, R., and Swift, D. L. (1998). The effect of nasal passage characteristics on particle deposition. *Journal of Aerosol Medicine and Pulmonary Drug Delivery*, 11(1), 27-39.

Kesavanathan, J., and Swift, D. L. (1998). Human nasal passage particle deposition: the effect of particle size, flow rate, and anatomical factors. *Aerosol Science and Technology*, 28, 457-463.

Kimbell, J. S. (2006). Nasal dosimetry of inhaled gases and particles: where do inhaled agents go in the nose? *Toxicology Pathology*, 34, 270-273.

Landahl, H. D., and Black, S. (1947). Penetration of air-borne particulates through the human nose. *Journal of Industrial Hygiene and Toxicology*, 29(4), 269-277.

Landahl, H. D., and Tracewell, T. (1949). Penetration of air-borne particulates through the human nose. *Journal of Industrial Hygiene and Toxicology*, 31(1), 55-59.

Lippmann, M. (1970). Deposition and clearance of inhaled particles in the human nose. Annals of Otology, *Rhinology and Laryngology*, 70, 519-528.

Liu, Y., Matida, E. A., Gu, J., and Johnson, M. R. (2007). numerical simulation of aerosol deposition in a 3-D human nasal cavity using RANS, RANS/EIM, and LES. *Journal of Aerosol Science*, 38(7), 683-700.

Liu, Y., Johnson, M. R., Matida, E. A., Kherani, S., and Marsan, J. (2009). Creation of a standardized geometry of the human nasal cavity. *Journal of Applied Physiology*, 106, 784-795.

Liu, Y., Matida, E. A., and Johnson, M. R. (2010). Experimental measurements and computational modeling of aerosol deposition in the Carleton-Civic standardized human nasal cavity. *Journal of Aerosol Science*, 41(6), 569-586.

Pattle, R. E. (1961). The retention of gases and particles in the human nose. In: C. N. Davies (Ed.), Inhaled Particles and Vapours. Pergamon Press: Oxford, pp.302-309.

Phalen, R. F., Oldham, M. J., and Mautz, W. J. (1989). Aerosol deposition in the nose as a function of body size. *Health Physics*, 57(Suppl. 1), 299-305.

Rasmussen, T. R., Swift, D. L., Hilberg, O., and Pedersen, O. F. (1990). Influence of nasal passage geometry on aerosol particle deposition in the nose, *Journal of Aerosol Medicine and Pulmonary Drug Delivery*, 3(1), 15-25.

Rasmussen, T. R., Anderson, A., Pedersen, O. F. (2000). Particle deposition in the nose related to nasal cavity geometry. *Rhinology*, 38, 102-107.

Scott, W. R., Taulbee, D. B., and Yu, C. P. (1978). Theoretical study of nasal deposition. *Bulletin of Mathematical Biology*, 40, 581-603.

Shi, H., Kleinstreuer, C., and Zhang, Z. (2007). Modeling of inertial particle transport and deposition in human nasal cavities with wall roughness. *Journal of Aerosol Science*, 38, 398-419.

Storey-Bishoff, J., Noga, M., and Finlay, W. H. (2008). Deposition of Micrometer-Sized Aerosol Particles in Infant Nasal Airway Replicas. *Journal of Aerosol Science*, 39, 1055–1065.

Swift, D. L. (1991). Inspiratory inertial deposition of aerosols in human nasal airway replicate casts: implication for the proposed NCRP lung model. *Radiation Protection Dosimetry*, 38, 29-34.

Swift, D. L. and Kesavanathan, J. (1996). The anterior human nasal passage as a fibrous filter for particles. *Chemical Engineering Communications*, 151(1), 65-78.

Thatcher, T. L., Fairchild, W. A., Nazaroff, W. W. (1996). Particle deposition from natural convection enclosure flow onto smooth surfaces. *Aerosol Science and Technology*, 25, 359-374.

U. S. EPA. (U.S. Environmental Protection Agency) (1994). Methods for derivation of inhalation reference concentrations and application of inhalation dosimetry. EPA/600/8-90/066F.

Vincent, J. H. (2005). Health-related aerosol measurement: a review of existing sampling criteria and proposals for new ones. *Journal of Environmental Monitoring*, 7, 1037-1053.

Wang, S. W., Inthavong, K., Wen, J., Tu, J. Y., and Xue, C. L. (2009). Comparison of micron- and nanoparticle deposition patterns in a realistic human nasal cavity. *Respiratory Physiology & Neurobiology*, 166, 142-151.

White, F. M. (1999). Fluid Mechanics (4th ed.). McGraw-Hill: Boston.

Wiesmiller, K., Keck, T., Leiacker, R., Sikora, T., Rettinger, G., and Lindemann, J. (2003). The impact of expiration on particle deposition within the nasal cavity. *Clinical Otolaryngology*, 28, 304-307.

Yeh, H. C., Brinker, R. M., Harkema, J. R., and Muggenburg, B. A. (1997). A comparative analysis of primate nasal airways using magnetic resonance imaging and nasal casts. *Journal of Aerosol Medicine*, 10(4), 319-329.

Yu, C. P., Diu, C. K., and Soong, T. T. (1981). Statistical analysis of aerosol deposition in nose and mouth. *American Industrial Hygiene Association*, 42, 726-733.

Zwartz, G. J., and Guilmette, R. A. (2001). Effect of flow rate on particle deposition in a replica of a human nasal airway. *Inhalation Toxicology*, 13, 109-127.

CHAPTER 4 : DEPOSITION OF INHALED MICROMETER-SIZED PARTICLES IN OROPHARYNGEAL AIRWAY REPLICAS OF CHILDREN AT CONSTANT FLOW RATES

A very similar version of this chapter is in press in *Journal of Aerosol Science* as: Golshahi, L., Noga, M. L., and Finlay, W. H. (2012). Deposition of inhaled micrometer-sized particles in oropharyngeal airway replicas of children at constant flow rates.

4.1 Introduction

Deposition in the extrathoracic region plays an important role in determining the delivered dose to the lungs since this region serves as a filter for both deleterious environmental particles and beneficial therapeutic aerosols. Extrathoracic deposition is a major determinant of variability in lung deposition (Borgstrom *et al*., 2006). Deposition in nasal airways, mostly among adults, has been the focus of several studies, a review of which is given by Cheng (2003). We have recently studied the deposition of micrometer-sized particles in the extrathoracic airways of infants (Storey-Bishoff *et al*., 2008) and children (Golshahi *et al*., 2011) during nose breathing. However, the preferred route of inhalation drug delivery to the lungs is the oral airways, due to their lower deposition. There are *in vivo* (e.g. Borgstrom, 1999; Bowes and Swift, 1989; Cass *et al*., 1999; Chan and Lippmann, 1980; Emmett *et al*., 1982; Foord *et al*., 1978; Lippmann and Albert, 1969; Pritchard *et al*., 1981; Stahlhofen *et al*., 1980, 1983, 1984; Svartengren *et al*., 1987, 1994, 1995) and *in vitro* (e.g. Cheng *et al*., 1999,

2001; DeHaan and Finlay, 2001, 2004; Grgic *et al*., 2004 a, b, 2006; Swift, 1992; Zhou *et al*., 2011) studies available with a focus on deposition of particles in oral airways of adults. Comprehensive evaluations and representative correlations based on the experimental data of *in vivo* adult studies have been given by Stahlhofen *et al*. (1989) and Cheng (2003). A recent review on *in vivo* and *in vitro* deposition in the oropharyngeal airways (mouth-throat) and lungs is given by Finlay and Martin (2008).

Little data exists on oral airway deposition in children. The lack of such data is unfortunate since inhalation drug delivery is an efficient common practice for the noninvasive treatment of pediatric lung diseases, and oropharyngeal deposition is of significant importance in the estimation of delivered drug dose to the lungs. A limited number of *in vivo* studies have been carried out to quantify the total deposition of particles in children's lungs during oral inhalation (Becquemin *et al*., 1991; Bennett and Zeman, 1998, 2004; Schiller-Scotland *et al*., 1992). In addition, *in vivo* oropharyngeal and lung deposition of aerosols (with radioactive tracers) emitted from specific types of aerosol inhalers such as the Turbuhaler® and QVAR® have been studied in children with cystic fibrosis (Devadason *et al*., 1997) and asthma (Devadason *et al*., 2003; Roller *et al*., 2007). However, comprehensive data on the deposition of particles of various sizes during inhalation at different flow rates in children's oral airways with known dimensions are missing from the literature.

In vitro deposition measurements using high-fidelity replicas have been considered as robust alternatives to *in vivo* measurements and have been validated

against *in vivo* deposition data in the literature (Cheng, 2003). However, one should be cautious in interpreting the data taken with cadaver-based replicas due to possible post-mortem changes in the airways and distortion of their geometry during the casting process involved in their fabrication (Pritchard *et al*., 2004; McRobbie *et al*., 2003). On the other hand, imaging of the oropharyngeal airways, which has been a core part of the recently common *in vitro* studies, is considered complex because of the time- and flow-dependent dynamics of the airways, especially around the larynx area (Martonen and Lowe, 1983). To address this issue, gated MRI images have been considered to keep the airways of adults open consistently during the time of imaging (McRobbie *et al*., 2003). Although, MRI gating could also be used for imaging the oropharyngeal airways of children, the long duration of this technique is considered a major drawback because of the short attention span common among the children as well as the discomfort due to wearing a neck coil during imaging. Note that the neck coil is used to reduce the motion artifacts and for consistent positioning of the region of interest during the imaging process (McRobbie *et al*., 2003).

Computed tomography (CT) is known as the fastest mode of imaging thus far, which is believed to result in the most anatomically-accurate replicas (McRobbie *et al*., 2003). However, exposure to unwarranted X-ray radiation is a concern. Therefore, it is important to recruit subjects from a population who require CT for their clinical diagnosis. This type of subject selection imposes the need for making the imaging as simple as possible, while the oropharyngeal airways are still required to stay open during imaging to mimic the inhalation

scenario. Delivering constant flow rates at the time of imaging is thus considered as a solution to keep the airways open in the imaging region, while making the timing as short as possible.

The present study examines the deposition of micrometer-sized particles in oropharyngeal airway replicas of nine children 6-14 years old during inhalation at constant flow rates. The CT images, taken while the subjects inhaled from a standard mouthpiece, were used to make anatomically accurate replicas in order to explore intersubject variation in the deposition. To reduce the scatter of the data we used the two non-dimensional numbers, Reynolds and Stokes number, calculated using the geometrical dimensions of the airways of each subject, in a predictive correlation. This correlation is used to estimate deposition of the particles among children during oral inhalation at moderate to high constant flow rates. Such a correlation may be used for better individualized dosing of inhaled medication delivered via inhalers such as dry powder inhalers (DPIs) or pressurized metered dose inhalers (pMDIs) with holding chambers.

4.2 Experimental Methods

4.2.1 Imaging of the Airways

An AKITA® inhalation system (Activaero GmbH, Germany) was used to deliver a fixed flow rate to children who required CT as a part of their clinical protocol at the PET/CT center of Stollery Children's Hospital under the approval of the University of Alberta Health Research Ethics Board (HREB). AKITA® is a nebulizer aerosol administration system and has been used by children 3 years of

age and older. In this study, however, this inhalation system was used in empty, dry mode (i.e. no liquid material or drug in the nebulizer). The smart card of the instrument was programmed to generate a fixed flow rate of 12 L/min over a fixed period of time (i.e. 10 seconds). While it would be preferable to obtain scans at the higher flow rates (30-150 L/min) used in our deposition measurements, this was not possible due to the mismatch between the short duration of inhalation at these flow rates and the CT acquisition time, and because of the relatively small inspiratory capacity of pediatric subjects. To ensure the oral cavity remains open, a mouthpiece is needed (Bowes and Swift, 1989). For this purpose, we used the PARI LC Star (PARI, Starnberg, Germany) nebulizer's mouthpiece for all individuals. The shape and dimensions of this mouthpiece are given in Figure 4.1. The children were asked to bite on the mouthpiece, while a plastic medical nose clip was used to prevent nasal breathing. To keep the geometry of the buccal cavity as natural as possible, the children were provided with no special instructions on how to position their tongue around the mouthpiece.

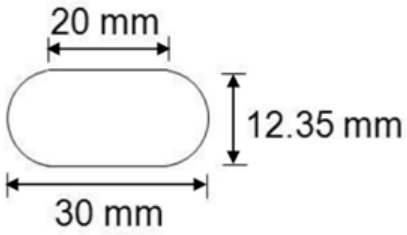

Figure 4.1 The dimensions of the mouthpiece (LC star nebulizer's mouthpiece), through which the children inhaled at the time of CT imaging.

The CT imaging, using a high-resolution Philips scanner (Philips, The Netherlands), was synchronized with inhalation by asking the subject to start inhaling the constant flow provided by AKITA at the time that the scanner was imaging their oral airways. The recorded raw images were then reconstructed at a slice thickness of one millimeter. The in-plane resolutions (pixel sizes) were in the range of 0.324-0.453 mm, with an average of 0.411±0.039 mm. The relevant subject information such as sex, age, height and weight were also recorded and are given in Table 4.1.

Table 4.1 Relevant information of the subjects including their sex, age (in years), height (in cm) and weight (in kg)

Subject	Sex	Age (yr)	Height (cm)	Weight (kg)
1	M	6	119.5	28
2	F	8	118	20
3	F	9	140	37.5
5	M	12	153	42.6
6	M	12	157.2	46.5
7	M	13	161	57
10	M	14	171	47.4
11	M	10	139	34
12	F	14	155	50.5

4.2.2. Fabrication of Replicas

Based on the grayscale level of air, the regions of interest (i.e. oropharyngeal airways and the first 3 cm of trachea) were identified in the CT images using the Mimics software package (Materialise, USA). The threshold level was kept consistent (-200 to -1024) for all layers of the CT images. Magics commercial software (Materialise, USA) was used for further processing of the

3D models imported from Mimics to build a two-millimeter thick shell of the airways. At this stage, a cylinder was added around the trachea for easier tube connection during the experiments. The mouthpiece was also subtracted in Magics. A rapid prototyping machine (Invision SR 3-D printer, 3D Systems, USA) was used for building the processed 3D computer models using acrylic plastic build material and wax as the support. The wax was removed from the airways afterwards by heating the replicas to ~60 ºC. The mouthpieces that were used for imaging were air-sealed to the built replicas using Parafilm® and putty prior to the experiments. Figure 4.2 shows our nine replicas at the final fabrication stage, prior to the experiments.

Figure 4.2 Nine oral airway replicas of children 6-14 years old. The replicas are arranged in an ascending order based on their numerical label from left to right on each row.

The replicas were re-scanned by CT after rapid prototyping to ensure the important anatomical features of the airways had been precisely maintained during fabrication. By segmenting these images, the geometrical dimensions of the airway replicas were measured (Table 4.2). Note that these data are the dimensions of the 3D airways truncated at the tip of the mouthpiece (the emission point of aerosols). Only the dimensions of the remaining part, i.e. excluding the mouthpiece, were used for further analysis.

Table 4.2 Geometrical parameters of the replicas post-build: volume (mm^3), surface area (mm^2) and length (mm)

Subject	Volume (mm^3)	Surface area (mm^2)	Length (mm)
1	17584.6	7680.9	125.7
2	19554.1	9172.5	130.4
3	39003.5	12557.8	154.9
5	33828.8	11711.1	167.6
6	31275.7	10181.3	158.8
7	38788.3	14428.3	160.3
10	50915.9	16735.5	171.6
11	35877.8	13112.2	150.9
12	30937.8	11229.8	136.9

We also fabricated a plastic version of the commercially-available adult idealized throat, known as the 'Alberta Idealized Throat', with the same rapid prototyping machine used to build our children's replicas. The details of the methodology, followed for the design of this Idealized Throat, have been noted in our previous study (Stapleton *et al*., 2000). This adult replica was utilized to validate our deposition measurements.

4.2.3. Deposition Measurement Experiments

Figure 4.3 shows a schematic diagram of the experimental setup that we used for measuring deposition in the replicas. To create the desired flow rates, dilution air was added to the setup via two openings in the two lines. The openings were covered with filters (303 Respirgard II^{TM}, Vital Signs Inc., USA) to remove ambient particles. Two vacuum pumps were used in series to generate five steady flow rates (Q_1=30 L/min, Q_2=33 L/min, Q_3=68 L/min, Q_4=107 L/min and Q_5=150 L/min) downstream of the replica to cover the range of typical peak inspiratory flow rates (PIF) generated by children during the use of inhalers. A digital mass flowmeter (Model 4043, TSI Inc., USA) was used downstream of each replica individually to record the flow rates through the blank and replica lines and the average of five measurements was used for the analysis of each data point. In line with balancing the flow in the whole setup, we controlled the ELPI's required sampling flow rate (30 L/min) by setting a rotameter at a certain reading while checking that zero flow occurred through the replica when the pumps were off.

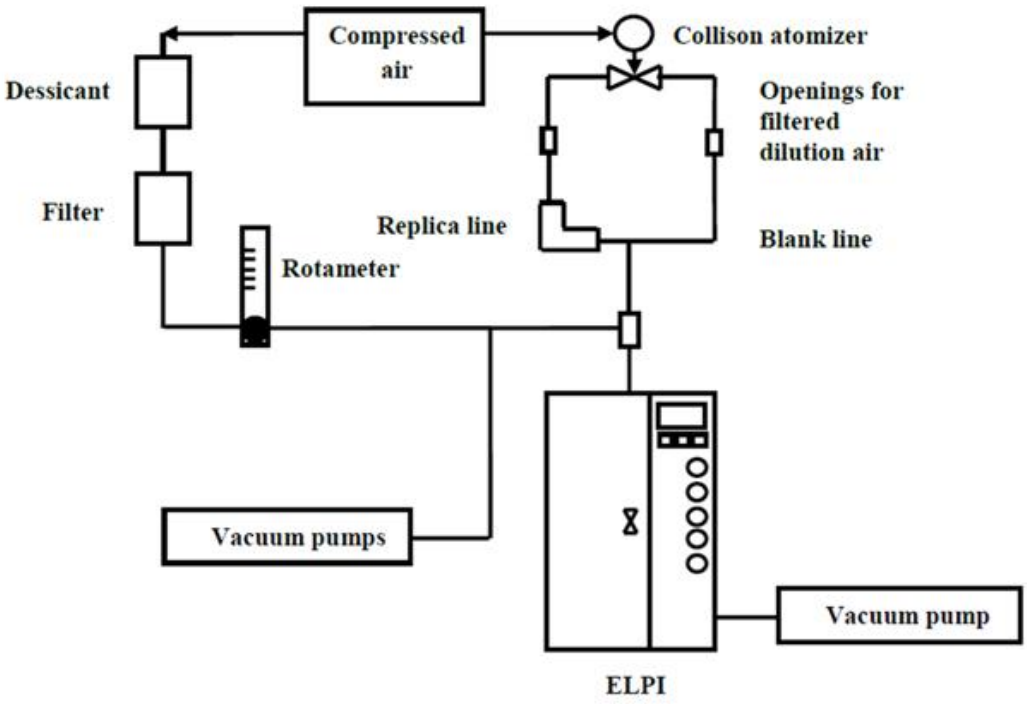

Figure 4.3 Schematic diagram of the experimental setup we used for measuring deposition of particles in oropharyngeal airway replicas of children and the 'Alberta Idealized Throat'.

We defined the deposition as the absolute difference in the number concentration of aerosol, at a given particle size and flow rate, penetrating through a tube with no replica and a tube with in-line replica. The number concentration and the size of particles were determined by an Electrical Low Pressure Impactor (ELPI, DEKATI, Finland). ELPI's built-in software was used to correct for diffusion and particle bounce and to record the number concentration at a current setting of 40,000 fA. Polydisperse jojoba oil (density 0.86 g/ml) particles were generated using a six-jet Collison atomizer (BGI Inc., USA). As previously noted (Golshahi *et al*., 2011), the deposition of particles smaller than 0.5 μm in diameter

is significantly affected by diffusion, unlike larger micrometer-sized particles. Also, the number of particles larger than 5.3 μm, emitted from our aerosol generator, was not large enough to allow meaningful data analysis. For these reasons, we only used the concentration data for the ELPI stages with aerodynamic cut sizes within 0.5- 5.3 μm at moderate flow rates, Q_1 and Q_2. The ELPI stage sizes thus considered were 0.5, 0.8, 1.3, 2.0, 3.2 and 5.3 μm. However, it should be noted that at higher flow rates the numbers of particles with larger sizes were too low due to the high losses that occurred in the lines; thus, we excluded 5.3 μm at Q_3, and both 3.2 and 5.3 μm at Q_4 and Q_5. Each single test was 5 minutes in duration, consisting of two one-minute samplings from the blank line, with a one-minute sampling from the replica line in between, and one minute stabilizing time after changing the direction of the gate valve. This additional stabilizing step was taken to exclude sudden changes in the concentration of aerosols.

To validate our method of deposition measurements, we initially tested our Idealized Alberta Throat using the setup detailed above. The average of five deposition measurements was used as a single data point, presented in the results section.

4.3. Results and Discussion

The deposition in the fabricated 'Alberta Idealized Throat' plastic replica was compared with previously-reported data (DeHaan and Finlay, 2001; Grgic *et al*., 2004; Zhou *et al*., 2011). Despite all the differences in the methodologies used

to measure the deposition in the Idealized Throat among all studies, our data was found to be in a good agreement with others (deposition measured by us differed by less than 5% from that reported elsewhere); this evidence convinced us that our deposition measurement method is acceptable. Therefore, we proceeded with obtaining deposition data with our children's replicas. Figure 4.4 shows deposition in the children's replicas versus the impaction parameter, $d_a^2 Q$, where d_a is the aerodynamic diameter of the particle and Q is the inhalation flow rate measured downstream of the replica.

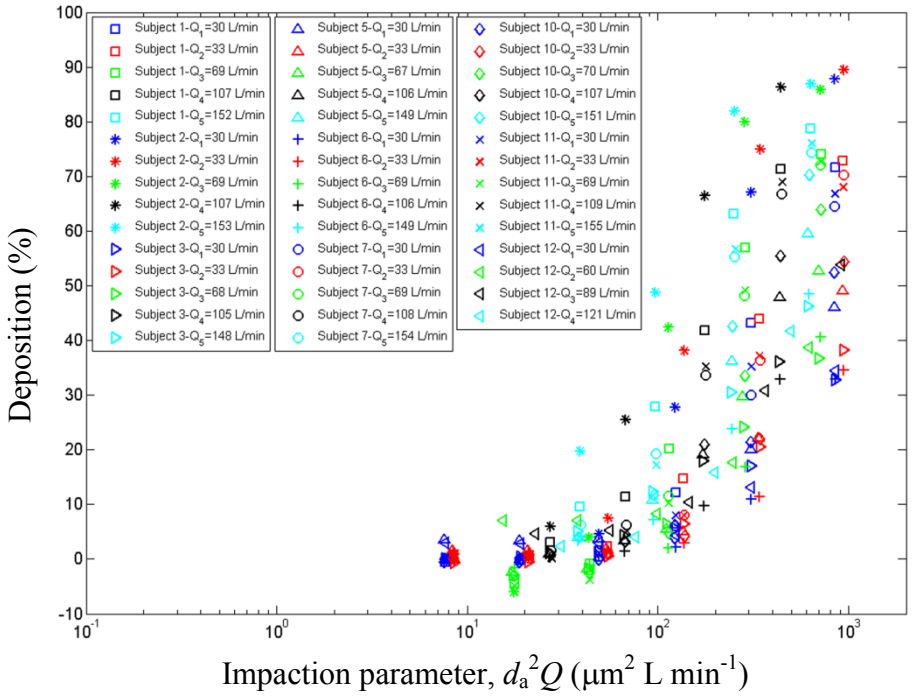

Figure 4.4 Deposition in children's replicas vs. the impaction parameter ($d_a^2 Q$) for flow rates of 30-150 L/min and particles in the aerodynamic size range of 0.5-5.3 μm.

Large scatter is observed in Figure 4.4 since the anatomical dimensions of the subjects have not been considered. To reduce this scatter, we included the dimensions of the airways in our analysis. In our previous studies with adults (Grgic *et al*., 2004), the use of the volume (V) and the length of a centerline (L) of the airway replica led to a minimized scatter, and as a result, the following curve-fit was given by Grgic *et al*. (2004) to predict the average deposition in the oral airways of adults:

$$\eta = [1 - 1/(11.5(\mathrm{StkRe}^{0.37})^{1.912} + 1)] \times 100 \tag{4.1}$$

where Stokes (Stk) and Reynolds (Re) numbers are defined as follows:

$$\mathrm{Stk} = \frac{\rho_p d_p^2 Q}{36\mu}\sqrt{\frac{\pi L^3}{V^3}} \tag{4.2}$$

$$\mathrm{Re} = \frac{2\rho Q}{\mu}\sqrt{\frac{L}{\pi V}} \tag{4.3}$$

In these equations, ρ_p is the density of the particle, ρ is the density of air, d_p is the particle diameter and μ is the dynamic viscosity of the air.

In Figure 4.5, we compare the deposition in our replicas with the deposition values estimated using the correlation developed for adults (Eq. 4.1), with the same x-axis containing the children's dimensions. This figure shows that including the children's geometrical information in the adults' deposition parameter (x-axis) somewhat reduces the scatter of deposition. However, the estimated deposition values from Eq. 4.1 underestimate the deposition among children. This discrepancy is probably due to the smaller oral airway dimensions of children compared to adults, which increases deposition to an extent that is not captured by extrapolating Eq. 4.1 to Stk, Re and x values associated with children.

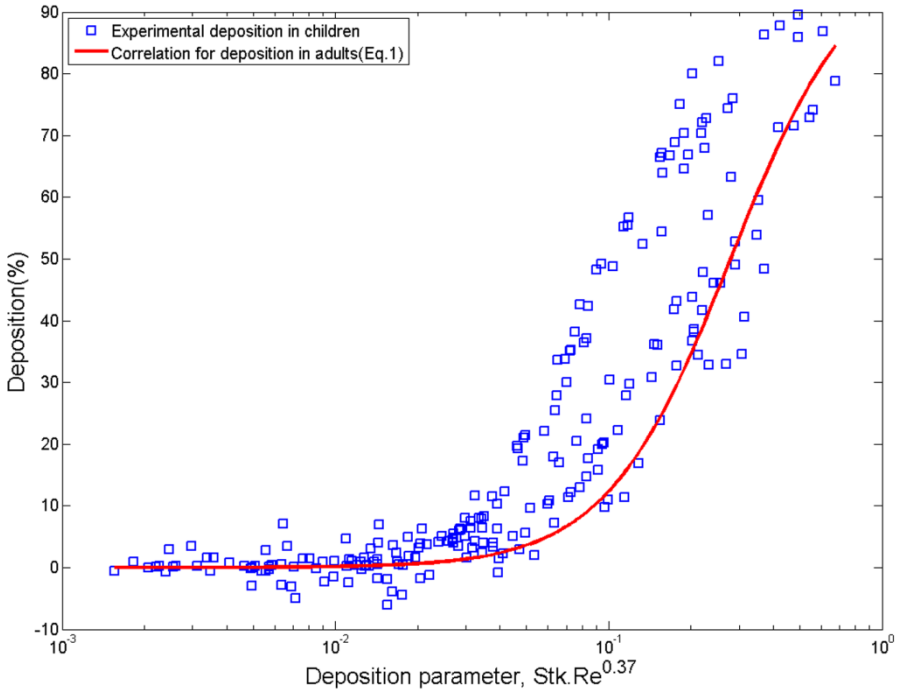

Figure 4.5 Comparison of the deposition in our children replicas with the estimated values using a correlation developed for adults by Grgic *et al*. (2004) (Eq. 4.1) when the x-axis contains the children's geometrical dimensions.

In order to further reduce the scatter, we developed a new least-squares curve-fit for children using a characteristic diameter, similar to the one used for adults (see above) in the form of $d_c=\sqrt{V/L}$. This diameter was used to calculate the Stokes and Reynolds numbers, defined as follows:

$$\mathrm{Re}=\frac{4\rho_{air}Q}{\pi\mu d_c} \tag{4.4}$$

$$\mathrm{Stk}=\frac{\rho_p {d_p}^2 C_c U}{18\mu d_c}=\frac{2\rho_{water} d_a^2 C_c Q}{9\pi\mu d_c^3} \tag{4.5}$$

where ρ_{air} (1.2 kg/m^3) is the density of air, ρ_{water} is the density of water (1000 kg/ m^3). C_c is the Cunningham slip correction factor. The subscripts 'p' and 'a' refer to the particle diameter (d_p) and aerodynamic diameter (d_a), respectively. C_c is defined as follows:

$$C_c = 1 + 2.52\lambda / d_p \tag{4.6}$$

where λ is the mean free path of air, which is 0.067 μm at the standard room conditions.

Figure 4.6 shows the correlation developed based on the approach explained above. Although the scatter has been further decreased compared to Figure 4.5, the R-squared value is still relatively poor (0.84).

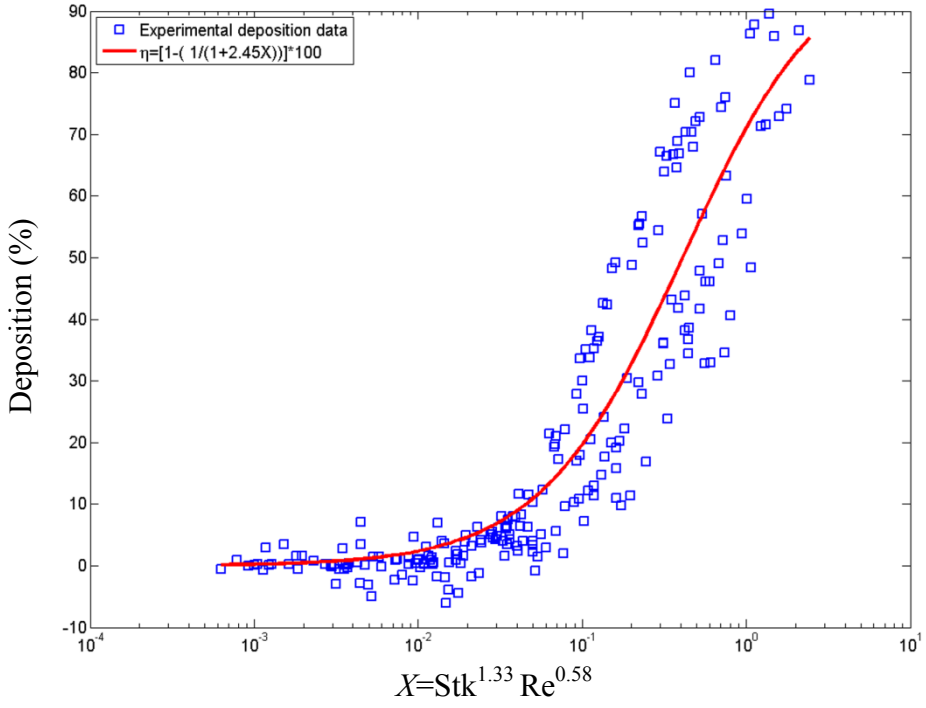

Figure 4.6 Deposition of micrometer-sized particles in oropharyngeal replicas of children vs. non-dimensional deposition parameter (X) as a combination of

Stokes and Reynolds numbers that include a characteristic diameter defined as $d_c = \sqrt{V/L}$.

In an attempt to further reduce the existing scatter of the deposition data apparent in Figure 4.6, we used the diameter $d_c = V/A_s$ in the calculation of the Stokes and Reynolds numbers using Eqs. 4.4 and 4.5. The parameter A_s is the total surface area of the airways. We considered this characteristic diameter since it successfully reduced the scatter in the deposition of inhaled micrometer-sized particles among infants (Storey-Bishoff *et al*., 2008). Figure 4.7 displays the developed correlation using this characteristic diameter. A high *R*-squared value of 0.94 was achieved using this approach.

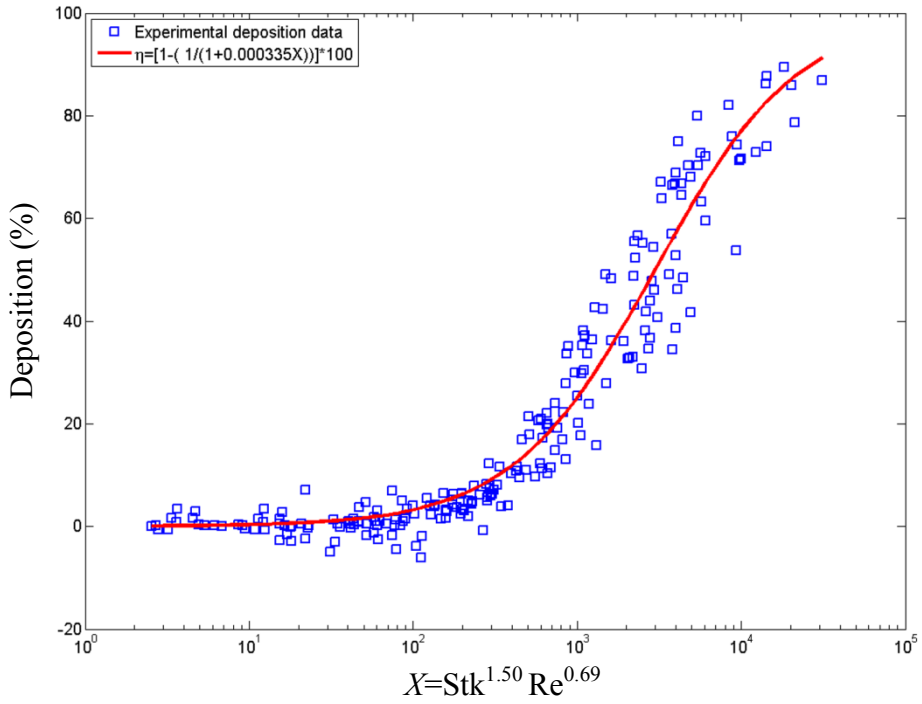

Figure 4.7 The deposition of micrometer-sized particles in oropharyngeal replicas of children vs. non-dimensional deposition parameter, X, as a combination of Stokes and Reynolds numbers. These numbers include a characteristic diameter defined as $d_c = V/A_s$.

It is speculated that the reason behind the success of the latter characteristic diameter in minimizing the scatter of deposition data lies in its increased sensitivity to the complexity of the geometry of the airways i.e. airway surface area (A_s) is more sensitive than the airway length (L) to differences in airway geometry between subjects. The complex cross-section of airways influences the dynamics of the fluid passing through, and consequently, the deposition of the particles. Although the defined characteristic diameter ($d_c = V/A_s$) results in a better predictive correlation, compared with $d_c = \sqrt{V/L}$,

in practice $\sqrt{V/L}$ may be preferred since the volume and the length of the airways can be measured *in vivo* by acoustic pharyngometry.

4.4 Conclusions

Large scatter was observed in the deposition of micrometer-sized particles in oropharyngeal airway replicas of children when intersubject variations in anatomical dimensions of the airways were not considered. The following correlations (Eqs. 7 and 8) can be used to reduce this scatter using either of the two subject specific characteristic diameters, $d_{c1} = \sqrt{V/L}$ or $d_{c2} = V / A_s$, where V, L and A_s are the given subject's oral airway volume, length and surface area, respectively:

$$\eta_1 = [1 - 1/(2.45(\mathrm{Stk}^{1.33}\mathrm{Re}^{0.58}) + 1)] \times 100 \tag{4.7}$$

$$\eta_2 = [1 - 1/(0.000335(\mathrm{Stk}^{1.5}\mathrm{Re}^{0.69}) + 1)] \times 100 \tag{4.8}$$

where Reynolds number (Re) is defined in Eq. 4.4 and Stokes number (Stk) is defined in Eq. 4.5. The average diameters for these equations are d_{c1}=1.46 ± 0.17 cm and d_{c2}=0.27 ± 0.03 cm for the nine children in our study. Of these two correlations, Eq. 4.8 resulted in a better fit. These correlations may be useful for better subject specific estimation of the delivered drug dose to the lungs of children using aerosol inhalers, such as pMDIs with holding chambers and DPIs.

4.5 Bibliography

Becquemin, M. H., Yu, C. P., Roy, M., and Bouchikhi, A. (1991). Total deposition of inhaled particles related to age: comparison with age dependent model calculations. *Radiation Protection Dosimetry*, 38, 23-28.

Bennett, W. D., and Zeman, K. L. (1998). Deposition of fine particles in children spontaneously breathing at rest. *Inhalation Toxicology*, 10, 831-842.

Bennett, W. D., and Zeman, K. L. (2004). Effect of body size on breathing pattern and fine-particle deposition in children. *Journal of Applied Physiology*, 97, 821-826.

Borgstrom, L. (1999). *In vitro*, *ex vivo*, *in vivo veritas*. *Allergy*, 54, 88-92.

Borgstrom, L. Olsson, B., and Thorsson, L. (2006). Degree of throat deposition can explain the variability in lung deposition of inhaled drugs. *Journal of Aerosol Medicine*, 19(4), 473-483.

Bowes, S. M., and Swift, D. L. (1989). Deposition of inhaled particles in the oral airway during oronasal breathing. *Aerosol Science and Technology*, 11, 157-167.

Cass, L. M. R., Brown, J., Pickford, M., Fayinka, S., Newman, S. P., Johansson, C. J., and Bye, A. (1999). Pharmacoscintigraphic evaluation of lung deposition of inhaled zanamivir in healthy volunteers. *Clinical Pharmacokinetics*, 36(Suppl. 1), 21-31.

Chan, T. L., and Lippmann, M. (1980). Experimental measurements and empirical modeling of the regional deposition of inhaled particles in humans. *American Industrial Hygiene Association Journal*, 41, 399-409.

Cheng, Y. S., Zhou, Y., and Chen, T. B. (1999). Particle deposition in a cast of human oral airways. *Aerosol Science and Technology*, 31, 286-300.

Cheng, Y. S., Yazzie, D., and Zhou, Y. (2001). Respiratory deposition patterns of salbutamol pMDI with CFC and HFA-134a formulations in a human airway replica. *Journal of Aerosol Medicine*, 14(2), 255-266.

Cheng, Y. S. (2003). Aerosol Deposition in the Extrathoracic Region. *Aerosol Science and Technology*, 37, 659-671.

DeHaan, W. H., and Finlay, W. H. (2001). *In vitro* monodisperse aerosol deposition in a mouth and throat with six different inhalation devices. *Journal of Aerosol Medicine*, 14(3), 361-367.

DeHaan, W. H., and Finlay, W. H. (2004). Predicting extrathoracic deposition from dry powder inhalers. *Journal of Aerosol Science*, 35(3), 309-331.

Devadason, S. G., Everard, M. L., MacEarlan, C., Roller, C., Summers, Q. A., Swift, P., Borgstrom, L., and Le Souef, P. N. (1997). Lung deposition from the Turbuhaler in children with cystic fibrosis. *The European Respiratory Journal*, 10, 2023-2028.

Devadason, S. G., Huang, T., Walker, S., Troedson, R., and Le Souef, P. N. (2003). Distribution of technetium-99m-labelled QVAR™ delivered using an Autohaler™ device in children. *The European Respiratory Journal*, 21, 1007-1011.

Emmett, P. C., Aitken, R. J., and Hannan, W. J. (1982). Measurements of the total and regional deposition of inhaled particles in the human respiratory tract. *Journal of Aerosol Science*, 13(6), 549-560.

Finlay, W. H., and Martin, A. R. (2008). Recent advances in predictive understanding of respiratory tract deposition. *Journal of Aerosol Medicine*, 21(2), 1-17.

Foord, N., Black, A., and Walsh, M. (1978). Regional deposition of 2.5–7.5 μm diameter inhaled particles in healthy male non-smokers. *Journal of Aerosol Science*, 9, 343-357.

Golshahi, L., Noga, M. L., Thompson, R. B., and Finlay W. H. (2011). *In vitro* deposition measurement of inhaled micrometer-sized particles in extrathoracic airways of children and adolescents during nose breathing. *Journal of Aerosol Science*, 42(7), 474-488.

Grgic, B., Finlay W. H., Burnell, P. K. P., Heenan, A. F. (2004a). *In vitro* intersubject and intrasubject deposition measurements in realistic mouth-throat geometries. *Journal of Aerosol Science*, 35, 1025-1040.

Grgic, B., Finlay W. H., Heenan, A. F. (2004b). Regional aerosol deposition and flow measurements in an idealized mouth and throat. *Journal of Aerosol Science*, 35, 21-32.

Grgic, B., Martin, A. R., and Finlay W. H. (2006). The effect of unsteady flow rate increase on *in vitro* mouth-throat deposition of inhaled boluses. *Journal of Aerosol Science*, 37, 1222-1233.

Lippmann, M., and Albert, R. E. (1969). The effect of particle size on the regional deposition of inhaled aerosols in the human respiratory tract. *American Industrial Hygiene Association Journal*, 30, 257-275.

Martonen, T. B., and Lowe, J. (1983). Assessment of aerosol deposition patterns in human respiratory tract casts. *In* Marple, V. A., and Liu, B. Y. H., eds. Aerosols in the mining and industrial work environments. Ann Arbor Science Publishers, Ann Arbor, 151-164.

McRobbie, D. W., Pritchard, S., and Quest, R. A. (2003). Studies of the human oropharyngeal airspaces using magnetic resonance imaging. I. Validation of a three-dimensional MRI method for producing *ex vivo* virtual and physical casts of the oropharyngeal airways during inspiration. *Journal of Aerosol Medicine*, 16(4), 401-415.

Pritchard, J. N., Black, A., Foord, N., Walsh, M. (1981). A comparison of the regional deposition of monodisperse polystyrene aerosols in the respiratory tracts of healthy male smokers and non-smokers. *Journal of Aerosol Science*, 12(3), Page 214.

Pritchard, S. E., and McRobbie, D. W. (2004). Studies of the human oropharyngeal airspaces using magnetic resonance imaging. II. The use of three-dimensional gated MRI to determine the influence of mouthpiece diameter and resistance of inhalation devices on the oropharyngeal airspace geometry. *Journal of Aerosol Medicine*, 17(4), 310-324.

Roller, C. M., Zhang, G., Troedson, R. G., Leach, C. L., Le Souef, P. N., and Devadason, S. G. (2007). Spacer inhalation technique and deposition of extrafine aerosol in asthmatic children. *The European Respiratory Journal*, 29, 299-306.

Schiller-Scotland, C. H. F., Hlawa, R., Gebhart, J., Wonne, R., and Heyder, J. (1992) Total deposition of aerosol particles in the respiratory tract of children

during spontaneous and controlled mouth breathing. *Journal of Aerosol Science*, 23(Suppl. 1), S457-S460.

Stahlhofen, W., Gebhart, J., and Heyder, J. (1980). Experimental determination of the regional deposition of aerosol particles in the human respiratory tract. *American Industrial Hygiene Association Journal*, 41(6): 385-398a.

Stahlhofen, W., Gebhart, J., Heyder, J., Scheuch, G. (1983). New regional deposition data of the human respiratory tract. *Journal of Aerosol Science*, 14(3), 186-188.

Stahlhofen, W., Gebhart, J., Heyder, J., Scheuch, G., Juraske, P. (1984). Particle deposition in extrathoracic airways of healthy subjects and of patients with early stages of laryngeal carcinoma. *Journal of Aerosol Science*, 15(3), 215-217.

Stahlhofen, W., Rudolf, G., and James, A. C. (1989). Intercomparison of experimental regional aerosol deposition data. *Journal of Aerosol Medicine*, 2(3), 285-308.

Stapleton, K. W., Guentsch, E., Hoskinson, M. K., and Finlay, W. H. (2000). On the suitability of k-ε turbulence modeling for aerosol deposition in the mouth and throat: a comparison with experiment. *Journal of Aerosol Science*, 31, 739-749.

Storey-Bishoff, J., Noga, M., and Finlay, W. H. (2008). Deposition of Micrometer-Sized Aerosol Particles in Infant Nasal Airway Replicas. *Journal of Aerosol Science*, 39, 1055–1065.

Svartengren, M., Falk, R., Linnman, L., Philipson, K., and Camner, P. (1987). Deposition of large particles in human lung. *Experimental Lung Research*, 12(1), 75-88.

Svartengren, K., Lindestad, A. P., Svartengren, M., Bylin, G., Philipson, K., and Camner, P. (1994). Deposition of inhaled particles in the mouth and throat of asthmatic subjects. *European Respiratory Journal*, 7, 1467-1473.

Svartengren, K., Lindestad, A. P., Svartengren, M., Philipson, K., Bylin, G., and Camner, P. (1995). Added external resistance reduces oropharyngeal deposition and increases lung deposition of aerosol particles in asthmatics. *American Journal of Respiratory and Critical Care Medicine*, 152(1), 32-37.

Swift, D. L. (1992). Apparatus and method for measuring regional distribution of therapeutic aerosols and comparing delivery systems. *Journal of Aerosol Science*, 23(Suppl. 1), S495-S498.

Zhou, Y., Sun, J., and Cheng Y. S. (2011). Comparison of deposition in the USP and physical mouth-throat models with solid and liquid particles. *Journal of Aerosol Medicine and Pulmonary Drug Delivery*, 24, 1-8.

CHAPTER 5 : AN IDEALIZED CHILD THROAT THAT MIMICS AVERAGE PEDIATRIC OROPHARYNGEAL DEPOSITION

A very similar version of this chapter is in press as an Aerosol Research Letter: Golshahi, L., and Finlay, W. H. (2012). An Idealized Child Throat that Mimics Average Pediatric Oropharyngeal Deposition. *Aerosol Science and Technology*, 46(5), i-iv.

5.1 Introduction

Extrathoracic deposition plays an important role in determining the total lung dose (TLD) of pharmaceutical inhalers (Borgstrom *et al*. 2006; Stahlhofen *et al*. 1989). Because of possible fluid mechanic interactions between the oral cavity and the flow exiting an inhaler (DeHaan and Finlay 2004), geometric mimics of the mouth-throat are useful in aiding inhaler design. Thus, there has been a long-term interest in simplifying the testing of drug delivery devices by having a simple geometry that can be used to mimic average extrathoracic deposition among adults and children.

In vitro methods using physical oral airway models have been successful in mimicking TLD for adult subjects (Delvadia *et al*. 2012; Ehtezazi *et al*. 2005; Finlay and Martin 2008). The use of a single geometry such as the United States Pharmacopeia (USP) induction port to mimic throat deposition and thereby measure TLD has been popular for testing inhalers due to its relative simplicity. However, the USP throat is far from resembling a realistic human airway; thus, it

has not been successful in replicating mouth-throat deposition of gently delivered aerosols (Srichana *et al*. 2000; Zhang *et al*. 2007; Zhou *et al*. 2011). To address these limitations of the highly simplified USP throat, an idealized adult throat, the 'Alberta Idealized Throat', has previously been developed by our group based on the actual geometry of human extrathoracic airways (Stapleton *et al*. 2000). This throat has been successful in replicating extrathoraic deposition (Zhang *et al*. 2007; Grgic *et al*. 2004 a, b; Zhou *et al*. 2011) and is commercially available (Copley Scientific, UK).

Due to recent interest in optimizing pediatric drug delivery, pediatric models are needed for *in vitro* testing. Studies have been done by our group (Storey-Bishoff *et al*. 2008; Golshahi *et al*. 2011a) and others (Janssens *et al*. 2001; Minocchieri *et al*. 2008; Corcoran *et al*. 2003; Laube *et al*. 2010) to mimic pediatric deposition with airway models, mostly among infants and young children who are nose breathers. However, as for adults, there is a need for a single idealized model to consistently predict average pediatric deposition. Previously, MRI scans of children, younger than five years old, have been used to modify the laryngeal region of the Alberta Idealized Throat to replicate the oral airway of a five year old child (Wachtel *et al*. 2010). This modified idealized throat was used to test Respimat® Soft Mist™ inhalers (Boehringer Ingelheim, Germany) with and without a holding chamber. The capability of this non-uniformly modified idealized throat to give average deposition among children younger than five years old remains to be examined. Since inhalers are more common among older children, we recently completed a systematic study to

examine and reduce the intersubject variability in deposition of micrometer-sized particles in oral airways of children aged 6-14 years (Golshahi *et al*. 2011b). The present communication examines the possibility of uniformly scaling the Alberta Idealized Throat to replicate average deposition among children with a single simplified geometry. This scaling is based on our recent measurements of the dimensions of children's oropharyngeal airways and deposition of micrometer-sized particles in replicas of these airways (Golshahi *et al*. 2011b). The development of such a simple geometry can be considered a major advance in the field of pediatric drug delivery since it will provide a standard platform for optimizing the treatment of children with inhaled pharmaceutical aerosols.

5.2 Methods

In our recent study with oropharyngeal airway replicas of children, the characteristic diameter that resulted in the most reduction in scatter due to intersubject variability was the ratio of the volume to the surface area of the airway ($d_c=V/A_s$) (Golshahi *et al*. 2011b). By examining CT scans of oral airways of children and adults, it appears that the main geometrical features of the child and adult airways are similar. Thus, it would seem logical that scaling the Alberta Idealized Throat by a uniform factor based on the average characteristic diameter would be suitable to mimic average oral deposition among children. The scale factor of 0.62 was thus used for scaling the Adult Idealized Throat in Magics software (Materialise, USA) based on the above reasoning. This scaling resulted in a characteristic diameter (V/A_s) of 2.7 mm, which is equal to the average of the

nine tested child replicas in our recent study (Golshahi *et al*. 2011b). Figure 5.1 shows our new 'Idealized Child Throat' and its main dimensions (i.e. a=62.7 mm, b=40.6 and c=38.7 mm) that are similar to the average of the main dimensions of our nine realistic children replicas (a=59.4±4.9, b=45.9±8.1 and c=46.2±3.9 mm). A 3D printer (Invision SR, 3D Systems, USA) was used to build the Idealized Child Throat using Visijet SR200, which is an acrylic material. A cylindrical shaped adaptor was made to connect the inlet of the throat to the tubing in the experimental setup. The inner diameter of that cylinder was 11 mm.

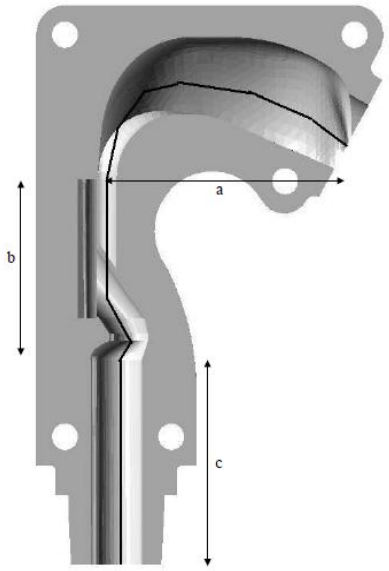

Figure 5.1 Schematic of the Idealized Child Throat. The lengths of the sections a, b and c (62.7, 40.6 and 38.7 mm, respectively) are the summations of polylines shown in each section.

The Idealized Child Throat was then tested in the same setup that we used for measuring deposition of micrometer-sized particles in the oral airways of children. The details of such measurements are given in Golshahi *et al*. 2011b. In

brief, an Electrical Low Pressure Impactor (Dekati, Finland) was used for measuring the size distribution of polydisperse jojoba oil aerosols, generated by a six jet Collison atomizer (BGI Inc., USA). The absolute difference between number concentration in the line with no replica and the line with the replica was defined as the deposition for each particle size, given as the cut sizes of ELPI, which were 0.5, 0.8, 1.3, 2.0, 3.2 and 5.3 micrometers. The tested flow rates were 30, 60, 90 and 120 L/min, which were generated using two vacuum pumps in parallel and recorded using a digital mass flow meter (TSI Model 4043, USA) for both lines (blank and replica line). At 60 L/min the number concentration of 5.3 μm particles was too low to be considered and at 90 and 120 L/min the number of 3.2 and 5.3 μm were too low; thus, those sizes were excluded at the associated flow rates. The variable dilution air, as a result of the resistance of the replica compared to the blank line, was corrected similar to our previous work (Storey-Bishoff *et al*. 2008; Golshahi *et al*. 2011 a, b). The replica was also removed and the difference between the number concentration through the blank line and the replica line was measured and defined as the baseline, which was then subtracted from the total deposition. Five measurements were made for each data point.

5.3 Results and Discussion

Figure 5.2 shows the deposition of particles in the "Idealized Child Throat" versus the impaction parameter (d_a^2Q, where d_a is aerodynamic diameter and Q is inhalation flow rate) compared with the nine children (aged 6-14 years) in our previous study (Golshahi *et al*. 2011b). It is observed that deposition in the

Idealized Child Throat lies in the middle of the data and may be used to mimic average deposition among children in that study.

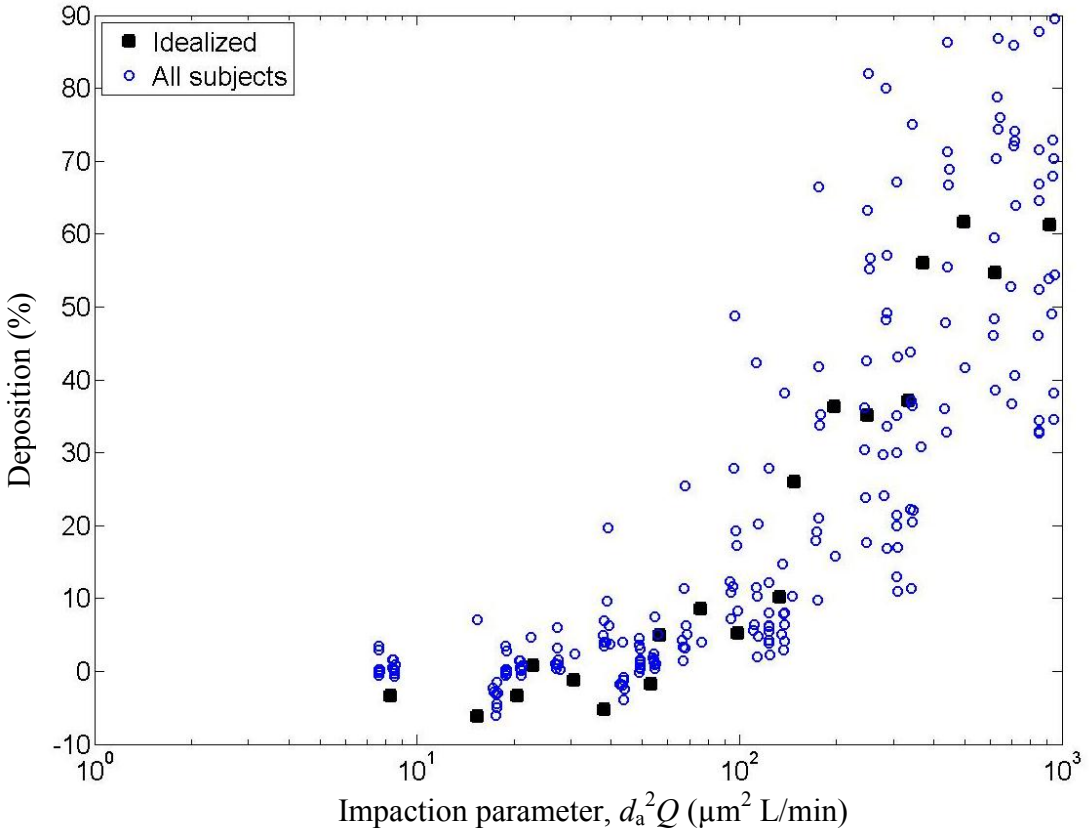

Figure 5.2 The deposition of orally inhaled micrometer-sized particles in the Idealized Child Throat versus the impaction parameter compared to that of nine children replicas in our previous study (Golshahi *et al*. 2011b).

Deposition in the Idealized Child Throat and the replicas of nine children's airways (Golshahi *et al*. 2011b) is plotted in Figure 5.3 versus a different deposition parameter, a combination of Stokes (Stk) and Reynolds (Re) numbers, which includes the characteristic diameter of V/A_s. This deposition parameter

successfully minimized the scatter of the deposition data among our child airway replicas (Golshahi *et al*. 2011b). It appears that deposition in the Idealized Child Throat for the deposition parameter in the mid range of 600-2000 is slightly (~10%) higher than the average predictive correlation given in Golshahi *et al*. 2011b for nine children 6-14 years old. This is presumably because the Idealized Child Throat is a simplified geometry and does not include all of the complex features of the anatomical airways. Hence, this simplification may affect the dynamics of aerosol and flow in a way that is reflected in the data. This slight overestimation was similarly observed in the data with our Adult Idealized Throat (Grgic *et al*. 2004 a). Despite this overestimation, however, the adult Alberta Idealized Throat was successful in replicating average *in vivo* deposition (Zhang *et al*. 2007; Grgic *et al*. 2004 a, b; Zhou *et al*. 2011).

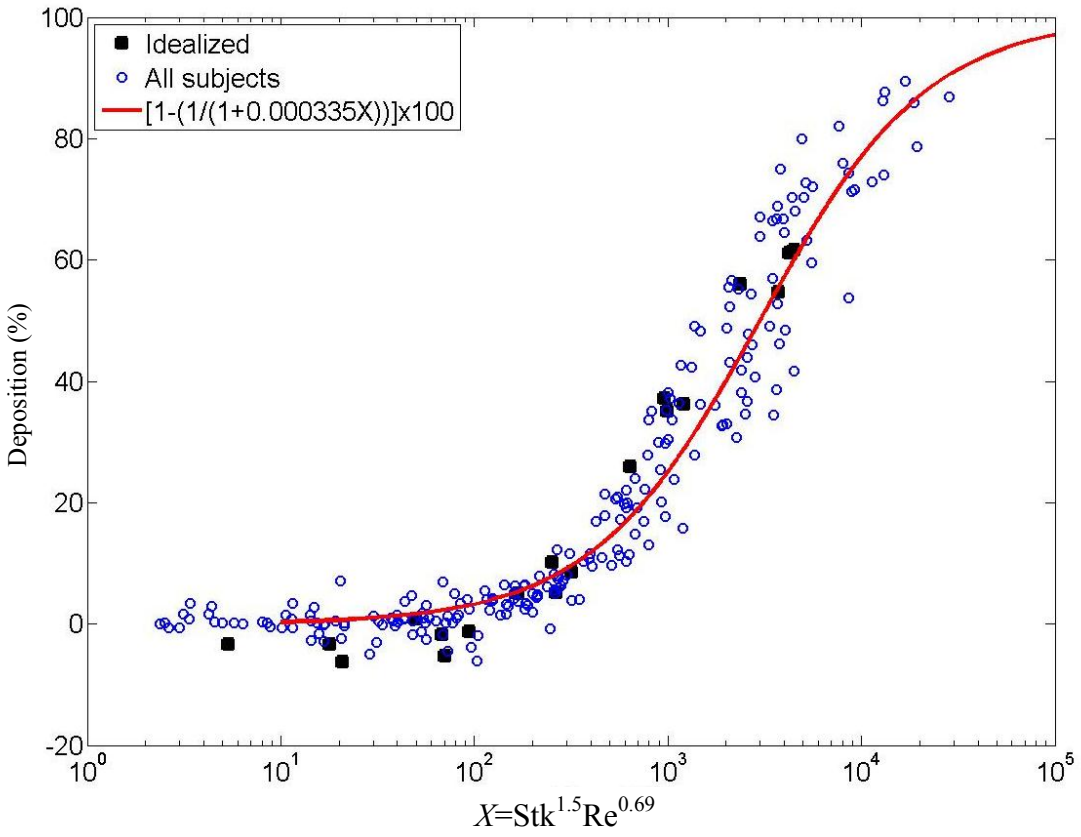

Figure 5.3 Deposition in the Idealized Child Throat and children's anatomically accurate replicas (Golshahi *et al*. 2011b) versus the deposition parameter X=Stk$^{1.5}$Re$^{0.69}$ where Stk and Re are Stokes and Reynolds numbers that use a subject specific length scale V/A_s.

5.4 Conclusions

Uniform scaling of the adult Alberta Idealized Throat by a factor of 0.62 resulted in an Idealized Child Throat with a characteristic diameter V/A_s that is equal to the average characteristic diameter of the children's airways (i.e. 2.7 mm) in our previous study (Golshahi *et al*. 2011b). This Idealized Child Throat mimics the average deposition during oral inhalation among children 6-14 years

old in that study. Thus, this geometry may be useful for substantially simplifying experimental studies involving the design and development of inhalers for oral inhaled aerosol drug delivery to the lungs in child patient populations.

5.5 Bibliography

Borgstrom, L., Olsson, B., and Thorsson, L. (2006). Degree of throat deposition can explain the variability in lung deposition of inhaled drugs. *Journal of Aerosol Medicine and Pulmonary Drug Delivery*, 19, 473-483.

Corcoran, T.E., Shortall, B.P., Kim, I.K., Meza, M.P., Chigier, N. (2003). Aerosol drug delivery using heliox and nebulizer reservoirs: Results from an MRI-based pediatric model. *Journal of Aerosol Medicine and Pulmonary Drug Delivery*, 16, 365-271.

DeHaan, W. H., and Finlay, W. H. (2004). Predicting extrathoracic deposition from dry powder inhalers. *Journal of Aerosol Science*, 35, 309-331.

Delvadia, R. R., Longest, P. W., and Byron P. R. (2012). *In vitro* tests for aerosol deposition. I: scaling a physical model of the upper airways to predict drug deposition variation in normal humans. *Journal of Aerosol Medicine and Pulmonary Drug Delivery*, 25(1), 32-40.

Ehtezazi, T., Southern, K. W., Allanson, D., Jenkinson, I., and O'Callaghan, C. (2005). Suitability of the upper airway models obtained from MRI studies in simulating drug lung deposition from inhalers. *Pharmaceutical Research*, 22, 166-170.

Finlay, W. H., and Martin, A. R. (2008). Recent advances in predictive understanding of respiratory tract deposition. *Journal of Aerosol Medicine and Pulmonary Drug Delivery*, 21, 189-205.

Golshahi, L., Noga M. L., Thompson, R. B., and Finlay W.H. (2011a). *In vitro* deposition measurement of inhaled micrometer-sized particles in nasal airways of children and adolescents during nose breathing. *Journal of Aerosol Science*, 42, 447-488.

Golshahi, L., Noga, M. L., and Finlay, W. H. (2011b). Deposition of inhaled micrometer-sized particles in oropharyngeal airway replicas of children at constant flow rates. Submitted to *Journal of Aerosol Science*.

Grgic, B., Heenan, A. F., Burnell, P.K.P., and Finlay, W. H. (2004a). *In vitro* intersubject and intrasubject deposition measurements in realistic mouth-throat geometries. *Journal of Aerosol Science*, 35, 1025-1040.

Grgic, B., Finlay, W. H., and Heenan, A. F. (2004b) Regional aerosol deposition and flow measurements in an idealized mouth and throat. *Journal of Aerosol Science*, 35, 21-32.

Janssens, H.M., De Jongste, J.C., Fokkens, W.J., Robben, S.G.F., Wouters, K., Tiddens, H.A.W.M. (2001). The Sophia anatomical infant nose-throat (saint) model: A valuable tool to study aerosol deposition in infants. *Journal of Aerosol Medicine and Pulmonary Drug Delivery*, 14, 433-441.

Laube, B.L., Sharpless, G., Shermer, C., Nasir, O., Sullivan, V., Powell, K. (2010). Deposition of albuterol aerosol generated by pneumatic nebulizer in the

Sophia Anatomical Infant Nose-Throat (SAINT) model. *Pharmaceutical Research*, 27,1722-1729.

Minocchieri, S., Burren, J.M., Bachmann, M.A., Stern, G., Wildhaber, J., Buob, S., Schindel, R., Kraemer, R., Frey, U.P., Nelle, M. (2008). Development of the premature infant nose throat-model (PrINT-Model)-an upper airway replica of a premature neonate for the study of aerosol delivery. *Pediatric Research*, 64,141-146.

Srichana, T., Martin, G., and Marriott, C. (2000). A human oral-throat cast integrated with a twin-stage impinger for evaluation of dry powder inhalers. *Journal of Pharmacy and Pharmacology*, 52, 771-778.

Stahlhofen, W., Rudolf, G., and James, A.C. (1989). Intercomparison of experimental regional aerosol deposition data. *Journal of Aerosol Medicine and Pulmonary Drug Delivery*, 2, 285-308.

Stapleton, K. W., Guentsch, E., Hoskinson, M. K., and Finlay W. H. (2000). On the suitability of the k-ε turbulence model for aerosol deposition in the mouth and throat: a comparison with experiments. *Journal of Aerosol Science*, 31, 739-749.

Storey-Bishoff, J., Noga, M. and Finlay, W. H. (2008). Deposition of micrometer-sized aerosol particles in infant nasal airway replicas. *Journal of Aerosol Science*, 39, 1055-1065.

Wachtel, H., Bickmann, D., Breitkreutz, J., Langguth, P. (2010). Can Pediatric Throat Models and Air Flow Profiles Improve Our Dose Finding Strategy. In *Respiratory Drug Delivery 2010*, pp. 195-204, ed. Dalby, R.N., Byron, P. R.,

Peart, J., Suman, J. D., Farr, S. J., Young, P.M., Davis Healthcare, Rivergrove, Illinois.

Zhang, Y., Gilbertson, K., and Finlay, W. H. (2007). *In vivo-in vitro* comparison of deposition in three mouth-throat models with Qvar and Turbuhaler inhalers. *Journal of Aerosol Medicine and Pulmonary Drug Delivery*, 20, 227-35.

Zhou, Y., Sun, J., Cheng, Y. S. (2011). Comparison of deposition in the USP and physical mouth-throat models with solid and liquid particles. *Journal of Aerosol Medicine and Pulmonary Drug Delivery*, 24(6), 277-284.

CHAPTER 6 : COMPARISON OF THE LUNG DOSE IN ADULTS AND CHILDREN USING THE DEVELOPED CORRELATIONS FOR EXTRATHORACIC DEPOSITION

A similar version of this chapter's analyses will appear in *Respiratory Drug Delivery* 2012 and is reprinted with permission:
Finlay, W. H., Golshahi, L., and Noga, M. L. (2012). New validated extrathoracic and pulmonary deposition models for infants and children. Accepted to appear in Respiratory Drug Delivery 2012 (ISBN Volume 3, 1-933722-59-2), Richard N. Dalby, Peter R. Byron, Joanne Peart, Stephen J. Farr, Julie D. Suman and Paul Young, Editors, Davis Healthcare, River Grove, Illinois (May, 2012).

6.1 Introduction

Several competing factors determine the fate of the inhaled medications among pediatric subjects. Smaller extrathoracic airways of children raise the expectation of higher deposition during inhalation; however, the effect of the size of airways is counterbalanced by the lower inhalation flow rate of children, which lowers the chance of impaction of particles on the surfaces of airways. It is equally important to consider that the common fashion for drug dose administration involves either the body mass or the body surface area of the subjects; thus, the smaller body size of the pediatric subjects should be considered in studies comparing the total lung dose among various age groups.

To address the above uncertainties, the possibility of combining all of the available extrathoracic correlations to perform a comparison of lung dose among infants, children and adults is explored in this brief note. In previous chapters, the development of new correlations to predict the deposition of inhalable aerosols in the extrathoracic airways of children was explained in detail. Similar correlations have previously been developed in our group for adults (Grgic *et al*., 2004). It is hoped that combining such correlations in the form of a comparative study can be useful in giving us a perspective on extending the current knowledge of drug dose administration in adults to yet not fully explored pediatric population.

6.2 Methods

The predictive correlations and their required parameters are listed in Table 6.1. The average height, weight and tidal breathing flow rates have been taken from the International Commission on Radiological Protection (ICRP, 1994). Body surface area (BSA) was calculated using Eq. 6.1 based on a study by Mosteller (1987).

$$\text{BSA } (\text{m}^2) = \sqrt{H(\text{cm}) \times W(\text{kg})} \tag{6.1}$$

Lung dose (LD) fraction was estimated by subtracting the extrathoracic (ET) deposition fraction from the inhaled dose as follows:

$$\text{LD}=1-\text{ET} \tag{6.2}$$

The exhaled fraction was assumed negligible considering the breath hold for the oral inhalation cases, which is typical during the use of single breath inhalers. For

nasal applications, the exhaled fraction is also reasonably negligible (Hoffmann *et al*. 1989).

Table 6.1 List of the developed extrathoracic deposition equations and their related parameters and references. Parameters V, L and A_s are the volume, centerline length and surface area of the airways, respectively.

Subject	Weight (kg)	Height (cm)	BSA (m^2)	Airway Characteristic Dimension	Flow Rates (L/min)	Extrathoracic Deposition Fraction η	Ref.
Adult male	73	176	1.89	D= $\sqrt{V/L}$ = 2.0 cm	30, 60, 90	$1-\frac{1}{11.5\mathrm{Stk}^{1.912}\mathrm{Re}^{0.707}+1}$	Grgic *et al*. 2004
Adult female	60	163	1.65	D= $\sqrt{V/L}$ = 2.0 cm	30, 60, 90	$1-\frac{1}{11.5\mathrm{Stk}^{1.912}\mathrm{Re}^{0.707}+1}$	Grgic *et al*. 2004
10 yr. old child oral inhalation	33	138	1.12	D=V/A_s= 0.27 cm	30, 60, 90	$1-\frac{1}{1+0.000335\mathrm{Stk}^{1.50}\mathrm{Re}^{0.69}}$	Chapter 4
10 yr. old child nasal tidal inhalation	33	138	1.12	D=A_s/L= 9.0 cm	12.7	$1-\left(\frac{4.21\times10^{-3}}{4.21\times10^{-3}+\mathrm{Stk}^{1.25}\mathrm{Re}^{1.32}}\right)^{0.55}$	Chapter 3
1 year old infant nasal tidal inhalation	10	75	0.46	D=V/A_s= 0.12 cm	8.8	$1-\left(\frac{2.164\times10^{5}}{2.164\times10^{5}+\left(\mathrm{Re}^{1.118}\mathrm{Stk}^{1.057}\right)}\right)^{0.851}$	Storey-Bishoff 2008

6.3 Results and Discussion

Figure 6.1 shows the calculated lung dose using Eq. 6.1 and the correlations given in Table 6.1 versus the aerodynamic particle size. All the lung dose data in this figure have been normalized by body mass and the adult inhaled

dose. The flow rate of 60 L/min was used for the calculation of constant-flow cases and the flow rates given in Table 6.1 were used for other age groups and breathing paths. The actual lung dose can be obtained by multiplying the values given in *y*-axis of Figure 6.1 by the adult inhaled dose.

Figure 6.1 illustrates that the 1-year old infant's lung dose is approximately triple the lung dose of an adult, while a 10-year old child breathing tidally through the nose receives almost double the adult dose. This observed trend is due to the large difference in the body mass of the studied age groups. When the 10-year old child breathes orally the lung dose is less than the adult dose for the two large sizes of particles (4 and 5 μm) examined herein. This is an interesting observation considering that the nose is normally considered a better filter compared to the oral airways. Our data, however, show that the lower breathing flow through the nose results in lower losses in nasal airways. Also, more losses occur in oropharyngeal airways of children during high constant flow rates that are typical of what happens during inhalation of the dose emitted from the common inhalers.

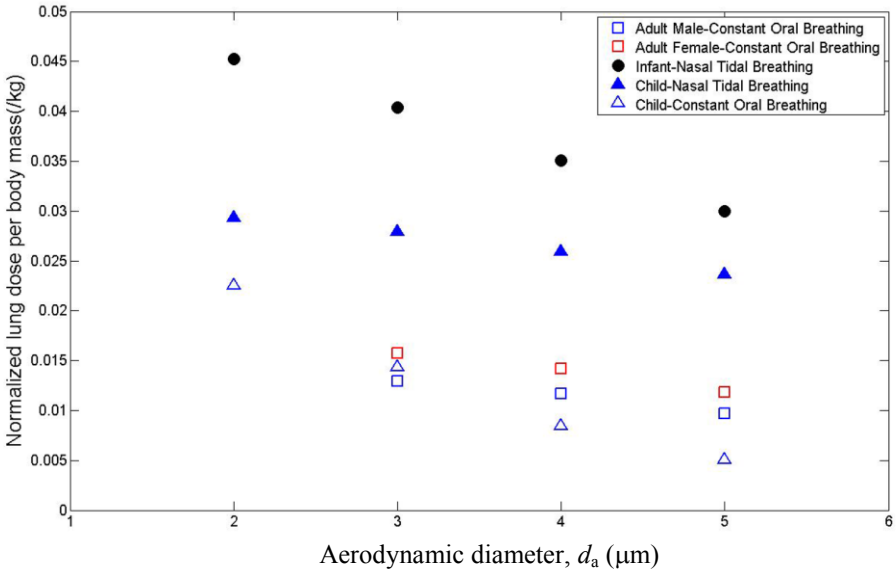

Figure 6.1 Lung doses for different age groups, normalized to the body mass and the adult inhaled dose, versus particle's aerodynamic diameter.

The lung doses for different age groups have been normalized by body surface area, using Eq. 6.1, and illustrated in Figure 6.2. For the cases of constant flow, 60 L/min was used as the flow rate while for tidal breathing cases, the related flow rates given in Table 6.1 were used. Body surface area is believed to result in a more accurate comparative dose prescription among subjects with different sizes (Mosteller 1987). This is in fact obvious in Figure 6.2 by noticing the reduced differences in the lung doses among different age groups (normalized by body surface area) compared to Figure 6.1, which was plotted based on the subjects' body mass.

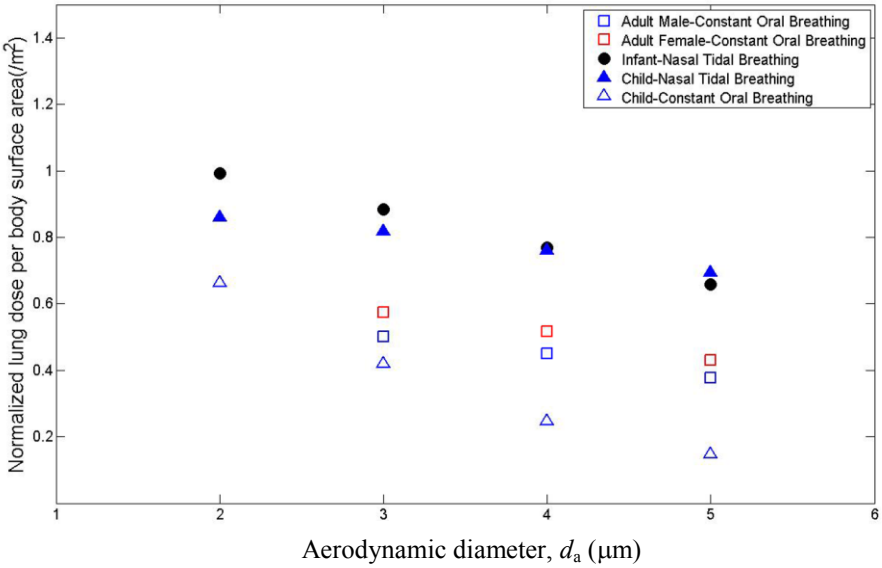

Figure 6.2 Lung doses for different age subjects, normalized to the adult inhaled dose and the subjects' body surface area, versus aerodynamic diameter of particles.

The 1-year old infant and 10-year old child receive approximately the same amount of lung dose; both less than double the adult's dose. However, high losses of the orally inhaled particles, particularly the larger ones, are again apparent in the oropharyngeal airways of 10-year old child. The lower tidal breathing flow rates result in less extrathoracic deposition in the same subject.

In order to examine the effect of breathing flow rate on the lung doses, the normalized lung dose values for different age groups (i.e. normalized by adult's inhaled dose and body surface areas of the subjects) have been plotted in Figure 6.3 versus the impaction parameter, $d_a^2 Q$. All flow rates given in Table 6.1 have been used in this Figure (i.e. 30, 60 and 90 L/min for constant flow cases). The

least square method was used in Matlab to fit a linear equation to the normalized lung dose. The approximate collapse of all the data (R^2=0.83) on a line suggests the possibility of correcting pediatric lung doses to achieve approximately uniform dose per body surface area among different age groups. For instance, by knowing that infant's breathing flow rate is about one-tenth of adult's breathing flow rate, for a known particle size released from an inhaler the impaction parameter of infant ($d_a^2 Q$) is also one-tenth of adult's case. By substituting the parameter x in the fitted equation (Eq. 6.2) with 1 and 0.1, the difference between the y values would be 0.44. This means that by prescribing approximately half (precisely 44%) of the labeled dose to an infant, the same dose per unit body mass as adults would be obtained by an infant.

$$y = 1.7 - 0.44 \log_{10} x \tag{6.2}$$

Note that different results would be obtained by considering different inhaled fractions by infants and children compared with adults. In Figures 6.1, 6.2 and 6.3 the infant's inhaled dose was considered as half of the adult's dose whereby child's inhaled dose was considered equal to the adult's inhaled dose (Chambers *et al*. 2009).

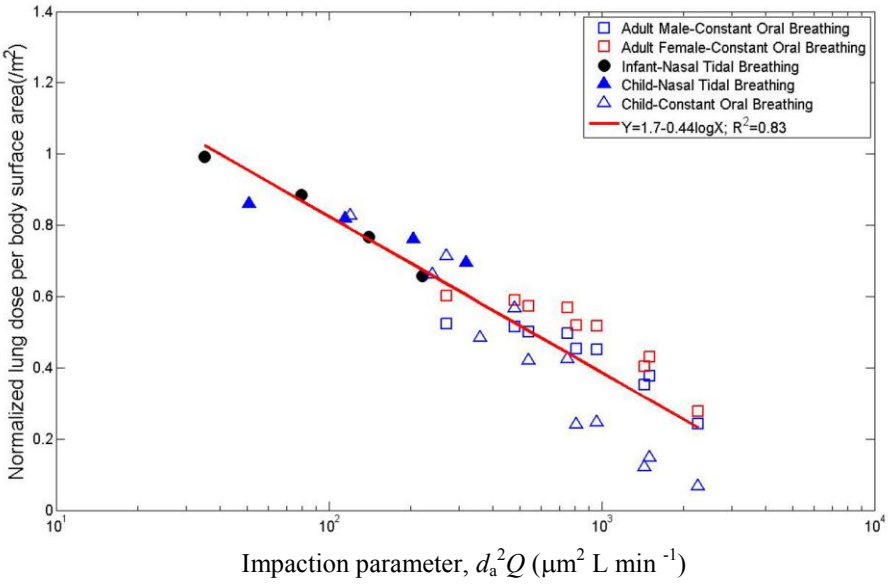

Figure 6.3 Lung doses for different age group subjects, normalized to the adult inhaled dose and the body surface area of different age groups, versus the inertial impaction parameter $d_a^2 Q$.

6.4 Conclusions

Application of the correlations, developed for the prediction of extrathoracic deposition, in the estimation of lung dose was examined. Also, relating the dose efficacious for adults to the pediatric subjects was learned to be promising with the use of Eq. 6.2. Such comparative estimations may be useful for developing new inhalers and improving the inhalation drug delivery to the children suffering from respiratory diseases.

6.5 Bibliography

Chambers, F. E., Brown, S., and Ludzik, A. J. (2009). Comparative *in vitro* performance of valved holding chambers with a budesonide/formoterol pressurized metered-dose inhaler. *Allergy and Asthma Proceedings*, 30(4), 424-432.

Grgic, B., Finlay W. H., Burnell, P. K. P., Heenan, A. F. (2004). *In vitro* intersubject and intrasubject deposition measurements in realistic mouth-throat geometries. *Journal of Aerosol Science*, 35, 1025-1040.

Hofmann, W., Martonen, T.B., Graham, R.C. (1989), Predicted deposition of nonhygroscopic aerosols in the human lung as a function of subject age. *Journal of Aerosol Medicine*, 2, 49-68.

ICRP (International Commission on Radiological Protection) (1994), Human respiratory tract model for radiological protection, *Annals of the ICRP*, ICRP Publication 66, Elsevier, New York.

Mosteller R. D. (1987), Simplified calculation of body surface area. *New England Journal of Medicine*, 317(17), 1098.

Storey-Bishoff, J., Noga, M. and Finlay, W. H. (2008). Deposition of Micrometer-sized Aerosol Particles in Infant Nasal Airway Replicas. *Journal of Aerosol Science*, 39, 1055-1065.

CHAPTER 7 : CONCLUSIONS

7. 1 Summary and Conclusions

In this thesis, a collection of *in vitro* predictive correlations were developed to estimate the deposition of aerosols of various sizes in the extrathoracic airways of children of different ages. The correlations will be useful for exposure studies and inhalation drug delivery. Intersubject variability was reduced by characterizing the geometry of the airways and relating the most relevant characteristic diameter to deposition in each case.

In summary, the deposition of ultrafine particles in nasal airways of infants was measured and a single predictive correlation was proposed to estimate the deposition of a known ultrafine particle in the range of 13-100 nm at a known breathing pattern for an individual (3-18 months) with a given airway volume and length. Airway volume and length can be relatively easily measured by acoustic rhinometry *in vivo*. Also, the deposition of micrometer-sized particles (0.5-5.3 μm) was measured in nasal airways of children 4-14 years old and a single predictive correlation was developed. The ratio of surface area to the length of airway was characterized as the most relevant characteristic diameter in this case. However, a second correlation based on the airway volume and the centerline length of the airways was presented as an alternative to simplify the *in vivo* measurements of the dimensions of the airways. In addition, the development of a technique to CT scan the oral airways of children 6-14 years of age was presented. *In vitro* measurement of the deposition of micrometer-sized particles (0.5-5.3 μm) in the oropharyngeal airway replicas, fabricated using the recorded

CT scans images and rapid prototyping, was related to the volume and surface area of the airway and a single predictive individualized correlation was introduced. An alternative equation was also proposed based on the volume and length of the centerline of the oral airways. Moreover, the development of an idealized child throat, based on our findings in Chapter 4, was presented here. Such an idealized child throat is hoped to significantly facilitate bench-top inhalation drug testing. As an illustrative example, the application of the developed correlations in the comparative studies, relating adult's lung dose to pediatric lung dose, was also reported as a part of this study.

7.2 Future Work

1. Deposition in Oropharyngeal Airways during Tidal Breathing

In this study, experiments were performed to measure the deposition of micrometer-sized particles in nine children replicas and the idealized child throat during tidal breathing. Completion of the analysis of recorded data will result in a predictive correlation with an application in drug delivery using nebulizers.

Computed tomography images of eleven adults were also recorded during this study, following the same methodology that was used for imaging children's oral airways. Eleven airway replicas of these adult subjects were rapid prototyped and further experiments similar to the ones completed for children will extend Stahlhofen's findings (Stahlhofen *et al*. 1989) for improved individualized drug delivery to adults using nebulizers. This will be invaluable to address the current

lack of individualized correlations including the airway dimensions of adult subjects.

There are *in vivo* data available on the lung dose of children during inhalation of specified medications (Devadason *et al*., 1997, 2003; Roller *et al*., 2007). Experiments are required to measure the deposition of the exact inhalers in the developed child throat to validate this throat based on the available *in vivo* data.

In this study, the focus has been on measuring the deposition during inhalation only since the lungs geometry was needed to simulate the exhaled breath realistically; thus, studies are needed to develop lung geometries and measure the deposition during exhalation. These experiments could be extended to measure regional deposition of aerosols in the developed lung geometries during both inhalation and exhalation.

Possible *in vivo* experiments are also recommended to validate the developed correlations for a known particle size during controlled breathing in subjects with known airway geometries.

7.3 Bibliography

Devadason, S. G., Everard, M. L., MacEarlan, C., Roller, C., Summers, Q. A., Swift, P., Borgstrom, L., and Le Souef, P. N. (1997). Lung deposition from the Turbuhaler in children with cystic fibrosis. *The European Respiratory Journal*, 10, 2023-2028.

Devadason, S. G., Huang, T., Walker, S., Troedson, R., and Le Souef, P. N. (2003). Distribution of technetium-99m-labelled QVAR™ delivered using an Autohaler™ device in children. *The European Respiratory Journal*, 21, 1007-1011.

Roller, C. M., Zhang, G., Troedson, R. G., Leach, C. L., Le Souef, P. N., and Devadason, S. G. (2007). Spacer inhalation technique and deposition of extrafine aerosol in asthmatic children. *The European Respiratory Journal*, 29, 299-306.

Stahlhofen, W., Rudolf, G., and James, A. C. (1989). Intercomparison of experimental regional aerosol deposition data. *Journal of Aerosol Medicine*, 2(3), 285-308.

Appendix A: Experimental Deposition Data

A.1 List of Deposition Data Presented in Chapter 2

Subject 2		
Q (L/min)	d_p (nm)	Dep (%)
3.12	13	9.301
3.12	20	7.091
3.12	30	6.817
3.12	40	3.531
3.12	50	1.868
3.12	60	1.063
3.12	70	0.220
3.12	80	0.039
3.12	90	0
3.12	100	0
5.26	13	13.967
5.26	20	9.855
5.26	30	8.362
5.26	40	4.805
5.26	50	4.025
5.26	60	1.324
5.26	70	0.368
5.26	80	0
5.26	90	0
5.26	100	0
6.81	13	13.486
6.81	20	10.456
6.81	30	8.713
6.81	40	5.216
6.81	50	2.396
6.81	60	1.058
6.81	70	0.004
6.81	80	0
6.81	90	0
6.81	100	0

Subject 3		
Q (L/min)	d_p (nm)	Dep (%)
2.99	13	9.684
2.99	20	8.344
2.99	30	7.780
2.99	40	4.033
2.99	50	1.169
2.99	60	0
2.99	70	0
2.99	80	0
2.99	90	0
2.99	100	0
-	-	-
-	-	-
-	-	-
-	-	-
-	-	-
-	-	-
-	-	-
-	-	-
-	-	-
-	-	-
7.23	13	13.643
7.23	20	11.564
7.23	30	9.239
7.23	40	5.785
7.23	50	1.958
7.23	60	0.129
7.23	70	0
7.23	80	0
7.23	90	0
7.23	100	0

Subject 4		
Q (L/min)	d_p (nm)	Dep (%)
3.15	13	14.271
3.15	20	10.727
3.15	30	9.076
3.15	40	6.125
3.15	50	2.387
3.15	60	0.864
3.15	70	0.052
3.15	80	0
3.15	90	0
3.15	100	0
-	-	-
-	-	-
-	-	-
-	-	-
-	-	-
-	-	-
-	-	-
-	-	-
-	-	-
-	-	-
7.00	13	15.280
7.00	20	13.267
7.00	30	11.755
7.00	40	6.738
7.00	50	3.283
7.00	60	0.266
7.00	70	0
7.00	80	0
7.00	90	0
7.00	100	0

Subject 5		
Q (L/min)	d_p (nm)	Dep (%)
3.19	13	11.7406
3.19	20	9.1568
3.19	30	6.9501
3.19	40	4.6690
3.19	50	2.5055
3.19	60	0.6095
3.19	70	0
3.19	80	0
3.19	90	0
3.19	100	0
-	-	-
-	-	-
-	-	-
-	-	-
-	-	-
-	-	-
-	-	-
-	-	-
-	-	-
-	-	-
7.17	13	15.3432
7.17	20	12.4052
7.17	30	10.4541
7.17	40	6.1814
7.17	50	2.4607
7.17	60	0.4250
7.17	70	0.0518
7.17	80	0
7.17	90	0
7.17	100	0

Subject 6		
Q (L/min)	d_p (nm)	Dep (%)
2.93	13	22.358
2.93	20	18.288
2.93	30	14.853
2.93	40	10.115
2.93	50	6.022
2.93	60	1.884
2.93	70	0
2.93	80	0
2.93	90	0
2.93	100	0
4.83	13	20.309
4.83	20	16.176
4.83	30	13.280
4.83	40	8.568
4.83	50	4.409
4.83	60	1.745
4.83	70	0
4.83	80	0
4.83	90	0
4.83	100	0
7.08	13	21.027
7.08	20	17.358
7.08	30	14.295
7.08	40	12.063
7.08	50	8.784
7.08	60	6.233
7.08	70	3.115
7.08	80	2.847
7.08	90	8.098
7.08	100	1.525

Subject 7		
Q (L/min)	d_p (nm)	Dep (%)
3.07	13	18.161
3.07	20	13.651
3.07	30	12.600
3.07	40	6.801
3.07	50	2.854
3.07	60	1.163
3.07	70	0.354
3.07	80	0
3.07	90	0
3.07	100	0
-	-	-
-	-	-
-	-	-
-	-	-
-	-	-
-	-	-
-	-	-
-	-	-
-	-	-
-	-	-
7.28	13	20.673
7.28	20	17.353
7.28	30	14.796
7.28	40	10.108
7.28	50	6.476
7.28	60	4.212
7.28	70	2.955
7.28	80	2.905
7.28	90	2.712
7.28	100	0.286

Subject 8		
Q (L/min)	d_p (nm)	Dep (%)
3.02	13	15.511
3.02	20	12.801
3.02	30	9.612
3.02	40	6.770
3.02	50	3.852
3.02	60	0.339
3.02	70	0
3.02	80	0
3.02	90	0
3.02	100	0
-	-	-
-	-	-
-	-	-
-	-	-
-	-	-
-	-	-
-	-	-
-	-	-
-	-	-
-	-	-
6.83	13	21.037
6.83	20	16.442
6.83	30	12.685
6.83	40	8.974
6.83	50	5.689
6.83	60	3.703
6.83	70	2.372
6.83	80	0.423
6.83	90	1.025
6.83	100	0.281

Subject 10		
Q (L/min)	d_p (nm)	Dep (%)
3.12	13	7.354
3.12	20	4.466
3.12	30	6.515
3.12	40	2.488
3.12	50	1.448
3.12	60	0.792
3.12	70	0
3.12	80	0
3.12	90	0
3.12	100	0
5.27	13	9.928
5.27	20	7.590
5.27	30	7.615
5.27	40	4.008
5.27	50	1.882
5.27	60	0
5.27	70	0
5.27	80	0
5.27	90	0
5.27	100	0
6.99	13	9.233
6.99	20	8.923
6.99	30	7.997
6.99	40	4.677
6.99	50	1.834
6.99	60	0.513
6.99	70	0
6.99	80	0
6.99	90	0
6.99	100	0

Subject 11		
Q (L/min)	d_p (nm)	Dep (%)
2.96	13	16.587
2.96	20	13.616
2.96	30	12.508
2.96	40	7.492
2.96	50	4.245
2.96	60	2.910
2.96	70	1.254
2.96	80	0.089
2.96	90	0
2.96	100	0
-	-	-
-	-	-
-	-	-
-	-	-
-	-	-
-	-	-
-	-	-
-	-	-
-	-	-
-	-	-
6.86	13	23.463
6.86	20	20.216
6.86	30	18.247
6.86	40	13.760
6.86	50	10.127
6.86	60	6.681
6.86	70	5.273
6.86	80	5.116
6.86	90	4.995
6.86	100	2.665

Subject 14		
Q (L/min)	d_p (nm)	Dep (%)
3.15	13	10.317
3.15	20	7.936
3.15	30	7.983
3.15	40	4.375
3.15	50	1.989
3.15	60	0.776
3.15	70	0
3.15	80	0
3.15	90	0
3.15	100	0
-	-	-
-	-	-
-	-	-
-	-	-
-	-	-
-	-	-
-	-	-
-	-	-
-	-	-
-	-	-
7.37	13	13.790
7.37	20	11.284
7.37	30	9.713
7.37	40	5.919
7.37	50	2.252
7.37	60	0.219
7.37	70	0
7.37	80	0
7.37	90	0
7.37	100	0

A.2 List of Deposition Data Presented in Chapter 3

Subject 1		
Q (L/min)	d_a (μm)	Dep (%)
9.771	0.505	4.105
9.771	0.794	4.071
9.771	1.280	3.864
9.771	2.031	4.466
9.771	3.208	8.776
9.771	5.322	19.230
12.724	0.505	1.688
12.724	0.794	1.740
12.724	1.280	1.898
12.724	2.031	4.270
12.724	3.208	1.374
12.724	5.322	31.409
18.343	0.505	3.922
18.343	0.794	4.084
18.343	1.280	6.009
18.343	2.031	14.015
18.343	3.208	30.317
18.343	5.322	50.199
24.601	0.505	0
24.601	0.794	0
24.601	1.280	4.967
24.601	2.031	21.913
24.601	3.208	45.042
24.601	5.322	63.017

Subject 2		
Q (L/min)	d_a (μm)	Dep (%)
10.083	0.505	1.889
10.083	0.794	1.830
10.083	1.280	1.647
10.083	2.031	1.762
10.083	3.208	3.407
10.083	5.322	9.887
13.285	0.505	1.352
13.285	0.794	1.278
13.285	1.280	1.334
13.285	2.031	1.842
13.285	3.208	5.213
13.285	5.322	12.693
19.273	0.505	2.042
19.273	0.794	2.075
19.273	1.280	2.446
19.273	2.031	4.528
19.273	3.208	12.422
19.273	5.322	28.951
26.046	0.505	0.856
26.046	0.794	0.913
26.046	1.280	1.957
26.046	2.031	6.589
26.046	3.208	19.412
26.046	5.322	40.059

Subject 3		
Q (L/min)	d_a (μm)	Dep (%)
9.997	0.505	1.811
9.997	0.794	1.826
9.997	1.280	1.773
9.997	2.031	1.997
9.997	3.208	3.883
9.997	5.322	11.267
13.242	0.505	2.815
13.242	0.794	2.780
13.242	1.280	2.708
13.242	2.031	3.479
13.242	3.208	8.660
13.242	5.322	21.860
19.139	0.505	3.863
19.139	0.794	3.892
19.139	1.280	4.409
19.139	2.031	8.377
19.139	3.208	21.502
19.139	5.322	43.417
25.732	0.505	1.302
25.732	0.794	1.428
25.732	1.280	3.433
25.732	2.031	13.045
25.732	3.208	34.087
25.732	5.322	57.004

Subject 5		
Q (L/min)	d_a (μm)	Dep (%)
10.046	0.505	3.373
10.046	0.794	3.371
10.046	1.280	3.175
10.046	2.031	3.113
10.046	3.208	3.809
10.046	5.322	5.005
13.099	0.505	0.875
13.099	0.794	0.930
13.099	1.280	0.735
13.099	2.031	1.047
13.099	3.208	2.906
13.099	5.322	9.768
19.386	0.505	3.323
19.386	0.794	3.742
19.386	1.280	3.573
19.386	2.031	6.122
19.386	3.208	11.153
19.386	5.322	21.527
25.914	0.505	0.351
25.914	0.794	0.612
25.914	1.280	1.146
25.914	2.031	4.993
25.914	3.208	17.581
25.914	5.322	33.579

Subject 6		
Q (L/min)	d_a (μm)	Dep (%)
9.817	0.505	2.211
9.817	0.794	2.400
9.817	1.280	2.762
9.817	2.031	4.780
9.817	3.208	13.623
9.817	5.322	31.464
12.811	0.505	1.114
12.811	0.794	1.091
12.811	1.280	1.936
12.811	2.031	7.200
12.811	3.208	23.695
12.811	5.322	45.236
18.592	0.505	4.121
18.592	0.794	4.395
18.592	1.280	7.475
18.592	2.031	20.945
18.592	3.208	44.610
18.592	5.322	66.419
24.790	0.505	3.245
24.790	0.794	6.105
24.790	1.280	13.079
24.790	2.031	36.644
24.790	3.208	59.654
24.790	5.322	75.843

Subject 7		
Q (L/min)	d_a (μm)	Dep (%)
9.818	0.505	0
9.818	0.794	0
9.818	1.280	0
9.818	2.031	0
9.818	3.208	1.790
9.818	5.322	11.778
13.088	0.505	2.643
13.088	0.794	2.608
13.088	1.280	2.663
13.088	2.031	3.991
13.088	3.208	10.031
13.088	5.322	25.233
19.139	0.505	4.090
19.139	0.794	4.197
19.139	1.280	5.118
19.139	2.031	10.632
19.139	3.208	24.418
19.139	5.322	48.159
25.400	0.505	0.101
25.400	0.794	0.305
25.400	1.280	3.481
25.400	2.031	16.487
25.400	3.208	37.861
25.400	5.322	62.419

Subject 8		
Q (L/min)	d_a (μm)	Dep (%)
9.998	0.505	0.314
9.998	0.794	0.387
9.998	1.280	0.279
9.998	2.031	0.409
9.998	3.208	2.060
9.998	5.322	9.476
13.203	0.505	1.928
13.203	0.794	1.814
13.203	1.280	1.662
13.203	2.031	2.180
13.203	3.208	6.430
13.203	5.322	18.151
19.231	0.505	3.332
19.231	0.794	3.216
19.231	1.280	3.686
19.231	2.031	7.114
19.231	3.208	18.152
19.231	5.322	38.279
25.752	0.505	0.800
25.752	0.794	0.955
25.752	1.280	2.984
25.752	2.031	11.662
25.752	3.208	28.933
25.752	5.322	51.448

Subject 9		
Q (L/min)	d_a (μm)	Dep (%)
10.022	0.505	1.449
10.022	0.794	1.533
10.022	1.280	1.464
10.022	2.031	1.658
10.022	3.208	3.144
10.022	5.322	9.036
13.029	0.505	0
13.029	0.794	0
13.029	1.280	0.085
13.029	2.031	0.984
13.029	3.208	4.031
13.029	5.322	15.892
19.216	0.505	2.843
19.216	0.794	2.836
19.216	1.280	3.376
19.216	2.031	6.641
19.216	3.208	17.668
19.216	5.322	36.070
25.569	0.505	0
25.569	0.794	0
25.569	1.280	1.776
25.569	2.031	9.811
25.569	3.208	27.053
25.569	5.322	49.692

Subject 10		
Q (L/min)	d_a (μm)	Dep (%)
10.029	0.505	1.994
10.029	0.794	2.079
10.029	1.280	2.094
10.029	2.031	2.439
10.029	3.208	4.660
10.029	5.322	11.431
12.988	0.505	1.838
12.988	0.794	1.747
12.988	1.280	1.818
12.988	2.031	2.882
12.988	3.208	8.216
12.988	5.322	19.878
18.950	0.505	1.505
18.950	0.794	1.562
18.950	1.280	2.367
18.950	2.031	6.433
18.950	3.208	19.060
18.950	5.322	39.172
25.356	0.505	0
25.356	0.794	0
25.356	1.280	2.199
25.356	2.031	11.419
25.356	3.208	31.734
25.356	5.322	54.257

Subject 11		
Q (L/min)	d_a (μm)	Dep (%)
9.459	0.505	0
9.459	0.794	0
9.459	1.280	0.546
9.459	2.031	4.782
9.459	3.208	19.273
9.459	5.322	42.093
12.603	0.505	2.672
12.603	0.794	2.827
12.603	1.280	4.880
12.603	2.031	14.414
12.603	3.208	35.926
12.603	5.322	55.708
17.706	0.505	2.558
17.706	0.794	3.368
17.706	1.280	9.274
17.706	2.031	28.953
17.706	3.208	55.191
17.706	5.322	73.262
23.750	0.505	0
23.750	0.794	0
23.750	1.280	10.650
23.750	2.031	40.430
23.750	3.208	66.126
23.750	5.322	78.247

Subject 12		
Q (L/min)	d_a (μm)	Dep (%)
9.832	0.505	0.494
9.832	0.794	0.548
9.832	1.280	0.604
9.832	2.031	1.593
9.832	3.208	6.604
9.832	5.322	20.761
12.988	0.505	1.891
12.988	0.794	1.908
12.988	1.280	2.325
12.988	2.031	5.239
12.988	3.208	15.828
12.988	5.322	34.489
18.706	0.505	2.483
18.706	0.794	2.700
18.706	1.280	4.578
18.706	2.031	13.232
18.706	3.208	31.990
18.706	5.322	56.413
24.965	0.505	0
24.965	0.794	0
24.965	1.280	4.037
24.965	2.031	21.013
24.965	3.208	44.965
24.965	5.322	67.193

Subject 14		
Q (L/min)	d_a (μm)	Dep (%)
9.764	0.505	0.754
9.764	0.794	0.968
9.764	1.280	1.232
9.764	2.031	2.547
9.764	3.208	6.543
9.764	5.322	18.183
12.988	0.505	3.059
12.988	0.794	3.156
12.988	1.280	3.770
12.988	2.031	6.810
12.988	3.208	14.582
12.988	5.322	29.343
18.651	0.505	4.528
18.651	0.794	4.819
18.651	1.280	6.725
18.651	2.031	14.792
18.651	3.208	28.464
18.651	5.322	48.461
24.376	0.505	0
24.376	0.794	0
24.376	1.280	1.770
24.376	2.031	17.488
24.376	3.208	37.160
24.376	5.322	60.522

Subject 15		
Q (L/min)	d_a (μm)	Dep (%)
10.098	0.505	1.922
10.098	0.794	2.063
10.098	1.280	1.969
10.098	2.031	2.137
10.098	3.208	2.944
10.098	5.322	8.881
13.584	0.505	2.477
13.584	0.794	2.291
13.584	1.280	2.000
13.584	2.031	2.169
13.584	3.208	4.442
13.584	5.322	13.187
19.670	0.505	3.465
19.670	0.794	3.354
19.670	1.280	3.510
19.670	2.031	5.394
19.670	3.208	13.333
19.670	5.322	33.581
25.653	0.505	0.118
25.653	0.794	0.145
25.653	1.280	1.245
25.653	2.031	6.642
25.653	3.208	22.108
25.653	5.322	48.401

Subject 4-Congested		
Q (L/min)	d_a (μm)	Dep (%)
7.039	0.505	8.048
7.039	0.794	10.991
7.039	1.280	25.606
7.039	2.031	51.029
7.039	3.208	70.941
7.039	5.322	76.217
8.986	0.505	8.074
8.986	0.794	14.070
8.986	1.280	37.004
8.986	2.031	64.327
8.986	3.208	79.107
8.986	5.322	77.775
11.580	0.505	12.532
11.580	0.794	22.009
11.580	1.280	49.243
11.580	2.031	74.244
11.580	3.208	85.432
11.580	5.322	86.822
14.971	0.505	1.903
14.971	0.794	21.321
14.971	1.280	57.961
14.971	2.031	80.862
14.971	3.208	88.224
14.971	5.322	87.072

A.3 List of Deposition Data Presented in Chapter 4

Subject 1		
Q (L/min)	d_a (μm)	Dep (%)
29.96	0.505	-0.556
29.96	0.794	-0.268
29.96	1.280	1.645
29.96	2.031	12.204
29.96	3.208	43.135
29.96	5.322	71.606
33.01	0.505	0.580
33.01	0.794	0.486
33.01	1.280	2.380
33.01	2.031	14.787
33.01	3.208	43.886
33.01	5.322	72.861
69.51	0.505	-4.463
69.51	0.794	-0.814
69.51	1.280	20.214
69.51	2.031	57.026
69.51	3.208	74.060
107.06	0.505	3.145
107.06	0.794	11.445
107.06	1.280	41.851
107.06	2.031	71.311
152.47	0.505	9.583
152.47	0.794	27.863
152.47	1.280	63.199
152.47	2.031	78.754

Subject 2		
Q (L/min)	d_a (μm)	Dep (%)
29.87	0.505	-0.092
29.87	0.794	0.191
29.87	1.280	4.600
29.87	2.031	27.804
29.87	3.208	67.156
29.87	5.322	87.770
33.39	0.505	-0.344
33.39	0.794	0.192
33.39	1.280	7.482
33.39	2.031	38.135
33.39	3.208	75.022
33.39	5.322	89.530
68.92	0.505	-6.017
68.92	0.794	3.971
68.92	1.280	42.369
68.92	2.031	79.976
68.92	3.208	85.908
107.17	0.505	5.998
107.17	0.794	25.506
107.17	1.280	66.454
107.17	2.031	86.315
153.37	0.505	19.747
153.37	0.794	48.826
153.37	1.280	81.986
153.37	2.031	86.905

Subject 3		
Q (L/min)	d_a (μm)	Dep (%)
29.99	0.505	0.053
29.99	0.794	0.290
29.99	1.280	1.300
29.99	2.031	5.453
29.99	3.208	16.989
29.99	5.322	32.686
33.37	0.505	-0.640
33.37	0.794	-0.616
33.37	1.280	0.450
33.37	2.031	6.461
33.37	3.208	20.544
33.37	5.322	38.220
68.01	0.505	-2.778
68.01	0.794	-1.738
68.01	1.280	6.478
68.01	2.031	24.060
68.01	3.208	36.673
105.11	0.505	1.064
105.11	0.794	4.275
105.11	1.280	17.947
105.11	2.031	36.074
148.43	0.505	5.002
148.43	0.794	12.285
148.43	1.280	30.454
148.43	2.031	46.154

Subject 5		
Q (L/min)	d_a (μm)	Dep (%)
29.84	0.505	3.484
29.84	0.794	3.424
29.84	1.280	3.663
29.84	2.031	6.243
29.84	3.208	19.982
29.84	5.322	46.046
32.85	0.505	1.607
32.85	0.794	1.524
32.85	1.280	1.876
32.85	2.031	5.085
32.85	3.208	22.197
32.85	5.322	49.078
67.55	0.505	-2.329
67.55	0.794	-1.712
67.55	1.280	5.578
67.55	2.031	29.751
67.55	3.208	52.741
105.69	0.505	0.939
105.69	0.794	3.378
105.69	1.280	19.191
105.69	2.031	47.876
149.14	0.505	3.993
149.14	0.794	10.815
149.14	1.280	36.242
149.14	2.031	59.507

Subject 6		
Q (L/min)	d_a (μm)	Dep (%)
30.03	0.505	0.242
30.03	0.794	0.165
30.03	1.280	0.540
30.03	2.031	2.250
30.03	3.208	10.990
30.03	5.322	32.927
33.19	0.505	1.610
33.19	0.794	1.471
33.19	1.280	1.544
33.19	2.031	2.996
33.19	3.208	11.355
33.19	5.322	34.598
69.29	0.505	-1.536
69.29	0.794	-1.193
69.29	1.280	2.029
69.29	2.031	16.908
69.29	3.208	40.650
106.35	0.505	0.326
106.35	0.794	1.464
106.35	1.280	9.737
106.35	2.031	32.879
149.53	0.505	3.443
149.53	0.794	7.164
149.53	1.280	23.811
149.53	2.031	48.445

Subject 7		
Q (L/min)	d_a (μm)	Dep (%)
29.92	0.505	0.130
29.92	0.794	0.033
29.92	1.280	0.445
29.92	2.031	6.096
29.92	3.208	30.022
29.92	5.322	64.591
33.34	0.505	0.105
33.34	0.794	0.173
33.34	1.280	0.943
33.34	2.031	8.075
33.34	3.208	36.426
33.34	5.322	70.337
6.89	0.505	-3.056
6.89	0.794	-1.954
6.89	1.280	11.556
6.89	2.031	48.226
6.89	3.208	72.038
107.85	0.505	1.528
107.85	0.794	6.339
107.85	1.280	33.709
107.85	2.031	66.808
153.98	0.505	6.261
153.98	0.794	19.247
153.98	1.280	55.251
153.98	2.031	74.326

Subject 10		
Q (L/min)	d_a (μm)	Dep (%)
29.87	0.505	-0.538
29.87	0.794	-0.511
29.87	1.280	-0.085
29.87	2.031	3.808
29.87	3.208	21.431
29.87	5.322	52.349
33.53	0.505	0.901
33.53	0.794	0.820
33.53	1.280	1.066
33.53	2.031	4.164
33.53	3.208	22.072
33.53	5.322	54.371
69.61	0.505	-2.946
69.61	0.794	-2.475
69.61	1.280	4.775
69.61	2.031	33.570
69.61	3.208	63.948
107.35	0.505	0.885
107.35	0.794	3.203
107.35	1.280	21.011
107.35	2.031	55.455
151.44	0.505	3.981
151.44	0.794	11.666
151.44	1.280	42.635
151.44	2.031	70.332

Subject 11		
Q (L/min)	d_a (μm)	Dep (%)
29.95	0.505	0.310
29.95	0.794	0.211
29.95	1.280	0.983
29.95	2.031	7.974
29.95	3.208	35.146
29.95	5.322	66.856
33.14	0.505	0.259
33.14	0.794	0.431
33.14	1.280	1.282
33.14	2.031	7.956
33.14	3.208	37.160
33.14	5.322	68.013
69.31	0.505	-4.934
69.31	0.794	-3.885
69.31	1.280	10.275
69.31	2.031	49.115
69.31	3.208	72.738
108.83	0.505	0.188
108.83	0.794	5.041
108.83	1.280	35.251
108.83	2.031	68.920
155.32	0.505	3.773
155.32	0.794	17.233
155.32	1.280	56.694
155.32	2.031	76.025

Subject 12		
Q (L/min)	d_a (μm)	Dep (%)
29.95	0.505	2.913
29.95	0.794	2.836
29.95	1.280	3.004
29.95	2.031	4.336
29.95	3.208	13.038
29.95	5.322	34.421
60.16	0.505	7.024
60.16	0.794	7.020
60.16	1.280	8.270
60.16	2.031	17.654
60.16	3.208	38.581
88.73	0.505	4.669
88.73	0.794	5.135
88.73	1.280	10.363
88.73	2.031	30.764
88.73	3.208	53.817
121.08	0.505	2.394
121.08	0.794	3.968
121.08	1.280	15.868
121.08	2.031	41.684

A.4 List of Deposition Data Presented in Chapter 5

Idealized Child		
Q (L/min)	d_a (μm)	Dep (%)
32.35	0.505	-3.33
32.35	0.794	-3.33
32.35	1.280	-1.81
32.35	2.031	10.23
32.35	3.208	37.10
32.35	5.322	61.23
60.29	0.505	-6.20
60.29	0.794	-5.29
60.29	1.280	5.19
60.29	2.031	35.14
60.29	3.208	54.73
89.95	0.505	0.80
89.95	0.794	4.94
89.95	1.280	25.93
89.95	2.031	55.99
120.39	0.505	-1.25
120.39	0.794	8.61
120.39	1.280	36.26
120.39	2.031	61.59